Elsevier Editorial System(tm) for Gondwana Research
Manuscript Draft

Manuscript Number: GR-D-18-00274R1

Title: The 2.0-1.88 Ga Paleoproterozoic evolution of the southern Amazonian Craton (Brazil): an interpretation inferred by lithofaciological, geochemical and geochronological data.

Article Type: Research Paper

Corresponding Author: Dr. Matteo Roverato, PhD

Corresponding Author's Institution: Yachaytech

First Author: Matteo Roverato, PhD

Order of Authors: Matteo Roverato, PhD; Daniele Giordano; Tommaso Giovanardi; Caetano juliani; Liza Polo

Abstract: The study of Paleoproterozoic rocks is crucial for understanding Earth's tectonic evolution during the time when most of the modern crust and ore deposits were formed. The rocks of the Brazilian Amazonian Craton record some of the most-complete and best-preserved Paleoproterozoic magmatic and volcanic episodes on Earth. Following previous investigations, we present new lithofaciological and stratigraphic records of the felsic rocks of the Tapajós Mineral Province (TMP) (~ 2-1.88 Ga) and the São Felix do Xingú region (SFX) (~ 1.88 Ga) which, combined with new petrological and geochronological data, help providing a more complete understanding of the tectonic, magmatic and volcanological evolution of the Amazonian Craton. This magmatism/volcanism is thought to be formed in a late-/post-orogenic to extentional regime confirmed by the new geochemical data presented here. The transition from late-convergent to extensional tectonic setting could register the beginning of the taphrogenesis that marked the Amazonian Craton throughout the Mesoproterozoic. The volcanological approach of this contribution can serve as a strategy for the modelling of the evolution of Precambrian volcano-sedimentary basins around the world. The large amount of rocks analyzed are divided into primary and secondary volcaniclastic products depending on if they resulted from a direct volcanic activity (pyroclastic) or processes that reworked pyroclastic fragments. Furthermore, the deposits are subdivided into massive and stratified, depending on their primary mechanisms of transport and emplacement. By confirming the results from previous studies, our study permits to depict a more precise paleo-environmental picture of the processes that occurred in the Amazonian Craton during the Late-Paleoproterozoic. In particular, the presence of large regional-scale fissural systems and caldera collapses produced large silicic explosive volcanic eruptions, also accompanied by the emission of large volume effusive products. Although studies on the Amazonian Craton are still scarce and controversial, the present study provides new evidence that this volcanism may have formed one of the largest Silicic Large Igneous Provinces (SLIP) on earth. Our data also confirm that at least two major Paleoproterozoic periods of formation of volcanic rocks exist in the Amazonian craton. This point is of great relevance for any future interpretation of the geological evolution of this craton.

Response to Reviewers: To reviewer 1 Nils Lenhardt:

Dear reviewer,
we respected and changed most of the corrections suggested in particularly we followed the suggestions to divide the lithofaciological description and simplify the geological framework.
Thank you for the time you spent reading this long manuscript.

To reviewer 2 Roberto Dall'Agnol:
Dear reviewer,
thank you for your suggestions especially those related to the geological framework and geochemical analyses. We considered and accepted most of the changes suggested.
Now, the manuscript appears more clear.

Research Data Related to this Submission

There are no linked research data sets for this submission. The following reason is given:
Data will be made available on request

Dear Editor of Gondwana Research,

Please find attached the manuscript: "*The 2.0-1.88 Ga Paleoproterozoic evolution of the southern Amazonian Craton (Brazil): an interpretation inferred by lithofaciological, geochemical and geochronological data.*" by Roverato M., Giordano D., Giovanardi T., Juliani C., and Polo L. which we would like to submit on Gondwana Research. This study documents in detail the extremely well preserved Paleoproterozoic architecture of a series of felsic volcanic and volcaniclastic rocks found in the southern part of the Amazonian Craton, Brazil. We aim to improve the current knowledge of the rare subaerial volcanism investigated in Precambrian volcanic regions by adding new textural data useful to better constrain this still poorly known volcanism. We provide also new geochemical and geochronological data that will increase the dataset of the study volcanic rocks. We use here a modern volcanological approach to describe the wide range of different lithofacies that our deposits display. We believe that this contribution will help to further our understanding of the geology of the Amazonian craton and, also, of other Precambrian volcanic areas worldwide.

We hope that the manuscript will be of interest for a first class international journal like GR.

Yours sincerely,

Dr. Matteo Roverato

Highlights

- The modern lithofaciological approach is used here to described the volcanic and volcaniclastic rocks of the Precambrian Amazonian Craton.
- The U-Pb geochronological data presented in the manuscript yielded three new ages of ca. 2.0 Ga and one new age of ca. 1.88 Ga that, linked with 31 geochemical analyses, increase the dataset available for the Amazonian craton and ancient terrains in general.
- The Paleoproterozoic volcanic activity that formed the large felsic rocks cropping out in the southern Amazonian craton is characterized by a fissure-fed and caldera volcanism with production of extensive lava flows and/or high-grade to rheomorphic ignimbrites, linked with other fragmental products of different type.

*Graphical Abstract

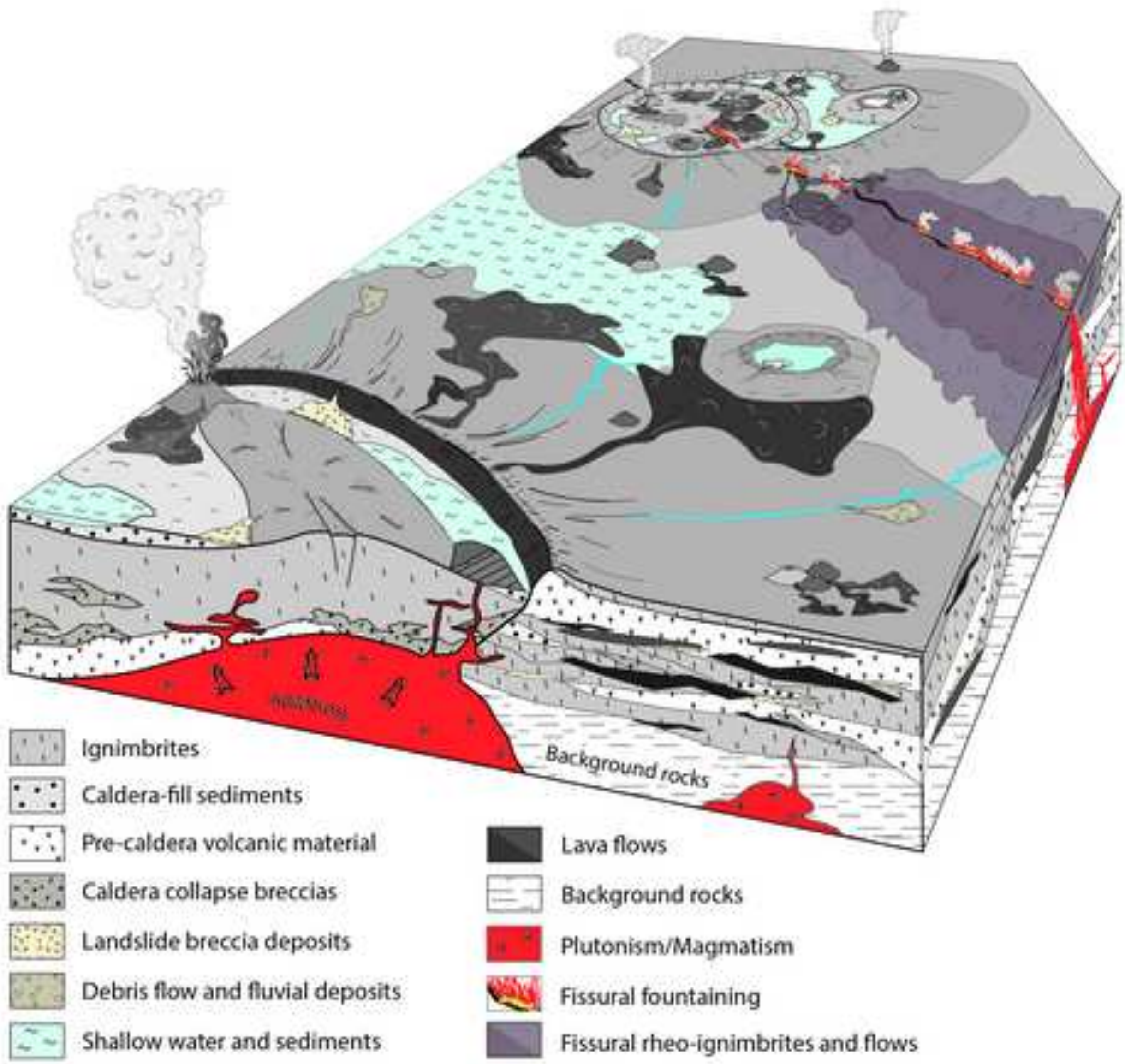

Reviewers' comments:

Reviewer #1: One of the main concerns of this manuscript is the lithofacies description and interpretation that oversimplifies the different lithofacies by only distinguishing them by their massive or stratified appearance. The observations and related interpretations seem to be of good value. However, I would suggest to make more subdivisions and adopt the terminology of McPhie et al. (1993) for non-genetic descriptive terms for each single lithofacies.
The manuscript contains too many different abbreviations for geological provinces, lithofacies types, etc. After a while, this appears rather confusing. Therefore, I would suggest to keep the abbreviations at a minimum, for instance for the lithofacies types and few other long terms that are constantly repeated throughout the text.
In the following paragraphs, some major suggestions are provided in detail. Further comments and suggestions (or questions) can be found in the attached commented manuscript.?

Author response:

Line 139:
Reviewer: What are the errors for the 2100 and 2875 Ma ages?
Line 148: What is the error for the 1880 Ma age?
Author: <u>The reviewer further on suggests to simplify this chapter. We deleted the paragraph as suggested.</u>

Lines 127-206:
Reviewer: A lot of information is presented here including many information on geochronology. Some of this information that is not particular of help for the understanding of the rest of the manuscript can probably be deleted or shortened. Furthermore, I suggest to show all mentioned locations on a map.
Author: <u>Done! As suggested by Reviewer 1 we reduced this part by keeping some of the literature information useful to put our study in a wider context.</u>

Rev: it would be good to see the detailed stratigraphy of the area: well we should wait for to more fieldwork.
Author: <u>That's the problem, very few data are available nowadays, and actually this is one of the first work that try to present more detailed stratigraphy. We should organize a fieldwork there together!</u>

line 226-229:
Rev: The way you describe the volcaniclastic rocks here, they are all fragmental rocks that are primary and syn-eruptive. However, effusive eruptions do not form fragments
Aut: <u>yes they do! One example is a basal breccia of a thick lava flow. You can find a very well developed clastic deposit underneath the flow. In any case we deleted the point to avoid confusion.</u>

Line 237:
Rev: Surely, no all volcanic products exhibit the same features. Otherwise, there would only be one lithofacies type. Please better describe what you mean.

Aut: Changed

Lines 239-243:
Rev: Not so many words are needed for this. Simply state that Table 1 shows all documented lithofacies including their descriptions and interpretations.
Aut: Done!

Lines 281-288
Rev: should be rephrased as they are difficult to read and understand. In particular, the paper of White and Houghton (2006) should be used here in order to define the terms pyroclastic and volcaniclastic. As it is, this part is not particularly clear. For once, effusive eruptions do not form volcaniclastic sediments. Furthermore, ignimbrites may also form due to PDCs.
Aut: Ok. We changed the sentence

Lines 297-486:
Rev.: There are some good observations and interpretations in here. However, the simplification into massive and stratified volcaniclastic rocks (containing everything from PDC deposits to autobreccias of a lava flow) and epiclastis rocks (containing everything from fluvial to mass-flow deposits) makes the chapter quite confusing. I suggest to make more subdivisions and describe the single lithofacies types one by one, probably adopting the non-genetic descriptive terms of McPhie et al. (1993). This way, the text may become slightly longer. However, the scientific value of the observations will significantly increase.
Aut.: Done! As the reviewer suggested, we divided the lithofacies descriptions and interpretations. Thank you for the suggestion!

Lines 785-789:
Rev: "Here we also image that an ideal late-convergent to extensional geotectonic environment was likely similar to that proposed in our discussion paragraph, where a post-orogenic to extensional regime for the period ~ 1.88 Ga was characterized by the emission of large volcanic felsic products." This sentence sounds very confusing and should be rephrased. For instance:
"The described volcano-sedimentary sequences that were characterized by the emission of large volcanic felsic products were formed in a post-orogenic to extensional regime during ~ 1.88 Ga."
Aut: Done! We changed the sentence!

Lines 789-791:
Rev:"With this contribution we want also stress the importance of the results obtained by investigating the lithofaciological character of the deposits instead of only carrying out geochemical studies." This should rather be obvious and can be omitted.
Aut: Done! We deleted the sentence

Reviewer #2: I appreciated your manuscript, in particular, the careful and detailed field and petrographic descriptions of lava flows and volcaniclastic sequences. Your data confirm the existence of, at least, two major Paleoproterozoic periods of formation of volcanic rocks in the Amazonian craton and this point is of great relevance for understanding the craton evolution. Your model to explain the origin of volcanic sequences is also a significant contribution. I made a series of comments and suggestions that I hope will help you to improve your manuscript. Most of them are not mandatory and should be evaluated for you. I have attached a pdf version indicating the main criticisms and indicating possible formal corrections.

Best regards,

Roberto Dall'Agnol

Author response:

1 - Abstract, p. 5, l. 41-45 - Please, rewrite. It is not clear.
Done

2 - Introduction, p. 5, l. 54-55 - I suggest to delete.
Done

3 - p. 5, l. 58-59 - References?
Done

4 - p. 5, l. 62 - the crust is...or the rocks are...???
Done

5 - p. 5, l. 63-67 - You are talking about the entire Amazonian craton but your references refer only to the regions of your direct interest. It is not reasonable to talk about mineral resources in the craton without any mention to the world-class mines of Carajás (iron, IOCG). I suggest to include also references of that province or to make clear that you are talking essentially about the Tapajós and Xingu regions.
Done

6 - p. 6, l. 71-74 - All this is the normal view of the Amazonian craton and it is correct in some degree. But I wonder if your contribution should not be directed to show that, in spite of the dominant conditions in the region, there are many areas where field information can be obtained and fresh rocks are available. This makes possible the petrological, geochemical and metallogenetic research on the craton that preserves better than one could imagine the signature of Precambrian events. You could illustrate this comment with the comproved occurrence in the Tapajós province of Paleoproterozoic allunite (Juliani et al., 2005). In other words, better than reinforce the general view, you should show that many things are possible in the geological studies of the craton.
We deleted the sentence

7 - p. 6, l. 84-89 - This is remark is very important but it looks contradictory with you have said before (cf. my remark 6) about the geological research in Amazonia. Please, make consistent changing the previous generic and not representative description of Amazonian conditions.
Done!

8. p. 66, l. 89-90 - This statement was entirely true in the pioneer works of the research group but now it looks not very appropriate to say that they 'are novel in this area'. You have said before that the present work is a continuity of previous research developed by the group in the last 15 years.

Changed it!

9 - p. 6, l. 99-101 - This description of the Amazonian craton evolution is oversimplified and do not give a clear idea of the more recent tectonic models proposed to explain it. You should present it more critically. E.g., the existence of a large Archean platform is not entirely demonstrated. You are mentioning the models of tectonic-geochronologic provinces and the existence of domains formed after the Trans-Amazonian event in the following. These topics should be better integrated and more consistent.

10 - p. 7, l. 104-107 - The relevance of the Uatumã Group in the Paleoproterozoic evolution of the craton is clearly demonstrated but it cannot be said that "All volcano/plutonic rocks forming the craton are attributed to the Uatumã Supergroup". There are many magmatic units, including Paleoproterozoic ones, that have nothing to do with the Uatumã Supergroup. You should clarify these points, showing the relevance of the Uatumã event but with a more rigorous description of it.

11 - p. 7, l. 108-110 - Your statement is not helping to show the real stage of knowledge of the Amazonian craton. I would say that we have now a general picture of the craton evolution and there are some portions of it relatively well studied, side by side with poorly known areas.

These last 3 points (9,10,11) are related to the geological framework chapter. We changed the chapter in accordance with the correct suggestions of reviewer 2 and, also the points commented by reviewer 1 who suggests to simplify the information. As suggested by Reviewer 2 we also changed figure 1 so to provide the wider context of application of our research

12 - p. 7, l. 116-119 - Is this context of ocean-continent subduction and flat subduction consistent with the hypothesis of "The transition from late-convergent to extensional tectonic setting could register the beginning of the taphrogenesis that marked the Amazonian Craton throughout the Mesoproterozoic (your abstract)"?
Yes, because the volcanic rocks studied (specially the andesitic rocks well described in Fernandes et al., 2011 and Roverato et al., 2017, but also the felsic older rocks in TMP) are related to a continental arc tectonic environment. The idea is that the system passes from an ocean-continent flat-subduction setting to a post-orogenic /extensional tectonism (as proved by the presence of younger felsic A-type rocks in SFX)

13 - p. 8, l. 148 - Some authors employ the term 'aluminous' for some A-type granites that vary generally from metaluminous to mildly peraluminous (e.g., King et al., 1997; Lamarão et al., 2002). However, this is a not rigorous term because these A-type granites are typically low Al_2O_3 granites (Dall'Agnol and Oliveira, 2007, Lithos). King et al. (Australian Journal of Earth Sciences, 2001, 48, p.501) have abandoned and advised against the use of this term because 'aluminous' can be related to S-type peraluminous granites that are entirely distinct of the A-type granites. For this reason, I suggest to the authors to avoid the use of the term 'aluminous' for A-type granites.
This is the only point where we used this term. In any case due to changes, we deleted the entire paragraph

14 - p. 8, l. 151 - Please, verify the error of 1870 +- 0.008 Ma.
It is correct in Juliani et al., 2005

15 - p. 8, l. 158 and 160 - alkaline is ambiguous in this context because it can be confused with peralkaline. I suggest to delete alkaline.
Done

16 - p. 9, l. 172, Fig. 1 and 2 - The presentation of the figures is very poor and should be improved. In figure 1, only the Brazilian part of the Amazonian craton is represented and the reference of the model of geochronologic provinces adopted is not informed in the caption of the figure. The Rio Negro province is not correctly represented.
The schematic geologic maps of Figure 2 do not follow the classical conventions. The colors adopted for different geologic units are inappropriate. I suggest to revise entirely figures 1 and 2.
Improved fig 1 and 2. **In figure 2 we added the location of the outcrops and rocks presented in the paper. I don t agree that about the geological unit, I'm using my symbols well expressed in the legend.**

17 - p. 9, l. 178-181 - It would be more appropriate to say that the basement of the volcano-plutonic complex is not exposed. It could be similar to the Mesoarchean units of the Carajás province, as suggested by Nd TDM ages obtained by Teixeira et al. (2002) in andesites and rhyolites of Xingu area. It was published recently a synthesis of new geochronological data about the 1.88 Ga granites of the Carajás province (Teixeira et al., 2018, J South American Earth Sci). The authors have also presented a discussion about the relevance of the 1.88 Ga event in the craton and elsewhere.
We deleted the paragraph.

19 - p. 10, l. 217-220 - Independent of the degree of alteration and lithification, pyroclastic and volcaniclastic sequences need to be defined in the field, because they mix igneous and sedimentary features. Hence, I suggest you to emphasize the relevance of field observations in your work better than to put in relief the restrictions you had. Another point is that 'alteration' should be possibly mean hydrothermal alteration and it should be distinguished of weathering alteration because readers can suppose that your rocks were intensely weathered and you are clearly showing that you were able to collect fresh samples for petrographic, geochemical and geochronologic studies.
We deleted the paragraph as also suggested by the other reviewer.

20 - p. 10, l. 230 - Coastal? Is it accurate?
YES

22 - p. 11, l. 250, Fig. 3 and its caption - It should be given a general idea of the location and informed the point of sampling where the photographs were taken and the units presented in each case. This should be done also in the captions of figures 4 and 5.
Done and thank you for the suggestion

24 - p. 11, l. 264 - 265 - pervasive does not give an idea of abundance. 10 vol % to how much in vol %?
Done!

25 - p. 13, l. 312, Fig. 5B - There is an euhedral crystal in the central lower part of Figure 5B that is named plg (plagioclase). I suspect that it can be a crystal of alkali-feldspar. Please, verify.
Sure! **Changed it!**

26 - p. 13, l. 326 -330, Fig. 6 - It is important to indicate the location of that sequence in the geological map of Figure 2.

Done

27 - Fig. 8, 9, 10, 11 - You present an extremely valious register of field and macroscopic aspects of the studied volcanic sequences. It looks very important to me that the location of the documented points should be given. These points will be a relevant reference for future studies.
Done

28 - p. 18, l. 491, Fig. 12 and its caption - In the caption of the figure are mentioned the TAS, AFM and SiO2-K2O digrams. However, in the available version of your manuscript the Figure 12 is identical to Figure 13 and the diagrams mentioned in Figure 12 are not presented. Without the figures it is difficult to evaluate the consistence of your text.
Done

29 - p. 18, l. 489 Geochemistry, Table 2 - You should give information about the methods employed and the laboratory where the chemical analyses were done.
we have added a small 'Analytical Methods' chapter to the text.

30 - Chemical Analyzes, Table 2 - It should be included on Table 2 the classification and the volcanic facies of the analyzed rock. It is important to distinguish, if possible, the rocks with I-type and A-type affinity. The meaning of V, I and R should be explained in the foot of the table.
the meaning of VC, I and R is already in the figure caption. We have reformulated the text to make it more clear. We have also added the classification of I- and A-type affinity

31 - p. 19. l. 524 - 529, Fig. 14 - The distribution of the studied rocks in the Pearce's diagram of 1984 suggest in fact that they can be related to a post-collisional setting (cf. Pearce, 1996, Episodes).
we have added the diagram to Fig. 14 and add it to the chapter.

32 - p. 20-23, l. 571-659; 7. Discussion
7.1 Subduction-related to extensional setting - In general, this topic of discussion section is well organized and looks consistent to me. I have some remarks that hope can help you in the review.
- p. 20, l. 573-576, Fig. 14 - As mentioned before, if you consider Pearce (1996), the distribution of the whole of your samples suggest a post-collisional setting for the studied rocks.
we have taken it into account and added some paragraphs at the discussion.

p. 20, l. 576-577, Fig 14, diagram FeOt/MgO vs. Zr+Nb+Ce+Y - The analyzed rocks plot mostly to the right of the fields of typical I and S granites because they are enriched in HFSE compared to these granites. It is not correct to say that your rocks have low HFSE. On the contrary, the relatively high HFSE contents distinguish your rocks of typical I and S granites and approach them of A-type rocks.
We agree. The sentence was not clear; we want to point out that TMP volcanics have enrichment in incompatible elements with respect HSFE which suggest the occurrence of crustal component in the melt. We have rephrased the sentence to make it more clear and pointing that our samples have also high HSFE content which shift the volcanics composition from the I- and S-type granites to the A-type field.

It is also relevant to mention that your ~2.0 Ga volcanic rocks are a little distinct in this respect of the Vila Riozinho formation rocks (Lamarão et al., 2002) that show a little lower HFSE contents when compared to your TMP samples. Besides, the hypothesis of a more evolved character for your rocks compared to VR of Lamarão et al. (2002), you should consider the possibility that the 2.0 Ga volcanism is not uniform in composition and avocate for TMP rocks an intermediate geochemical character between the VR and MA. The rocks of TMP analyzed (Fig. 2) are dispersed in a large area and not restricted to the VR type area. So, is it is reasonable that some geochemical variations could occur.

notwithstanding we think that the TMP derived from more evolved melts with respect to the VR, as observed by higher Si, K, trace elements and evidences of fractional crystallization in the TMP melts, we agree that these features could be possibly related to 'heterogeneiteis' in the magmatism. We have added a paragraph to point out this possibility,

- p. 22, l. 631-639 - The 2.0-1.88 Ga event in the craton and also in the scale of the planet, as indicated by Antonio et al. (2018), has effectively great relevance. A similar discussion about the 1.88 Ga anorogenic granites of the Carajás province was recentely presented (Teixeira et al., 2018; SAMES) and it can allow you to go deep in this point of the discussion.

we appreciate the indication and we have provided to discuss a little further the geodynamic setting of the TMP and SFX magmatism.

*Revised manuscript with changes marked
Click here to view linked References

The 2.0-1.88 Ga Paleoproterozoic evolution of the southern Amazonian Craton (Brazil): an interpretation inferred by lithofaciological, geochemical and geochronological data.

Roverato*[1,2] M., Giordano[3,4] D., Giovanardi[5] T., Juliani[2] C., Polo[2] L.

1. YachayTech University, School of Geological Sciences and Engeneering, Hacienda San José, Urcuquí, Ecuador.
2. Departamento de Geologia Sedimentar e Ambiental (GSA), Instituto de Geociências (IGC), Universidade de São Paulo, INCT – Geociam, SP, 05508080, Brazil.
3. Universitá degli studi di Torino, Dipartimento di Scienze della Terra, via Valperga Caluso 35, 10125, Torino, Italy.
4. Centro Nazionale delle Ricerche (CNR), Istituto di Geoscienze e Georisorse (IGG), via G. Moruzzi 1, 56124, Pisa, Italy.
5. Universitá di Modena e Reggio Emilia, Dipartimento di Scienze Chimiche e Geologiche, 41125, Modena, via Campi 103, Italy.

*Corrisponding Author: matteomroverato1809@yachaytech.edu.ecgmail.com

Formatted: Default Paragraph Font, Font: 12 pt

Keywords: Paleoproterozoic volcanism; Amazonian craton; Fissure eruption; Felsic volcanism; Lithofacies analyses

Abstract

The study of Paleoproterozoic rocks is crucial for understanding Earth's tectonic evolution during the time when most of the modern crust and ore deposits were formedPaleoproterozoic rocks represent some of the most interesting rocks to comprehend Earth's tectonic evolution during the Precambrian Supereon when most of modern crust and ore deposits formation occurred. The rocks of the Brazilian Amazonian Craton record one of the most-complete and best-preserved Paleoproterozoic magmatic episodes on Earth. Amazonian rocks record one amongst the most complete and best-preserved Paleoproterozoic magmatic episodes on Earth. Following previous investigations, we present new lithofaciological and stratigraphic records of the felsic rocks of the Tapajos Mineral Province (TMP) (~ 2-1.88 Ga) and the São Felix do

Formatted: Font: Times New Roman, No underline, Not Highligh

Formatted: Font: Times New Roman, No underline, Not Highligh

Formatted: Font: Times New Roman, No underline

Xingu region (SFX) (~ 1.88 Ga) which, combined with new petrological and geochronological data, help providing a more complete understanding of the tectonic, magmatic and volcanological evolution of the Amazonian Craton. This magmatism/volcanism is thought to be formed in a late-/post-~~-~~orogenic to extentional regime confirmed by the new geochemical data presented here. The transition from late-convergent to extensional tectonic setting could register the beginning of the taphrogenesis that marked the Amazonian Craton throughout the Mesoproterozoic. The modern volcanological approach of this contribution can serve as a model for the evolution of Precambrian volcano-sedimentary basins around the world. The large amount of rocks analyzed are divided into primary and secondary volcaniclastic ~~volcaniclastic and sedimentary~~ products depending on if they resulted from a direct volcanic activity (pyroclastic) or reworked processes that reworked pyroclastic fragments. In this second group are also included the epiclastic rocks constituted by all sediments that had been reworked before, independent of their source and composition. Furthermore, ~~,~~the deposits are divided in~~and~~ massive and~~to~~ stratified, depending on their different transport and emplacement mechanisms. By confirming the results from previous studies, our study permits to depict a more precise paleo-environmental picture of the processes that occurred in the Amazonian Craton during the Late-Paleoproterozoic. In particular, the presence of large regional-scale fissural systems with caldera collapses produced large silicic explosive volcanic eruptions, which were also accompanied by the emission of large volume effusive products. Although studies on the Amazonian Craton are still scarce and controversial, the present study provides new evidence that this volcanism may have formed one of the largest Silicic Large Igneous Provinces (SLIP) on earth.

1. Introduction

The Proterozoic Eon (2500 – 541 Ma) is the longest and youngest part of the Precambrian Supereon. This E~~e~~on represents the time just before the proliferation of oxygen accumulation and complex life on Earth. This period was likely the most tectonically active in Earth's history. In fact, it is also the period during which the largest portion of the modern crust (43%) and mineral ores were produced (Condie, 2000). Studies by Condie (2000) and Rino et al. (2004) suggest that crust production took place episodically, forming predominantly granitoidal crust and secondary volcanic and metamorphic rocks, some of which are extraordinarily well preserved.

Formatted: Font: Times New Roman, 12 pt, No underline

Formatted: Font: Times New Roman, 12 pt, No underline

Formatted: Indent: First line: 0 cm

The Amazonian Craton (AC) is one of the largest Precambrian terrains in the world ($4.6x10^{6}$ km^{2}) (Almeida et al., 1981). It occupies approximately half of the Brazilian territory and it is the location of important mineral resources such as gold, iron, copper, and tin, among others (Faraco et al., 1997; Bahia and Quadros, 2000; Juliani, 2002; Klein et al., 2002, ; Klein et al., 2004; Reis et al., 2006; Klien and Carvalho, 2008; Monteiro et al., 2008; Juliani et al., 2014, Dall'Agnol et al., 2017). Although the geological investigation of the AC has recently seen a renewed interest of the national and international scientific community, mainly because of the massive presence of ore deposits, a general consensus related to the interpretation of its complex -Paleoproterozoic evolution is still missing. Ancient volcanic regions represent a challenge for the understanding of emplacement dynamics especially when the stratigraphic relationships are difficult to decipher or blurred by erosion or vegetation cover.,

In fact, the difficult access to the outcrops, due to dense forest cover and to the presence of extensive water basins together with, in most cases, the bad preservation of the ancient outcrops with frequently obliterated structures and textures, significantly complicate this task.

The present work constitutes the natural prosecution of previous investigations, carried out by our research group (Juliani et al., 2005, ; Juliani et al., 2010, 2014;; Fernandes et al., 2011; Juliani et al., 2014; da Cruz et al., 2015; Roverato, 2016; , 2015; Roverato et al., 2016; Roverato, 2016; Roverato et al., 2016, 2017), which are devoted to characterize the dynamics of emplacement of Precambrian volcanic rocks and their relationships to sedimentary facies. The study area comprises of the Tapajóos Mineral Province (TMP) and the São Felix do Xingúu (SFX) region, Pará state, northern Brazil. This contribution provides a means to interpret the volcanic processes active in this region during the Precambrian, mainly based on field observation and detailed lithofacies analyses. In addition, -new geochemical and geochronological data are provided. The superb preservation of the rock-textures investigated here is such that they help us to better constrain the genetic mechanisms that brought to the formation of the investigated felsic deposits. -Our study demonstrates how powerful is the approach of rock structure and texture characterization to the interpretation of the eruptive processes that governed the emplacement of volcanic and volcaniclastic sequences. The detailed lithofacies characterization and the stratigraphic reconstruction are novel important in this area and constitute a powerfulnew key-tool to appropriately interpret

Formatted: No underline, Superscript

Formatted: No underline, Superscript

Formatted: Indent: First line: 0 cm

Formatted: No underline, Font color: Auto, Highlight the evolution of Precambrian volcano-sedimentary basins. Such an approach would turn to be useful when employed to investigate ancient terrains associated both to the ancient Amazonian felsic volcanism and Precambrian terrains in general.

2. Geological evolution of the southern portion of the Amazonian craton

The AC (Almeida et al., 1981) is located in the northern part of South America and is divided into two Precambrian shields, the Central-Brazil (or Guaporé, southern portion) and Guiana Shields (northern portion), which are separated by the Phanerozoic Amazonian Sedimentary Basin (Fig. 1) (Almeida et al., 1981). The entire craton has become stable before the end of the Precambrian (Dall'Agnol et al., 1994).

The AC (Almeida et al., 1981) has been considered (Amaral, 1974; Hasui et al., 1993; Costa and Hasui, 1997) asis a large Archean platform that had been reworked and reactivated during the ca. 2100 Ma Trans-Amazonian event (Amaral, 1974; Hasui et al., 1993; Costa and Hasui, 1997). The AC is located in the northern part of South America and is divided into two Precambrian shields, the Central-Brazil (or Guaporé) and Guiana Shields, which are separated by the Fanerozoic Amazonian Sedimentary Basin (Fig. 1) (Tassinari and Macambira, 1999; Santos et al., 2000). All igneous rocks forming the craton are attributed to the Uatumã Supergroup, which extends to an area of at least 1,500,000 km^2 (Dall'Agnol et al., 1999; Lamarão et al., 1999).

Alternative ideas Although several approaches have been used to unravel the complex tectonic evolution of these huge and frequently inaccessible territories, a clear understanding of the geological past of this area is still largely unknown. bBased on geochronological and isotopic data, Teixeira et al. (1989), (Teixeira et al., 1989; Tassinari and Macambira, (1999;), and Santos et al., (2000) divided the craton into several, predominantly NW-oriented geochronological provinces, which have been interpreted as successive continental accretionary events, followed by granitic magmatism and tectonic reworking (. Tassinari and Macambira (1999), Santos, (2003); and Vasquez et al., (2008) identified six and eight geochronological provinces, respectively (Fig. 1).

In a recent review Teixeira et at. (2019) report that the AC is the host of four LIP-scale (or SLIP) magmatic events discriminated by the Orocaima, Uatumã, Avanavero and Rincón del Tigre events, among other intra-plate activity through time and space. The igneous rocks described in the present manuscript are widely attributed to the Uatumã event (Dall'Agnol et al., 1999; Lamarão et al., 1999). More recently,

Formatted: Indent: First line: 0 cm

Formatted: Adjust space between Latin and Asian text, Adjust space between Asian text and numbers

Formatted: No underline, Not Highlight

The studied ~~Juliani and Fernandes (2010), Fernandes et al. (2011) and Roverato et al. (2017) suggested that the entire~~ region is located between TMP and SFX, which ~~may be~~is considered to be related to a continental arc, with a NE-SW arc migration as suggested by Juliani and Fernandes (2010), Fernandes et al. (2011) and Roverato et al. (2017). According to these authors a migration from the Serra do Cachimbo graben (in TMP where the subduction trench is located) towards the SFX could be explained by a change in the subducting angle of the oceanic plate beneath the continental plate. This is in agreement with the flat-subduction plate settings proposed by previous authors in other parts of the world (Ferrari et al., 2012; Gutscher et al., 2000; Kay et al., 2005; Mori et al., 2007; Manea et al., 2012~~; Fernandes et al., 2011; Juliani et al., 2014~~).

2.1. The TMP (Tapajós Mineral Province)

Formatted: Indent: First line: 0 cm

The TMP (F~~f~~ig. 2a) is primarily situated in the Tapajós–Parima geochronological/tectonic province (Santos et al., 2000) with the eastern part belonging to the Amazonia Central geochronological/tectonic province (Fig. 1). Based on Sm–Nd data and U–Pb ages (2100–1870 Ma), Santos et al. (2001, 2004) and Vasquez et al. (2008), identified several different domains for the Tapajós–Parima geochronological province and consider the TMP as a sequence of continental magmatic arcs (Ferreira et al., 2000; Santos et al., 2000, 2004; Vasquez et al., 2000; Klein et al., 2001; Lamarão et al., 1999, 2002). ~~The oldest granitoids and gneisses in this region belong to the Cuiú-Cuiú magmatic arc complex; the Conceição tonalite (Cuiú-Cuiú magmatism) yielded a U-Pb zircon age of 2019 ± 23 Ma (Santos et al., 2000). The supracrustal sequences of the Jacareacanga Group are considered broadly coeval with the Cuiú-Cuiú complex. Both units are related to early stages of magmatic arc development (Ferreira et al., 2000; Klein et al., 2001). Detrital zircon ages of ca. 2100 and ca. 2875 Ma have been obtained for the Jacareacanga Group (Santos et al., 2000). Stratigraphically above the Jacareacanga Group is the Vila Riozinho Formation, formed by ca. 2000-1990 Ma intermediate to felsic volcanic rocks (Lamarão et al., 2002). These units are intruded by the ca. 2000-1970 Ma syn- to late-orogenic calc-alkaline granitoids of the Creporizão suite (Lamarão et al., 1999; Vasquez et al., 2000). Following this first intrusive event, a second intrusive event was characterized by the 1907 ±9 and 1892 ±6 Ma granitoid rocks of the Tropas Suite (Santos et al. 2001, 2004). The ca. 1880 Ma Parauari suite corresponds to a younger generation of post-orogenic, calc-alkaline granitoids and is mainly exposed in the northeastern part of the~~

Formatted: Indent: First line: 1.27 cm

~~region. The Maloquinha ca. 1880 Ma aluminous A-type granite plutons are also found in the province and closes the sequence.~~ Late Paleoproterozoic volcanism of the Tapajós domain is represented~~-~~ by the Vila Riozinho Formation, formed by ca. 2000-1990 Ma intermediate to acid volcanic rocks (Lamarão et al., 2002), and by the Iriri Group that can be divided into the Bom Jardim (Almeida et al., 2000), Salustiano (1870 ± 0.008 Ma; Juliani et al., 2005) and Aruri (Pessoa et al., 1977) formations.

~~-~~The Bom Jardim Formation (1898 ± 5 Ma, Santos et al., 2001) consists of mafic to intermediate high-K to shoshonitic calc-alkaline rocks while the latter formations are characterized by rhyolites, dacites and their pyroclastic and epiclastic derivatives. Juliani et al. (2005) considered the Bom Jardim volcanism as a preliminary step of the Iriri event representing pre-caldera volcanism followed by the Salustiano and Aruri caldera-related felsic activity. Post-caldera volcanism is characterized by ring-felsic volcanic structures that produced ~~alkaline~~ A-type (Vasquez and Dreher, 2011) rhyolitic lavas and volcaniclastic deposits. Lamarão et al. (2002, 2005) described the ~~alkaline~~ felsic A-type Moraes Almeida volcanic sequence (1890 ± 6 Ma ryolite, 1875 ± 4 Ma ignimbite) represented by lavas and ignimbrites as part of the Iriri Group. Juliani et al. (2014) consider these last A-type ~~alkaline~~ rocks as similar in composition and age to the Santa Rosa Formation that crops out in the São Felix do Xingú region (SFX), which is considered to have formed by the same fissural-type volcanism (Juliani and Fernandes, 2010; Fernandes et al., 2011; Roverato et al., 2016). Preliminary data indicate that these rocks, for both ~~-~~TMP and SFX, display a very low grade of metamorphism, falling into the prehnite-pumpellyite field (Echeverri-Misas, 2010; Lagler et al., 2011; Fernandes et al., 2011).

2.2. The SFX (São Felix do Xingú region)

Formatted: Indent: First line: 0 cm

According to the work of Santos (2003) and Vasques et al. (2008) the SFX region belongs to the Amazonia Central province (F~~f~~ig. 1). The study area (Fig. 2b) is located near to São Felix do Xingú~~u~~ c~~C~~ity, which corresponds to the southern portion of the Carajás Province. ~~The geographical limits of SFX are still uncertain, mainly due to the difficult access to the area. The eastern limit is marked by the Archean TTG rocks several km east to Xingu River while the dense vegetation-cover does not permit access to the south. The northern limit is roughly marked by the Archean Xingu complex and younger intrusive formations (Macambira and Vale, 1997). The basement of the SFX region is represented by the Archean Rio Maria Granite–Greenstone~~

~~Terrain and the metavolcano-sedimentary units of the Itacaiúnas Supergroup (Araújo et al., 1988).~~ The Paleoproterozoic volcanic sequences in the SFX comprise the basal Sobreiro and upper Santa Rosa formations (Macambira and Vale, 1997; Juliani and Fernades, 2010), which are crosscut by the Sn-bearing A-type granitoids of the Velho Guilherme Suite (Teixeira et al., 2002). Antonio et al. (2017) published the first U-Pb ages on zircons for the Santa Rosa Formation with 1877.4 ± 4.3 Ma for a rhyolite and 1895 ± 11 Ma for a dike. Recent geochronological data on a felsic porph~~fyi~~ritic dike belonging to the Velho Guilherme suite yielded an age of 1857 ± 8.4 Ma (Shrimp U/Pb zircon analyses; Roverato, 2016). Other available geochronological data yielded ca. 1880 ± 6 Ma (TIMS Pb–Pb in zircon) for the Sobreiro Formation and ca. 1879 ±2 Ma (TIMS Pb–Pb in zircon) for the Santa Rosa Formation (Fernandes et al., 2011; Pinho et al., 2006; Teixeira et al., 2002). Despite their similar ages, their geochemical compositions, geological features and eruption styles point to their non-cogeneticity (Fernandes et al., 2011). ~~The Sobreiro Formation was defined for the first time by Macambira (1997) and Macambira and Vale (1997) as constituted by andesitic, trachy-andesitic and trachytic magmatism.~~ The Sobreiro Formation (SF) comprises basaltic andesite, andesite and less dacite massive lava flows and volcanoclastic rocks with high-K calk-alkaline signature (Fernandes et al., 2011; Roverato et al., 2017). According to da Cruz et al. (2015) late- to post-magmatic hydrothermal alteration in these rocks is responsible for a secondary paragenesis characterized by epidote, chlorite, carbonate, clinozoisite, sericite, quartz, albite, hematite and pyrite. The Santa Rosa Formation (SRF) is described by Fernandes et al. (2011) as characterized by four lithological facies with A-type signature: (i) rhyolitic lava flow and thick dikes of banded rhyolite and ignimbrite; (ii) highly rheomorphic felsic ignimbrite associated with un-welded ash tuff; (iii) felsic crystal tuff, lapilli-tuff and co-ignimbritic breccias; (iv) granitic porphyry stocks and dikes and subordinate equigranular granitic intrusions.

~~3. Results~~

~~Lithofaciological, petrological, geochemical and geochronological analyses were carried out in the course of this study in order to understand the geodynamic evolution of the study area. 31 new geochemical data for the TMP rock samples are presented here and compared with published data of Lamarão et al. (2002) and SFX previous results (Fernandes et al. (2011). The geochemical signature of SFX rock samples have~~

Formatted: Indent: First line: 0 cm

~~already recently been reported by Fernandes et al. (2011) who made unnecessary new analysis for our study. Four new geochronological data of rock samples from the TMP (3 samples) and SFX (1 sample) are also provided to compare with dating available for the AC. Finally, so far it concerns with the lithofaciological analysis we remind that a characterization of the granulometry of the deposits and of the shape of the fragments was qualitatively defined in the field, since the degree of alteration and lithification would have been impossible in the laboratory.~~

3~~4~~. Lithofacies analyses ~~and stratigraphy~~

Formatted: Indent: First line: 0 cm

Lithofaciological analyses were carried out in the course of this study in order to understand the geodynamic evolution of the study area. Here we report on~~f~~ the lithofacies analysis of rocks recognized during our field campaigns (and after in petrological thin section) at the TMP and SFX provinces. Within the study area (TMP and SFX), massive to banded lava flows and rheomorphic ignimbrites (Fig. 3) as well as felsic volcaniclastic rocks of various origin (Figs. 4-8, 11) are frequently found. ~~Massive and banded lava flows and rheomorphic ignimbrites deposits (fig. 3) as well as volcaniclastic felsic rocks of various origin (e.g. pumiceous, effusive, ignimbritic) (fig. 4,5,6,7,8,11) are frequently found in both the studied areas (TMP and SFX).~~ Reworked (secondary) volcaniclastic rocks (F~~f~~ig. 9,10) and sedimentary alluvial/coastal clastic deposits (epiclastic) are also widely distributed in both TMP and SFX areas. Primary v~~V~~olcaniclastic rocks are here defined as those fragmental products formed during a syn-eruptive explosion~~ve or effusive events~~, which were deposited regardless of whether their transport occurs through air, water, granular debris or a combination of them (McPhie et al., 1993; White and Houghton, 2006, Manville et al., 2009; Roverato et al., 2017). On the other hand, all the units deposited as a consequence of a reworking process of pre-existing volcanic units are defined here as ~~sedimentary/reworked~~secondary volcaniclastic rocks. We also introduce into this group all those epiclatic products that constitute sediments that had been reworked before, independent of their source and composition~~All TMP and SFX volcanic products share the same features both at outcrop scale and at hand specimen scale and for such a reason they will be presented together in the lithofaciological description~~. ~~In~~ T~~t~~able 1 ~~we propose~~shows a description and interpretation of the volcaniclastic

Formatted: Font: Times New Roman, 12 pt, No underline lithofacies, both primary ~~(volcaniclastic)~~ and ~~- reworked (~~secondary~~sedimentary)~~, for the deposits identified in the study areas~~. In the following we will also provide an interpretation of the processes involved in their transport and emplacement~~.

~~4.1~~4. ~~.~~ Lava flows and rheo-ignimbrites

Formatted: Indent: First line: 0 cm

As already discussed by Roverato et al. (2016), the absence of unequivocal vitroclastic textures complicates the distinction between volcaniclastic and layered lava flows in general and, more in particular, for the ancient volcanic rocks investigated here. Lava flows found in the TMP and SFX provinces have both massive and banded structures (F~~f~~ig. 3) while still maintaining, in some cases, glassy (obsidian) and aphanitic to porfiritic texture. Their composition varies from trachytic to rhyolitic with various content of alkalies (see section ~~5~~8). The phenocryst assemblage consists mainly of plagioclase, quartz, Fe–Ti oxides and accessory-amount of zircon and apatite. Plagioclase and bipiramidal quartz crystals (F~~f~~ig. 3a), with a maximum size of 3-4 mm, range from euhedral to anhedral, showing moderate to intense resorption. Plagioclase shows sieve texture indicating non-equilibrium conditions likely determined by magmatic transport. ~~Potassic~~ K-feldspar is also present as anhedral crystals in the groundmass often associated with sericite as alteration phase. Samples are generally affected by variable intensity of hydrothermal alteration. Plagioclase phenocrysts, in particular, present diffuse potassic and minor propylictic alterations. Abundant spherulites and lithophysaes of variable size, from millimetric to decimetric, were recognized in almost every sample and are thus common in these rocks (F~~f~~ig. 3b, c). The spherulites (radiating fibers of K-feldspar and cristobalite), ranging from few millimeters to 2 cm, are typically associated with perlitic fractures. Their content can vary from 10 vol% to ~~pervasive~~ 70% in the investigated rocks. A large amount of the spherulites developed into lithophysae commonly reaching 10-12 cm as a consequence of cooling and degassing processes. In the obsidian-type lavas (F~~f~~ig. 3c), the groundmass is characterized by a micro-granophiric-like devitrification texture characterized by crystallization of amorphous quartz and alkali feldspar, a process that occurred after the emplacement of lava bodies. Several rocks show textures that are not easy to be associated to either lava flows or flows of fragmented material which underwent rheomorphism (F~~f~~ig. 3d-g). Both banded lavas and rheo-ignimbrites display folds (F~~f~~ig. 3d~~-/~~g, see also F~~f~~ig. 11e) and sub-parallel bands on mm- to dm-scale, planar to wavy (F~~f~~ig. 3e, see also F~~f~~ig. 6 and 7) (parataxitic fabric), that deform and flattened around lithic fragments and crystals which alignment suggests the flow direction. In thin sections, the bands are characterized by extremely flattened vitroclastic textures with the former glass completely replaced by a mixture of quartz and feldspar (Roverato et al., 2016).

5.~~4.2.~~ ~~V~~Primary vo~~o~~lcaniclastic rocks

We consider primary volcaniclastic rocks those dense, scoriaceous and pumiceous products of fragmental character emplaced by ~~primary low intensity~~ explosive processes~~, frequently associated to effusive manifestations or highly explosive events associated to fall out, small pyroclastic density currents (PDC) or ignimbrites~~. With pyroclastic we refer to fragmental material generated by any kind of explosive volcanic activity and transported as ash-fall and pyroclastic density currents ~~by an explosive volcanism~~ (Manville et al., 2009), which deposition occurs by suspension settling, from traction, by en masse freezing, or any combination of these (White and Houghton, 2006). Depending on the mechanism of transport and the eruptive style these clastic rocks were distinguished into two different categories, i.e. massive and stratified; and they can vary from well sorted, poorly sorted or unsorted. The rocks are predominantly rhyolitic in composition (Fernandes et al., 2011, Roverato et al., 2016) and there is no significant geochemical difference from the lava flows. Nine main lithofacies (Lf) have been recognized for the volcaniclastic rocks: six of them are massive and three are stratified.

5.1. ~~4.2.1.~~ Massive

Six massive lithofacies (mAL, mLA, mLB, *l*-*g*wLA, *m*-*g*wLA and *h*-*g*wLA) were recognized during our field campaign, three of them belong to the welded ignimbrites sub-group (Table 1). By using the granulometric classification proposed by Fisher (1961), ash is defined as any fragment with size <2 mm, lapilli are fragments with size between 2 to 64 mm and blocks (or bombs) have sizes > 64 mm. Massive lithofacies includes all those deposits that display a massive coherent structure. Outcrops of such kind of lithofacies are constituted by a high percentage of ash up to block-rich textures. Most of the observed samples appear to have been affected by devitrification processes of the juvenile pyroclastic fragments and matrix. The presence of juvenile material linked with other observed textures such as broken crystals (Best and Christiansen, 1997) and eutaxitic fabric allows us to confirm that the rocks

Formatted: Indent: First line: 0 cm

Formatted: Indent: First line: 0 cm

Formatted: Font: Not Italic, No underline

Formatted: Font: Not Italic

belonging to lithofacies mAL, mLA, *l-g*wLA, *m-g*wLA and *h-g*wLA are fragmental and pyroclastic in origin. We discuss the meaning of Lf mLB below in section 5.1.2.

Formatted: Indent: First line: 0 cm

5.1.1. Lf mAL; mLA (massive Ash to Lapilli; massive Lapilli *and* Ash)

Description: the ash to lapilli (mAL) and lapilli *and* ash (mLA) deposits (Fig. 4a-e, Fig.6) are heterolithologic, matrix supported, containing angular to sub-rounded medium to coarse devitrified lapilli (displaying axiolitic fabric), banded fragments, occasional (or absent) lithics and angular-shaped broken crystals of plagioclase, bipiramidal quartz and rare oxides (Fig. 5). In mLA, clasts <25 cm in size are randomly immersed in the groundmass (Fig 4d and 4e, 11d). Some of them are altered by carbonate minerals. Groundmass of mAL and mLA is formed by K-feldspar and quartz crystals, devitrified ash fragments and sericite crystals as phase of alteration (Fig. 5).

Interpretation: the general massive aspect and the poor sorting of mAL and mLA point to a laminar granular flow transport regime and the fine content suggests the deposition from a dilute fluid escape-dominated flow-boundary zone in which turbulent shear-induced tractional segregation is suppressed (Branney and Kokelaar, 2002; Sulpizio et al., 2007, Roverato et al., 2017). These lithofacies are interpreted as ash flow deposits suggesting the deposition from a pyroclastic density current (PDC) (Lenhardt et al., 2011; Sulpizio et al., 2014; Roverato et al., 2017). The coarser lithofacies mLA (fig. 4e) could be related to proximal co-ignimbritic breccias as result of deposition by denser pyroclastic granular flows (Branney and Kokelaar, 2002). The angular aspect of the clasts indicates short-period transport.

5.1.2. Lf mLB (massive Lapilli and Block)

Description: this lithofacies (fig. 4f, fig.7) represents monolithologic coarse-grained rocks having high-clast content (clast:matrix ratios up to 3:1). Angular/sub-angular coarse lapilli and blocks up to 50-60 cm of devitrified banded or massive lava fragments are immersed in a devitrified fine lapilli and coarse ash matrix.

Interpretation: the blocky and monolithologic coarse-grained aspect of the lithofacies mLB and its position underneath thick flow-deposits is attributed to the basal auto-brecciation of lava flows and/or rheo-ignimbrite flows. Despite the lithofacies is likely a consequence of an effusive volcanic activity (in the lava-flow case) it is considered anyway as part of the volcaniclastic group due to its fragmental character.

5.1.3. Lf *l-g*wLA; *m-g*wLA; *h-g*wLA (welded Ignimbrites)

Description: all massive deposits displaying welding characteristics have been grouped in the “welded ignimbrites” group (table 1), following the idea of “grade of welding” (Walker, 1983) (i.e. the amount of welding and compaction exhibited by deposits). The rocks are matrix-supported with sub-rounded to angular lapilli and ash lithic clasts, euhedral, subhedral and broken crystals (plagioclase and less quartz) and deformed devitrified juvenile fragments (*fiamme*). Slightly- (low-grade, *l-g*wLA), medium- (medium-grade, *m-g*wLA), well-stretched (high-grade, *h-g*wLA) *fiamme* (Fig. 6), as well as, devitrified shards define the eutaxitic fabric (Roverato et al., 2016). These fragments varying from millimetric to 3–4 cm in size are immersed in a homogeneous micro-granophiric-like devitrified groundmass (see Roverato et al., 2016 for details). Figure 6 shows a stratigraphic column representing a 35 m thick sequence of ignimbrite deposits found in the TMP, displaying very low-grade to high-grade welded fabric where the grade of welding increases toward the top of the succession. The very top of the sequence is characterized by columnar jointing.

Interpretation: the massive aspect and the poor sorting of the lithofacies *l-g*wLA, *m-g*wLA and *h-g*wLA point to a laminar granular flow transport regime, interpreted to be deposited from a pyroclastic density current (PDC). The welded character of these lithofacies is indicative of hot PDC emplacement and compaction that result into the low- up to high-grade eutaxitic fabric. This process is favored by loading-compaction, low-viscosity fragments, high temperature (i.e. > 900°C), cooling of gas-permeable fragments (pumices) and dissolved water (Branney and Kokelaar, 2002; Roverato et al., 2016 and references therein).

~~Six massive lithofacies were recognized during our field campaign, three of them belong to the ignimbrites sub-group (Table 1). By using the granulometric classification proposed by Fisher (1961), ash is defined as any fragment with size <2 mm, lapilli are fragments with size between 2 to 64 mm and blocks (or bombs) have sizes > 64 mm. Massive lithofacies includes all those deposits that display a massive coherent structure. Outcrops of such kind of lithofacies are constituted by a high percentage of ash up to block-rich textures.~~ The ash to lapilli (mAL) and lapilli *and* ash

Formatted: Indent: First line: 0 cm

Formatted: Font: Not Italic, No underline

Formatted: Font: Not Italic, No underline

Formatted: Font: Not Italic, Font color: Black

Formatted: Font color: Auto

Formatted: Font: Not Italic, Font color: Auto

Formatted: Indent: First line: 0 cm

(mLA) deposits (fig. 4a/b/c/d/e, fig.6) are heterolithologic, matrix supported, containing angular to sub-rounded medium to coarse devitrified lapilli (displaying axiolitic fabric), banded fragments, occasional (or absent) lithics and angular-shaped broken crystals of plagioclase, bipiramidal quartz and rare oxides (fig. 5). In mLA, clasts <25 cm in size are randomly immersed in the groundmass (Fig 4d/e, 11d). Some of them are altered by carbonate minerals. Groundmass of mAL and mLA is formed by K-feldspar and quartz crystals, devitrified ash fragments and sericite crystals as phase of alteration (Fig. 5). mLB (massive Lapilli *and* Block) facies (fig. 4f, fig.7) represent monolithologic coarse-grained rocks having high-clast content (clast:matrix ratios up to 3:1). Angular/sub-angular coarse lapilli and blocks up to 50-60 cm of devitrified banded or massive lava fragments are immersed in a devitrified fine lapilli and coarse ash matrix.

All massive deposits displaying welding characteristics have been grouped in the "ignimbrites" group (table 1), following the idea of "grade of welding" (Walker, 1983) (i.e. the amount of welding and compaction exhibited by deposits). The rocks are matrix-supported with sub-rounded to angular lithic clasts, euhedral, subhedral and broken crystals (plagioclase and less quartz) and deformed devitrified juvenile fragments (fiamme). Slightly- (low-grade, l-gwLA), medium- (medium-grade, m-gwLA), well-stretched (high-grade, h-gwLA) fiamme (Fig. 6), as well as, devitrified shards define the eutaxitic fabric (Roverato et al., 2016). These fragments varying from millimetric to 3–4 cm in size are immersed in a homogeneous micro-granophiric-like devitrified groundmass (see Roverato et al., 2016 for details). Figure 6 shows a stratigraphic column representing a 35 m thick sequence of ignimbrite deposits found in the TMP, displaying very low-grade to high-grade welded fabric where the grade of welding increases toward the top of the succession. The very top of the sequence is characterized by columnar jointing.

4.2.2. Interpretation

Most of the observed samples appear to have been affected by devitrification processes of the juvenile pyroclastic fragments and matrix. The presence of juvenile material linked with other observed textures such as broken crystals (Best and Christiansen, 1997) and eutaxitic fabric allows us to confirm that the rocks belonging to lithofacies mAL, mLA, l-gwLA, m-gwLA and h-gwLA are fragmental and

~~pyroclastic in origin. The general massive aspect and the poor sorting of mAL and mLA point to a laminar granular flow transport regime and the fine content suggests the deposition from a dilute fluid escape-dominated flow-boundary zone in which turbulent shear-induced tractional segregation is suppressed (Branney and Kokelaar, 2002; Sulpizio et al., 2007, Roverato et al., 2017). These lithofacies are interpreted as ash flow deposits suggesting the deposition from a pyroclastic density current (PDC) (Lenhardt et al., 2011; Sulpizio et al., 2014; Roverato et al., 2017). The coarser lithofacies mLA (fig. 4e) could be related to proximal co-ignimbritic breccias as result of deposition by denser pyroclastic granular flows (Branney and Kokelaar, 2002). The angular aspect of the clasts indicates short-period transport. The blocky aspect of the lithofacies mLB is attributed to the basal auto-brecciation of lava flows and/or rheo-ignimbrite flows. The welded character of the lithofacies l-gwLA, m-gwLA and h-gwLA is indicative of hot PDC emplacement and compaction that result into the low-up to high-grade eutaxitic fabric. This process is favored by loading-compaction, low-viscosity fragments, high temperature (i.e. > 900°C), cooling of gas-permeable fragments (pumices) and dissolved water (Branney and Kokelaar, 2002; Roverato et al., 2016 and references therein).~~

Formatted: Font color: Black

5.~~4.2.~~2~~3~~. Stratified

Formatted: Indent: First line: 0 cm

These lithofacies, although commonly associated with ignimbrites, are not very spread in the studied areas. We also didn't find any alternation between massive and stratified deposits even if this association is a common occurrence in PDC deposits (Sulpizio et al., 2014; Roverato et al., 2017), alternating dilute (stratified deposits resulting) and concentrated (massive deposits resulting) regimes during transport (Sulpizio et al., 2014). Just one example has been found in TMP and is reported in the stratigraphic reconstruction of fig.11.

5.2.1 Lf sA; xsA; dsAL (stratified Ash; cross-stratified Ash; diffusely stratified Ash to lapilli)

Formatted: Indent: First line: 0 cm

Description: t~~T~~he stratified samples and outcrops analyzed comprise well sorted very fine to fine ash organized in millimetric to sub-millimetric parallel (sA) or cross-stratified (xsA) layers, with sharp or gradational changes in grain size (Fig. 8). The fragments are represented by devitrified shards, crystals (plagioclase), and rare (or absent) lithics (fig. 8d) immersed in a devitrified groundmass. Diffuse-stratified lithofacies dsAL display a coarser character with coarse lithic and devitrified ash and lapilli fragments forming well developed parallel continuous meter-long stratification (or very-low angle cross-stratification) at centimeter scale (fig. 11b), with gradational changes in grain-size. The sorting varies from well to moderate.

~~4.2.4.~~ Interpretation:

t~~T~~he fine parallel layering of shards material displayed by lithofacies sA is interpreted here as being deposited under the product of sedimentation by the upper and highly dilute ash-cloud that accompany a pyroclastic-density current. We don't exclude the direct sedimentation from tephra fall-out activity. Cross-stratified (Lf xsA) and diffuse-stratified (Lf dsAL) deposits indicate tractive processes usually attribute to pyroclastic surge-type depositional condition from dilute currents (Cas and Wright 1987; Lenhardt et al., 2011; Roverato et al., 2017). We interpreted these as pyroclastic surge deposits although Lf dsAL could also be the product of coarse ash fall-out processes. Pyroclastic surge deposits usually display small volume and rarely reach more than 10 km from their source (Lenhardt et al., 2011). Conversely, fall-out deposits could emplace tens of kilometers from their source.

6. ~~4.3.~~ Secondary volcaniclastic/epiclastic~~Sedimentary~~ rocks

The nomenclature of Fisher et al. (1961) is applied also for the ~~sedimentary~~ secondary volcaniclastic rocks as follow: silt (2<>64µm), sand (64µm<>2 mm), gravel (2<>64 mm), cobble (64<>256mm). These rocks are considered as the product of reworking and erosive processes. The clasts belonging to this group show a wide range of composition, size and shape variations. Based on their component, texture and fabric, we recognized five massive, both matrix- and clast-supported, and four stratified lithofacies (fig. 9).

6~~4.3.1~~.1. Massive

6.1.1. Lf mS (massive Sand)

Description: this lithofacies consists of reddish moderately to well-sorted, massive, fine- to medium grained sand forming parallel strata intercalated to clast-supported conglomerate deposits (Lf csG) (fig. 9a). The sandstone strata extend tens of meters and present thinness between 0.4-0.8 m. Lf mS is predominantly composed of

> **Formatted:** Font: Not Italic, No underline, Font color: Auto
>
> **Formatted:** Font: Not Italic, No underline, Font color: Auto
>
> **Formatted:** Indent: First line: 0 cm
>
> **Formatted:** Font: Not Italic, No underline, Font color: Auto
>
> **Formatted:** Font: Not Italic

quartz, feldspar and minor rock fragments. Contacts between mS and csG are sharp with rare slightly erosional surfaces. The tops of the sandstone are characterized by the presence of centimeters ripples (fig. 9b).

Interpretation: the massive sand (mS) and the small ripples found at the top of the strata indicate low energy under tractional currents in shallow water conditions (Collison and Thompson, 1982; Lenhardt et al., 2011). The alternation of Lf csG and mS indicates changes in energy conditions of sedimentation. We interpret these oscillations as belonging to a subaqueous-subaerial fan-delta interface setting where continental supply of material alternates to under-water sand accumulation (Lf mS).

6.1.2. Lf csG (clast supported Gravel)

Description: this lithofacies~~The Lf csG~~ (Fig. 9a, c, d) is massive, clast to matrix supported, with heterolithologic felsic rounded high-spherical coarse gravel with a sandy inter-clast matrix. Clasts are mainly characterized by massive and banded medium- to coarse-size felsic lava fragments (and rare quartz; size does no~~n'~~t exceed 5 cm) and present rounded with low- to high-sphericity. We found lithofacies csG also associated to xsSG (see below section 6.2.2.) (F~~f~~ig. 9c, 10b).

Interpretation: lithofacies csG is dominated by water flow processes where matrix plays a secondary role. The clast-supported character and less matrix content indicates that water removed the finer particles during transport and deposition. Lf csG display rounded clasts and well-sorting indicative of good selection during transport and emplacement. The rounded character of csG and the presence of matrix in the deposits suggest a laminar debris-flow regime in medial reaches of stream-dominated fluvial/alluvial fans (Mueller and Corcoran, 1998).

6.1.3. Lf csGS (clast supported Gravel to Sand)

Description: Lf csGS (F~~f~~ig. 9e, 11c) is massive, moderately well-sorted and clast-supported. Clasts (gravel to sand) present sub-rounded to sub-angula~~ou~~r~~s~~ with low/medium sphericity with maximum size of 2-3 cm. The rocks belonging to this lithofacies are mainly formed by massive felsic lava fragments with different color and crystallinity.

Interpretation: Lf csGS is dominated by water flow processes where matrix plays a secondary role. The clast-supported character and less matrix content indicates that water removed the finer particles during transport and deposition. This lithofacies

Formatted: Level 1, Adjust space between Latin and Asian text, Adjust space between Asian text and numbers

Formatted: Indent: First line: 0 cm

represents deposition within a debris-flow dominated fluvial/alluvial environment. Poor sorting, clast-supported and sub-angular clasts point to deposition by localized laminar hyperconcetrated-flows in volcanic fans fringing flanks of volcanic edifices. Single cross-beds are usually ca. 1 cm thick

6.1.4. Lf csGC (clast supported Gravel and Cobble)

Description: Lithofacies csGC (F~~f~~ig. 9f) is massive, low-sorted and clast-supported. The clast population is characterized by sub-rounded, low/medium sphericity, massive felsic porfiritic fragments with maximum size up to 20 cm. This lithofacies has an interstitial matrix characterized by medium to coarse sand.

~~4.3.2.~~ Interpretation:

Lf ~~csG, csGS and~~ csGC ~~(fig. 9a/d/f)~~ is~~are~~ dominated by water flow processes where matrix plays a secondary role. The clast-supported character and less matrix content indicates that water removed the finer particles during transport and deposition. This ~~Lf csG display rounded clasts and well-sorting indicative of good selection during transport and emplacement. The rounded character of csG and the presence of matrix in the deposits suggest a laminar debris-flow regime in a medial reaches of stream-dominated fluvial/alluvial fans (Mueller and Corcoran, 1998). The alternation of Lf csG and mS (fig. 9a) indicates changes in energy conditions of sedimentation. We interpret these oscillations as belonging to a subaqueous-subaerial fan-delta interface setting where continental supply of material alternates to under-water sand accumulation (Lf mS). The massive sand grain size (mS) and the small ripples found at the top of the strata indicate low energy under tractional currents in shallow water conditions (Collison and Thompson, 1982; Lenhardt et al., 2011).~~ l~~L~~ithofacies ~~csGS and csGC~~ represents deposition within a debris-flow dominated ~~fluvial/~~alluvial environment. Poor sorting, clast-supported and sub-angular clasts likely points to deposition by localized ~~laminar hyperconcetrated-flows (csGS) and~~ non-cohesive debris-flows ~~(csGC).~~. ~~in volcanic fans fringing flanks of volcanic edifices. Single cross-beds are usually ca. 1 cm thick.~~

6.~~4.3.~~2~~3~~. Stratified

6.2.1 Lf xsS (cross-stratified Sand)

Formatted: Indent: First line: 0 cm

Formatted: None, Don't adjust space between Latin and Asian text, Don't adjust space between Asian text and numbers

Formatted: Font: Not Italic, No underline, Font color: Auto

Formatted: None, Don't adjust space between Latin and Asian text, Don't adjust space between Asian text and numbers

Formatted: Font: Not Italic, No underline, Font color: Auto

Formatted: Font: Not Italic

Formatted: Indent: First line: 0 cm

Formatted: Font: Not Italic, No underline, Font color: Auto

Formatted: Font: Not Italic, No underline, Font color: Auto

Formatted: Font: Not Italic

Description: l~~L~~ithofacies cross-stratified S~~s~~and~~stone~~ ~~(xsS)~~ (F~~f~~ig. 10a) consist of white to brownish low-angle cross-stratified coarse quartzitic sandstone. The sandstones are characterized by lobe to sheet-shaped bodies. Major bedsets are recognized ranging in thickness from 0.5 to 1.5 m, composed of fine-grained sandstone dominated by medium-angle cross strata (18-20º). Single cross-beds are usually 0.7-1cm thick. The outcrops displaying this lithofacies extend tens of meters with sharp upper and lower contact.

Interpretation: the cross-stratification of xsS is interpreted as formed in fluvial channels attesting the deposition from crested dune bed-forms that formed under condition of lower flow regime (Collinson, 1996; Miall, 1996; Capuzzo and Wetzel, 2004; Went, 2016). The deposition of medium-angle cross-bedding within large-scale examples of beds indicates that these larger beds are likely a product of bar migration. The beds are interpreted as channel-fill deposits (Lenhardt et al., 2017) related to a fluvial environment likely associated to meandering or braided rivers. Shoreline deposition developed around margins of immature marine basins is also considered.

Formatted: Font color: Custom Color(RGB(35,31,32))

Formatted: Indent: First line: 0 cm

6.2.2. Lf xsSG (cross-stratified Sand and Gravel)

Description: Lf xsSG ~~Lf xsSG~~ (F~~f~~ig. 10b) is characterized by crystal-lithic fine to coarse sand and fine gravel (max 5-6 mm in size) organized in cross-bedded stratification. Clasts display medium roundness and sphericity and are mostly composed by felsic fragments. Stratification is defined by alternating of well to poorly sorted, fine to coarse millimeters-thick strata. The finer black layers are formed by sub-millimetric hematite sand.

Interpretation: Lf xsSG correspond to cross-stratified water reworked deposits. The cross-stratified thicker fine gravelly strata, alternated with sandy layers laterally discontinuous, were interpreted as different pulses as the result of rapid deposition from hyperconcentrated flows (Zanchetta et al., 2004) in a stream-dominated fluvial/alluvial setting. Alternation with csG (Fig. 9c) represents difference of energy condition.

Formatted: Font color: Text 1

Formatted: Indent: First line: 0 cm

6.2.3. Lf dsSt (diffusely layered Silt)

Description: ~~Lf dsSt~~ this lithofacies consists of parallel, lenticular, truncated, and locally low-angle cross-stratified multicolor millimetric well-sorted fine- to very fine-grained sand and silt strata (F~~f~~ig. 10c). Within the sandy bedset, a thinning- and fining-upward trend may be distinguished. Small and straight groove marks have been detected and reduced tiny slump folding is also presence in some parts.

Interpretation: lithofacies dsSt displays diffuse fine stratification with tiny ripples, suggesting transport and sedimentation in shallow water. The thin sheet-shaped is interpreted as flood sediments (Lenhardt et al., 2011). These deposits are interpreted to have been formed in low energy lacustrine environment or ponds (Collinson, 1996; Roverato et al., 2017) characterized by small turbidities successions affected by scouring and tiny deformations (slumps) of the sediments.

6.2.4. Lf bChS (bedded Chert and Sand)

Description: t~~T~~he bedded chert lithofacies (with sand) (bChS) (F~~f~~ig. 10d) crops out in both regions and it is characterized by outcrops that can be traced on strike for hundreds of meters. The facies consist of thin laminated pinkish chert (layers < 1mm in thickness) with darker laminae intercalated, formed predominantly by hematite (Lenhardt et al., 2017). The layers are composed by microcrystalline quartz. In some portions, these lithofacies are associated with fine to medium sand composed mainly by quartz and less volcanic fragments.

~~4.3.4~~ ~~.~~Interpretation: this lithofacies is interpreted as inorganic precipitation of silica in a closed lake basin mainly due to its association with volcanic rocks and fine sandstone (Blatt et al., 1980; Eriksson et al., 1994). The picture in figure 10d shows elongated ripped-up millimetric fragments of chert immersed in the sandstone eroded by low-energy stream flow or local lacustrine turbidites. As suggests by Lenhardt et al. (2017) the chert may have formed during repeated pulses of hydrothermal fluids that circulated into the lake water during hiatuses in the volcanism (Van Kranendonk, 2006).

7. Analytical methods for geochemistry and geochronology

A total of 19 new samples (9 volcaniclastics and 10 lava flows) from the Tapajos region (associated with the data published in Roverato et al., 2016; Table 2) were analysed for bulk rock major and trace elements. Major element bulk rock analyses were performed by X-ray fluorescence, using a wavelength dispersive Philips PW 2400 spectrometry, using fused glass disks according to procedures described by

Formatted: Indent: First line: 0 cm

Formatted: Font: Not Italic, No underline, Font color: Auto

Formatted: No underline, Font color: Text 1

Formatted: No underline, Font color: Text 1

Formatted: Font color: Text 1

Formatted: Left, Indent: First line: 1.27 cm, Line spacing: 1.5 lines

Mori et al. (1999). Accuracy was greater than 2%. Trace element analyses in selected samples were performed by Inductively Coupled Plasma-Mass Spectrometry (ICP-MS) using the procedure described by Navarro et al. (2008). Accuracy, determined with respect to the reference standards BHVO-2 and BR, was 0.5–2%.

Zircon grains were examined with a FEI-QUANTA 250 scanning electron microscope equipped with secondary-electron and cathodoluminescence (CL) detectors at the Instituto de Geociências - Centro de Pesquisas Geocronologicas - Universidade de São Paulo (IGc-CPGeo-USP); the most common conditions used in CL analysis were 60 µA of emission current, 15.0 kV of accelerating voltage, 7 µm of beam diameter, 200 µs of acquisition time, and a resolution of 2048x1887 pixels and 345 dpi. Selected samples were analyzed for U-Pb isotopes using a SHRIMP-IIe also at IGc-CPGeo-USP, following the analytical procedures of Williams (1998) as reported by Giovanardi et al. (2015). Correction for common Pb is based on the measured ^{204}Pb, and the typical error for the ^{206}Pb/^{238}U ratio is less than 2%; U abundance and U-Pb ratios were calibrated against the TEMORA-II standard. The dataset consists of 56 new U-Pb SHRIMP-II analyses and is reported in Table 3. Thirty-five analyses were performed on zircon grains from the Tapajos region as follow: 11 analyses on sample NP380-C, 11 analyses on sample NP183 and 13 analyses on sample NP396-B. Eleven analyses were performed on zircon grains from Xingu sample XU08. For all samples, ^{207}Pb/^{235}U and ^{206}Pb/^{238}U concordia ages (with 95% of confidence level and 2σ error) are calculated using Isoplot 4.1 software (Ludwig, 2009).

Formatted: Font: Not Italic, No underline, Font color: Auto

The cross-stratification of lithofacies xsS is interpreted as formed in fluvial channels attesting the deposition from crested dune bedforms that formed under condition of lower flow regime (Collinson, 1996; Miall, 1996; Capuzzo and Wetzel, 2004; Went, 2016). The deposition of medium-angle cross-bedding within large-scale examples of beds indicates that these larger beds are likely a product of bar migration. The beds are interpreted as channel-fill deposits (Lenhardt et al., 2017) related to a fluvial environment likely associated to meandering or braided rivers. Shoreline deposition developed around margins of immature marine basins is also considered. Lf xsSG correspond to cross-stratified water reworked deposits. The cross-stratified thicker fine gravelly strata, alternated with sandy layers laterally discontinuous, were interpreted as different pulses as the result of rapid deposition from hyperconcentrated

~~flows (Zanchetta et al., 2004) in a stream-dominated fluvial/alluvial setting. Alternation with csG (fig. 9c) represents difference of energy condition. Lithofacies dsSt display diffuse fine stratification with tiny ripples, suggesting transport and sedimentation in shallow water. The thin sheet-shaped is interpreted as flood sediments (Lenhardt et al., 2011). These deposits are interpreted to have been formed in low energy lacustrine environment or ponds (Collinson, 1996; Roverato et al., 2017) characterized by small turbidities successions affected by scouring and tiny deformations (slumps) of the sediments. The Lf bChS is interpreted as inorganic precipitation of silica in a closed lake basin mainly due to its association with volcanic rocks and fine sandstone (Blatt et al., 1980; Eriksson et al., 1994). The picture in figure 10d shows elongated ripped-up millimetric fragments of chert immersed in the sandstone eroded by low-energy stream flow or local lacustrine turbidites. As suggests by Lenhardt et al. (2017) the chert may have formed during repeated pulses of hydrothermal fluids that circulated into the lake water during hiatuses in the volcanism (Van Kranendonk, 2006).~~

8~~5~~. Geochemistry of the TMP samples

Formatted: Indent: First line: 0 cm

Independently of their nature (lavas or volcani~~o~~clastic), the rocks of the TMP follow a typical calc-alkaline trend (Fig. 12). They are mostly rhyolitic in composition (Table 2), with four exceptions which fall in the trachytic field. In addition, their low LOI values (0.32-3.51%) and the low FeO content (0.78 – 3.26%) together with the negative correlation FeO vs SiO_2 appears to indicate that the investigated volcanic rocks neither underwent significant alteration processes nor they belong to sedimentary suites which commonly contain water rich clay minerals. TMP volcaniclastic and lava flows show similar negative correlation between TiO_2, Al_2O_3, MgO, FeOt, CaO, Na_2O and P_2O_5 with SiO_2. A negative correlation between K2O and SiO2 also exists for the volcanoclastic, but not for the lava flows. The similar trends observed suggest that both these kind of rocks are originated by similar ~~the same~~ magmatic sources. Such a conclusion is supported by similar variation paths, although with different values, of minor and trace elements (Fig~~s~~. 13). In particular, TMP lava flows show LREE enrichment ($(La/Yb)_N$=10.68-21.45; normaliz~~t~~at~~z~~ion to Chrondrite I from Anders & Ebihara, 1982) and a negative Eu anomaly which increases from trachytes ($(Eu/Eu^*)_N$=0.89-0.78) to rhyolites ($(Eu/Eu^*)_N$=0.69-0.31) (Fig. 13). The Eu negative anomaly, shown from all the samples, is expression of feldspar fractionation. On the other hand, volcaniclastics rocks show similar LREE enrichment ($(La/Yb)_N$=11.12-28.10) and negative Eu anomaly ($(Eu/Eu^*)_N$=0.97-0.37) (Fig. 13). In addition, volcaniclastics have higher LREE abundances with respect to lavas (La between 35.5-91.3 ppm and between 40.5-71.9 ppm, respectively) while they have similar MREE and HREE contents (Yb between 1.56-3.43 ppm and between 1.83-4.11 ppm, respectively). Volcaniclastics commonly show higher Rb (121-272.9 ppm) and Pb (4.5-137.1 ppm) with respect to lavas (Rb=96.1-232 ppm and Pb=2.7-45.8 ppm). Volcaniclastics are enriched in LILE, Th and U with respect to MORB (Fig. ~~REE~~13; normalization to MORB from Hoffman, 1988), with the exception of Sr, which commonly show a pronounced negative anomaly ($(Sr/Sr^*)_N$=0.55-0.05). The Sr negative anomaly is consistent with feldspar fractionation. Negative anomalies are also present for Nb and Ta, while Ba and Pb are commonly enriched (Fig. 13). Lavas show a similar trace pattern, but higher values dispersion (Fig. ~~REE~~13). The Ba enrichment is less pronounced with respect to volcaniclastics (Ba between 75-1965 ppm and 310-2245 ppm, respectively) and the Nb/Ta ratio show higher dispersion (3.29-14.63 and 6.73-13.9, respectively), indicating more limited fractionation of feldspar.~~.~~ ~~According to the fractionation of feldspar, the trachytes have less pronounced negative Sr anomalies with respect rhyolites ($(Sr/Sr^*)_N$=0.61-0.35 and 0.34-0.04, respectively).~~ Geochemical affinity of Tapajó~~o~~s volcaniclastics and lava flows suggests that the magmatism occurred in active continental ~~margin~~ setting (Fig. 14). Using the tectonic discriminant diagrams of Zr+Nb+Ce+Y (ppm) vs FeOtot/MgO (wt.%), Yb vs Ta and Th-Ta-Hf/3 (Wahlen et al., 1987; Pearce et al., 1984; Wood, 1980), the magmatism in the Tapajos region appears related to a syn- to post-collisional setting with few samples falling into the intraplate field (Fig. 14). According to the refined diagram Nb+Y vs Rb of Pearce (1996), all the Tapajos volcanics, together with the majority of volcanic rocks from the Sobreiro formation (Fernandes et al., 2011) are consistent with a late- to post-collisional setting (Fig. 14).

9~~6~~. U-Pb zircon Geochronology

Formatted: Indent: First line: 0 cm

Zircons from Tapajos samples are colo~~u~~rless, sometimes fractured and euhedral to sub-euhedral. They can contain inclusions of apatite or spinel and ~~are~~ display commonly low emission in Cathodoluminescence (CL). All crystals show magmatic oscillatory zoning and commonly a dark core which, in most cases, appears to be homogenous. Nonetheless, in few cases an inner core with discordant and partially reabsorbed domains is recognized. Some of the zircons also show a bright CL rim with transgressive or sub-concordant contacts with the inner oscillatory zoning. Zircons from sample XU08 from the Xingu region are colourless, rarely fractured and sub-euhedral. Inclusions of apatite or spinel are also observed sometimes. Crystals are medium in CL emissions and commonly show a homogeneous core and a concordant magmatic oscillatory zoning. Few zircons show a core with discordant zoning. No transgressive bright CL rims were recognized. Analyses were carried out on zircons that do not show transgressive or resorption features and discordant inner cores. Zircons from sample NP183 (Ignimbrite) provide 4 discordant ~~ages~~ and 7 concordant analyses that provide ~~for~~ an upper intercept at 1984 ±8.5 Ma (95% confident decay-const. errs included, MSWD 1.09) and a concordia age at 1986 ±8.2 Ma (2σ, decay-const. errs included, MSWD 1.08, Probability of concordance = 0.30; Fig. 15). Single spot $^{206}Pb/^{207}Pb$ ages range between 2010 ±17 Ma and 1909 ±53 Ma with an average age of 1985 ±11 Ma (95% confident decay-const. errs included, MSWD 1.6, Probability of concordance = 0.15; Fig. 15). Zircons from sample NP380 (Ignimbrite) show slightly older single spot $^{206}Pb/^{207}Pb$ ages between 2023 ±31 Ma and 1981 ±24 Ma with an average age of 1998 ±5.9 Ma (95% confident decay-const. errs included, MSWD 0.74, Probability of concordance = 0.68; Fig. 14). Analyses are slightly discordant (up to 4%) providing an upper intercept at 1998 ±7.7 Ma (95% confident decay-const. errs included, MSWD 0.74). Zircons from sample NP396 (Banded lava) provide 5 discordant ages and 8 concordant analyses, which provide ~~for~~ an upper intercept at 1994 ±8.2 Ma (95% confident decay-const. errs included, MSWD 1.40) and a concordia age at 1997 ±7.0 Ma (2σ, decay-const. errs included, MSWD 5.70, Probability of concordance = 0.02; Fig. 15). Single spot $^{206}Pb/^{207}Pb$ ages range between 2014 ±14 Ma and 1973 ±8 Ma with an average age of 1994 ±8.7 Ma (95% confident decay-const. errs included, MSWD 1.6, Probability of concordance = 0.12; Fig. 14). Pooling togheter the analyses of the Tapajós samples provides an average age of 1991 ±12 Ma (2σ, MSWD 1.50, Probability of concordance = 0.06). Zircons from sample XU08 (Lava flow) provide a concordia age at 1882 ±6.4 Ma (2σ, decay-const. errs included, MSWD 2.70, Probability of concordance = 0.10; Fig. 16). Single spot $^{206}Pb/^{207}Pb$ ages range between 1899 ±10 Ma and 1875 ±13 Ma, with an average at

1884 ±5.2 Ma (95% confident decay-const. errs included, MSWD 0.60, Probability of concordance = 0.82).

10~~7~~. Discussion

~~7.1~~ 10.1. Subduction-related to extensional setting

The geochemistry of the TMP samples presented in this work display a high-K calc-alkaline signature (F~~f~~ig. 12); ~~most of them are related to a volcanic arc setting (fig. 14), although few samples display a geochemical signature that vary from the trend and~~they majorly fall into the A-type intra-plate granite field and tectonic discriminant diagrams suggest a late- to post-collisional setting for the TMP volcanism (F~~f~~ig. 14). This interpretation is also supported by enrichment in ~~low HSFE and the high~~ LILE, Th, U and LREE ~~contents~~ of our samples, which suggest a strong crustal component in the parent melt ~~,~~ consistent with a subduction/post orogenetic geodynamic setting (Fig. 12), and the high HSFE which shifted the TMP volcanics composition in the A-type granites showing however FeO/MgO which are low and comparable with I- and S-types granites (Fig. 14). Similar features are~~.~~ ~~These two distinct signatures are also well~~ reported in previous works (Lamarão et al., 1999; Lamarão et al., 2002) for volcanics in the Tapajós region, which are grouped into the Vila Riozinho (VR) and Maraes Aldeida (MA) formations, respectively. The Vila Riozinho rocks are intermediate to felsic in composition (Lamarão et al., 2002) with a calc-alkaline signature, while the rhyolites and ignimbrites of Moraes Almeida are slightly enriched in silica compared to the rhyolites of Vila Riozinho and are geochemically similar to evolved A-type granites (Lamarão et al., 2002). Our results show similarities with these data, suggesting that our specimens could be part of the VR and/or MA formations. The identification of two volcanic series has important implications for the understanding of the magmatic evolution of the Amazonian craton in late Paleoproterozoic. A model for the evolution of the TMP involves a first stage of subduction-related magmatism followed by an intracontinental magmatism related to a distensional event (Lamarão et al., 2002). Geochronological analyses by Lamarão et al. (2002) yielded ages of ca. 2 Ga for the VR rocks and ca. 1.88-1.87 Ga for the MA volcanism. The three new U-Pb geocronological analyses reported in this study yielded ages of ca. 2000 Ma (fig. 15) are~~,~~ concordant with the ages presented by Lamarão et al. (2002) for the VR magmatism, thus suggesting that the TMP rocks could be part of the VR volcanic sequence. However, TMP rocks are geochemically more evolved with

Formatted: Indent: First line: 0 cm

Formatted: No underline, Font color: Text 1

Formatted: Normal, No bullets or numbering

Formatted: Font: Not Italic, No underline, Font color: Auto

Formatted: Font color: Text 1

respect to VR in terms of SiO2 (63.8-76.6 wt.% and 54.4-71.8 wt.%, respectively), K2O (2.3-7.1 wt.% and 2.1-5.8 wt.%, respectively) and REE abundances (Fig. 12) and are more similar to MA rocks (Fig~~.~~s. 11, 12 and 13). In particular, REE patterns of the TMP samples are comparable with the rocks of the MA formation (Fig. 12) while they are more enriched in REE with respect to VR rocks. Conversely, TMP rocks are enriched in Ba (Fig. 12), while ~~A~~MA are depleted, and have compositions for Rb/Zr and Nb, considered as a proxy for arc maturity (Brown et al., 1984), similar to VR and different from MA (Rb/Zr between 0.3-1.1 in TMP, 0.2-0.7 in VR and 0.2-1.7 in MA; Lamarã~~a~~o et al., 2002). Thus, according to geochronological and petrological data, we proposed that the TMP rocks in this study ~~represent the more felsic and evolved facies of the VR magmatism and~~ must be ascribed ~~at thi~~to the VR~~s~~ formation. ~~-~~Geochemical differences in our rocks and VR volcanics could be explained by a more evolved character of the TMP rocks. The ~~The~~ evidences of plagioclase fractionation from the parent melts of the TMP (negative Eu and Sr anomalies, Fig. 12) and their absence in less evolved VR rocks reinforce this interpretation, and suggest fractional crystallization as the prominent process controlling the VR magmatism evolution. However, we want to point out that due to the large area covered by the presented investigation (Fig. 2), together with the VR area, the geochemical variations between our rocks (TMP) and VR could be the result of local/regional heterogeneities in the magmatism. This hypothesis is supported by the intermediate characteristics of the TMP samples with respect to the VR and MA volcanics (Figs 11, 12 and 13).

Recently, new authors (Juliani et al., 2014) suggest the geochemical and geocronological signature of the MA ~~(TMP)~~ formation could be correlated to the felsic Santa Rosa (SR) formation cropping out in the SFX region. Our new U-Pb geocronological analyses on one rock sample from the SR formation yielded an average age of 1884 ±5.2 Ma (Fig. 16~~8~~) that is consistent with previous Pb-Pb ages on other locations. Juliani and Fernandes (2010) published two Pb-Pb ages on zircons of 1879 ± 2 Ma and 1884 ± 1.7 for a rhyolite and an ash tuff, respectively. Recently Antonio et al. (2017) publishes the first U-Pb ages on zircons for the Santa Rosa Formation with 1877.4 ± 4.3 Ma for a rhyolite and 1895 ± 11 Ma for a dike. All geochronological results support a ca. 1880 Ma age for the emplacement of these rocks.

The southern Amazonian craton, as well as other P~~p~~recambrian terrains worldwide (Condie, 2002; Hoffman, 1988; Zhao et al., 2002), are considered to be characterized by a series of orogenic to post-orogenic events from 2.0 up to 1.88 Ga. The amalgamation of cratonic blocks worldwide established connections between South America and West Africa and other cratonic terrains such as Western Australia and South Africa, Laurentia and Baltica, Siberia and Laurentia, Laurentia and Central Australia, etc (Zhao et al., 2002). These late-Paleoproterozoic collisional processes likely formed the controversial supercontinent Columbia (Zhao et al., 2004). This period also coincides with a major peak in orogenic gold resources (Goldfarb et al., 2001, Juliani et al., 2014) and understanding the geodynamic of this period is crucial for economic interests. Antonio et al. (2017) highlight that for the period 1.88 Ga, many cratonic terrain have been characterized by extensive magmatism. These authors report as examples the 1880 Ma NE-trending Ghost dike swarm and the 1880 Ma Circum-Superior LIP in the Canadian shield (Minifie et al., 2013), the 1880 Ma Southern Bastar- Cuddapah LIP in India (French et al., 2008), the Mashonaland sills and the Post-Waterberg dolerites in Kalahari craton (Hanson et al., 2004), an extensive A-type magmatism in Baltica and in Siberia. The A-type affinity of the 1.88 Ga rocks is widely described by other authors in different regions into the Amazonian craton (Ferron et al., 2010; Pierosan et al., 2011; Fernandes et al., 2011; Klein et al., 2012; Barreto et al., 2014; Teixeira et al., 2018). Currently, the significance of the 1.88 Ga A-type magmatism in the Amazonian craton is still matter of debate, also due to the extremely large aerial cover which interested several different domains with different basements and geologic evolutions. For example, studies on the Carajas region suggest that the 1.88 Ga anorogenic magmatism in this domain was provoked by delamination and fusion of the Archean basement by a mantle plume which originated an extensional setting (Dell'Agnol et al., 2005; Silva et al., 2016; Teixeira et al., 2018; Teixeira et al., 2019).

Conversely, the geochemical features of the TMP and SFX magmatism presented in this work and in literature (Lamarão et al., 2002, 2005; Fernandes et al., 2011) mainly support an extensional regime of these regions related to a late- to post-collisional event, being possibly related to the end of the subduction process.~~).~~

~~According to these authors we suggest that the A-type rocks emplaced during the period 1.88 Ga in both TMP and SFX are related to an intraplate environment in an extensional regime.~~ The transition from convergent (syn/post-orogenic) to extensional tectonic setting could register the beginning of the taphrogenesis that marked the Amazonian Craton throughout the Mesoproterozoic (Brito Neves, 1999; Lamarão et

Formatted: Font: (Default) Times New Roman, No underline, Font color: Text 1

Formatted: Font: (Default) Times New Roman, Font color: Text 1, English (United States)

Formatted: Font: (Default) Times New Roman, No underline, Font color: Auto

Formatted: Font: (Default) Times New Roman, No underline

Formatted: Font: (Default) Times New Roman, No underline, Font color: Auto

Formatted: Font: (Default) Times New Roman, No underline

Formatted: Font: (Default) Times New Roman, No underline, Font color: Auto al., 2002). The ca. 1.88 Ga felsic magmatism in different provinces of the Amazonian craton could represent the oldest magmatism related to this event. It should be mentioned that in term of textural features, the products emitted during the transition between the post-collisional to extensive events don't display substantial variations. In other words, the lithofaciological signature of the volcanic and volcaniclastic rocks that characterized the 2 Ga VR event (subduction related) is similar for those products erupted during the 1.88-1.87 Ga extensional volcanism that characterized the MA and SR events. Moreover, the post-orogenic to extensional setting emphasizes the continental setting where the studied volcanic products have been emitted. Following the idea of Roverato et al. (2017) for the Late-Paleoproterozoic andesitic Sobreiro Formation, we stress the lack of any evidences in favour of subaqueous eruptions for the emitted felsic products such as pillow lavas as well as hyaloclastites. This suggests the subaerial character of the volcanism and its emitted products acted in both regions.

10~~7~~.2. Eruptive style and emplacement

The study areas are widely characterized by volcanic deposits whose eruptive style is hard to differentiate. Distinguishing between banded lavas and high grade ignimbrites is, sometime, extremely challenging (Henry and Wolff, 1992; Manley, 1995). This is made even more complicated when the investigated deposits are ancient and the outcrops intensely eroded, such as those Precambrian terrains investigated here (Lenhardt et al., 2012; Roverato et al., 2016; Lenhardt et al., 2017). Evidences in the field show that a great volume of the volcanic activity is represented by the emission of lava flows and/or high-grade to rheomorphic ignimbrites, although an important amount of other fragmental products of different type (Lf mAL, mLA, *l-g/m-g/h-g*wAL) are also well represented in both regions. High-grade welded and rheomorphic (up to lava-like) ignimbrites share similar features with lavas, displaying banding and ductile folds formed by the elongation of fiamme and vesicles (Schmincke and Swanson, 1967; Chapin and Lowell, 1979; Wolff and Wright, 1981; Branney et al., 1992; Sumner and Branney, 2002; Pioli and Rosi, 2005; Andrews and Branney, 2011; Brown and Bell, 2013). Although the ignimbrites investigated here have a fragmental derivation their origin largely differ from those characteristic of fallout deposits that form by a sustained column explosive-driven eruption. High-grade welded and rheomorphic ignimbrites are correlated with highly explosive plinian-type eruptions

Formatted: Font: (Default) Times New Roman, No underline

Formatted: Font: (Default) Times New Roman, No underline

Formatted: Font: (Default) Times New Roman, No underline, Font color: Auto

Formatted: Font: (Default) Times New Roman, No underline, Font color: Auto

Formatted: Indent: First line: 0 cm

Formatted: Font: Not Italic, No underline

Formatted: Font: Not Italic, No underline which produce, during their column collapse stage, large PDC. In addition, high-grade rheomorphism of silicic products, either deriving from an explosive or effusive eruption, are favored by high temperature low-viscosity emplacement conditions and the presence of some residual water. The high temperatures condition of our deposits is also confirmed by the pervasive presence of spherulites and lithophysae formed during the slow-cooling regimes of large silica-rich lavas and welded ignimbrites (Lofgren, 1971; Breitkreuz, 2013). The eruptive scenario showed in figure 17 giving origin to the frequent eruption of large volume and high discharge rate lava flows and ignimbrites was likely characterized by fissure-fed and caldera collapses systems as those described by previous authors (Legros et al., 2000; Aguirre et al., 2003; Cas et al., 2011; Lesti et al., 2011; Lenhardt et al., 2012; Willcock et al., 2013). Eruptions fed by extensive fissures of large size, in fact, appear to be the most favourable volcanic systems to minimize cooling during emplacement and produce an alternance of low-height sustained column eruptions feeding PDC and eruptions characterized by the effusion of low viscosity lava flows, coulees and domes, while maintaining high discharge rates (e.g. Bachmann et al., 2000; Aguirrez-Diaz & Labarthe-Hernandez, 2003; Polo et al., 2018a, b; Simões et al., 2017). The sustained fountaining and entrainment of air in the eruptive jet is strongly influenced by the geometry of the conduit (Legros et a., 2000) as well as the transition from sustained to collapsing eruptive column. A wide-geometry conduit would impede much air entrainment into the pyroclastic fountain and, at the same time, would favors magmatic escape of volcanic gases, favoring the low fountaining and promoting a “boil-over” style eruption (Branney and Kokelaar, 1992, 2002; Lenhardt et al., 2017) with high discharge rate. Moreover, the low air injection would inhibit the dilution of the eruptive material making it thermodynamically isolated from the surrounding environment (Lesti et al., 2011), preserving the high temperatures and enhancing the agglutination of fragments (welding) (~~e.g.~~ Quane and Russell, 2004; Russell and Quane 2005; Giordano et al., 2005). When the low-altitude pyroclastic fountaining or the emission of high temperature lavas would be maintained for long time the high flow-mobility is ensured (Sulpizio et al., 2014). If the material supply from the vent continues for long time and with high discharge rate, the mobility could be maintained even on very low slope angles (Sulpizio et al., 2014; Giordano et al., 2017; Kolzenburg et al., 2017), and flowing various kilometers up to hundreds of kilometers far from the vent (Aguirre-Diaz et al., 2008; Cas et al., 2011; Giordano et al., 2017). This could explain the presence of large silicic volcanic areas characteristic of the ancient Amazonian volcanism (Roverato et al., 2016). Although, volcaniclastic rocks seem to be volumetrically less important in the study areas than the lava flows and/or rheomorphic ignimbrites the recognition of fragmental rocks during our field campaigns is important to understand their significance into our paleogeographic reconstruction (Fig. 17). An idealized deposit sequence of a caldera forming eruption displays an air-fall deposit overlain by an ignimbrite (Druitt and Sparks, 1984) and the transition from the sustained column phase to the pyroclastic flow phase is often accompanied by a strong increase in the discharge rate (Bursik and Woods, 1996). The stratigraphic sequence of figure 11 shows this association of a possible air-fall deposit (Lf dsAL) linked with pyroclastic flow-dominated deposits (Lf mAL and *m*-*g*wLA). In some cases, pyroclastic eruptions commonly precede lava emplacement (Fink 1983; Heiken and Wohletz 1987). The sequence presented in figure 7 shows a low-grade welded ignimbrite deposit (Lf *l*-*g*wAL) overlaid by a thick banded body that we are interpreting here as a lava flow. At the base of the banded lava is a breccia (Lf mLB) consisting of clasts of a mix of lava textural types, including massive, vesicular, flow banded and flow-folded, glassy, pumiceous and devitrified. Autobrecciation in lavas or rheomorphic ignimbrites occurs when more rigid layers and the external parts are broken in response to the applied shear stress locally exceeding the tensile strength (Fink and Manley; 1987). Some polymictic breccia deposits (Lf mLA) are characterized by lithic angular clasts and devitrified fragments that could point to co-ignimbritic breccias with short transport of the emitted material. These deposits could be also related to collapse-caldera-breccias falling down into the caldera ring during the roof subsidence (Fig. 8). Air-fall (sA) and dilute pyroclastic flow (xsA) deposits (surge type) crop out in both regions. These, linked with the glassy and lithic pyroclastic material described above, are evidence of intense explosive phases from more sustained column eruptions of smaller intra-caldera volcanic centers and/or associated to events of caldera collapse (Fig. 17).

10.2.1 The sedimentary response

Formatted: Font: Not Italic, No underline

Formatted: Font: Not Italic

Sets of small basins intra-calderas and probable relatively immature shallow marine deposits are interpreted as forming part of a tectonically unstable setting of a young extensional environment that characterized the southern Amazonian craton during the Paleoproterozoic. Reworked sediments can accumulate into volcano-tectonic depressions created by the eruption, which often collects an intra-caldera lake (Heiken et al., 2000 Németh et al., 2009, Manville et al., 2009). The sedimentation into intra-volcano shallow-water lacustrine basins would have be facilitated (F~~f~~ig. 17). The alternation of subaerial to shallow-water sedimentation displayed by the alternation of Lf mS and csG is indicative of this volcano-tectonic depressions, which could be also interpreted as immature marine depressions. Subaerial and subaqueous talus coarse-grained up to finer grained turbidites (dsSt) and suspension deposits formed during quiescent periods into lakes or pounds is also inferred (Bacon et al., 2002). Silica-rich accumulations into shallow water basins (Chipera et al., 2008; Manville et al., 2009) deriving from hydrothermal activity in a dynamic volcanic context is also thought to be responsible for the formation of chert accumulation (Lf bChS). Post caldera uplifting (F~~f~~ig. 17), resurgence or central volcanism could also contribute to produce new sediments to be reworked and transported. Fluvial erosion and reworking of primary deposits produced wide range of different sediments from localized cross-bedded, well-sorted sand (Lf xsS) and gravel (Lf xsSG) beds to massive clast-supported sand and gravel (Lf csGS, csG) and cobble (Lf csGC) deposits. Fluvial deposits occur throughout all successions, representing periods of stream and river reworking and re-establishment after an eruptive phase (Zernack et al., 2011; Roverato et al.~~.~~, 2017). Debris-flows, hyperconcentrated flows, sheet-floods and active sandy braided river systems existed and the ~~probable~~ absence of vegetation during the Precambrian (Oberholzer and Eriksson, 2000; Roverato et al., 2017) permitted that copious rainfalls easily reworked the available sediments.

11~~9~~. Conclusion

This study is the result of the lithofaciological analysis carried out during the 2013, 2014 and 2015 field campaigns in the Amazon Craton in the TMP and SFX regions and the successive geochemical and geochronological analysis of samples collected in the field. This work constitutes a further step ahead toward the comprehension of significance, chronostratigraphic distribution and the dynamic of eruption and emplacement of felsic volcanic products in the region. Our results complete previous studies and confirm that products present in the Amazonia Craton could be related either to caldera-type systems (e.g. Lamarão et al., 2002; Juliani et al., 2005; Lamarão et al., 2005; Pierosan et al., 2011) and to fissure-fed eruptive environment following the model proposed by Aguirre-Diaz and Labarthe-Hernandez (2003) for the "Sierra Madre Occidental" formation and by Juliani and Fernandes (2010) for the Xingu region. The two models are in fact very similar only differing for the size of the hypothesized magma chambers and the shape of the fissural vents. The described volcano-sedimentary sequences that were characterized by the emission of large volcanic felsic products were likely formed in a late- to post-orogenic (~ 2 Ga) to extensional regimes (~ 1.88 Ga).

~~Here we also image that an ideal late-convergent to extensional geotectonic environment was likely similar to that proposed in our discussion paragraph, where a post-orogenic to extensional regime for the period ~ 1.88 Ga was characterized by the emission of large volcanic felsic products. With this contribution we want also stress the importance of the results obtained by investigating the lithofaciological character of the deposits instead of only carrying out geochemical studies.~~

Acknowledgments

This work was supported by the project CAPES/CNPq 402564/2012-0 (Programa Ciências sem Fronteiras) to Caetano Juliani and Matteo Roverato. M. Roverato acknowledges the grant of the Brasilian CAPES/ CNPq Programa Ciências Sem Fronteiras, Atração de Jovem Talento 402564/2012-0. We acknowledge the CNPq/CT-Mineral (Proc. 550.342/ 2011-7) and the INCT-Geociam (573733/2008-2) — (CNPq/MCT/ FAPESPA/PETROBRAS). Furthermore, the first author would like to thank Jeovaci Jr. Martins da Rocha, Diego Felipe Gomez Gutierrez, Lucas Villela Cassini for the help in the field ~~-~~and Carlos Marcelo Diaz Fernandez for the help ~~in the field~~ and very useful discussions. Dr. Giordano acknowledges the financial support for this research from the CAPES project (proposal 302827) of the Ciências Sem Fronteiras program (Brazil) and the local research funds (2012, 2013, 2014) of the University of Turin (Ex60-2015). We are indebted to ~~……~~Nils Lenhardt and Roberto Dall'Agnol~~……~~ for the dedication in reviewing this manuscript and ~~i~~important comments and reviews, which improved considerably this work. ~~, ………~~

Formatted: Indent: First line: 0.75 cm

References

Aguirre-Diaz, G.J., Labarthe-Hernández, G., 2003. Fissure ignimbrites: fissure-source origin for voluminous ignimbrites of the Sierra Madre Occidental and its relationship with Basin and Range faulting. Geology 31, 773-776.

Aguirre-Diaz, G.J., Labarthe-Hernàndez, G., Tristàn-Gonzàlez, M., Nieto-Obregòn, J., Isaac Gutiérrez-Palomares, I., 2008. The ignimbrite flare-up and graben calderas of the Sierra Madre Occidental, Mexico. In: Martí, J., Gottsman, J. (Eds.), Caldera Volcanism: Analysis, Modelling and Response. Developments in Volcanology 10, 143-180.

Almeida, F.F.M., Hasui, Y., Brito Neves, B.B., Fuck, R.A., 1981. Brazilian structural provinces: an introduction. Earth Science Reviews 17, 1-29.

Almeida, M.E., Brito, M.F.L., Ferreira, A.L., Monteiro, M.A.S., 2000. Projeto Especial Província Mineral do Tapajós. Geologia e recursos minerais da Folha Vila Mamãe Anã (SB.21-V-D). Estados do Pará e Amazonas. CPRM, Brasília. [CD-ROM].

Amaral, G., 1974. Geologia Pré-Cambriana da Região Amazônica. Tese de Livre Docência, IG/USP (212 pp.).

Anders, E., Ebihara, M., 1982. Solar system aboundances of the elements. Geochim. Cosmochim. Ac. 46, 2363-2380.

Andrews, G.D.M., Branney, M.J., 2011. Emplacement and rheomorphic deformation of a large, lava-like rhyolitic ignimbrite: Grey’s Landing, southern Idaho. Geological Society of America Bulletin 123, 725-743.

Antonio, P., D'Agrella-Filho, M.S., Trindade, R.I.F., Nédélec, A., de Oliveira, D.C., da Silva, F.F., Roverato M., Lana, C., 2017. Turmoil before the boring billion: Paleomagnetism of the 1880–1860 Ma Uatumã event in the Amazonian craton. Gondwana Research 49, 106-129.

Araújo, O.J.B., Maia, R.G.N., Jorge, João, X.S., Costa, J.B.S., 1988. A megaestruturação arqueana da folha Serra dos Carajás. In: SBG (Ed.), Congresso Latinoamericano de Geologia, seventh ed. Belém. 324-333.

Bacon, C.R., Gardner, J.V., Mayer, L.A., Buktenica, M.W., Dartnell, P., Ramsey, D.W., Robinson, J.E., 2002. Morphology, volcanism, and mass wasting in Crater Lake, Oregon. Geological Society of America bulletin 114, 675-692.

Bahia, R.B.C., Quadros, M.L.E.S., 2000. Geologia e recursos minerais da Folha Caracol SB.21-X-C. Estados do Pará e Amazonas. Escala 1:250.000. Brasília: CPRM, 2000. 1 CD ROM.

Barreto, C.J.S., Lafonb, J.M., da Rosa Costac L.T., Fernandes-Limad, E., 2014. Palaeoproterozoic (~1.89 Ga) felsic volcanism of the Iricoumé Group, Guyana

Shield, South America: geochemical and Sm-Nd isotopic constraints on sources and tectonic environment. International Geology Review, 2014. http://dx.doi.org/10.1080/00206814.2014.930800

Best, M.G., Christiansen, E.H., 1997. Origin of broken phenocrysts in ash-flow tuffs. GSA Bulletin, 109 (1), 63-73.

Blatt, H., Middleton, G., Murray, R., 1980. Origin of Sedimentary Rocks. Prentice-Hall, Englewood Cliffs, 634.

Branney, M.J., Kokelaar, B.P., 1992. A reappraisal of ignimbrite emplacement: progressive aggradation and changes from particulate to non-particulate flow during emplacement of high-grade ignimbrite. Bull. Volcanol. 54, 504-520.

Breitkreuz, C., 2013. Spherulites and lithophysae—200 years of investigation on high temperature crystallization domains in silica-rich volcanic rocks. Bull. Volcanol. 75:705.

Brito-Neves, B.B., 2011. The Paleoproterozoic in the South-American continent: Diversity in the geologic time. Journal of South American Earth Sciences 32, 270-286.

Brown, D.J., Bell, B.R., 2013. The emplacement of a large, chemically zoned, rheomorphic, lava-like ignimbrite: the Sgurr of Eigg Pitchstone, NW Scotland. Journal of the Geological Society 170, 753-767.

Brown, G.C., Thorpe, R.S., Webb, P.C., 1984. The geochemical characteristics of granitoids in contrasting arcs and comments on magma sources. Journal of the Geological society 141, 413-426.

Bursik, M.I., Woods, A.W., 1996. The dynamics and thermodynamics of large ash flows. Bull. Volcanol. 58, 175-193.

Capuzzo, N., Wetzel, A., 2004. Facies and basin architectural of the Late Carboniferous Salvan-Dorénaz continental basin (Western Alps, Switzerland/France). Sedimentology 51, 675-697.

Cas, R.A.F., Wright, J.V., 1987. Volcanic Successions, Modern and Ancient. Unwin Hyman, Boston. 528.

Cas, R.A.F., Wright, H.M.N., Folkes, C.B., Lesti, C., Porreca, M., Giordano, G., Viramonte, J.G., 2011. The flow dynamics of an extremely large volume pyroclastic flow, the 2.08-Ma Cerro Galán Ignimbrite, NW Argentina, and comparison with other flow types. Bull. Volcanol. 73, 1583-1609.

Chipera, S.J., Goff, F., Goff, C.J., Fittipaldo, M., 2008. Zeolitization of intracaldera sediments and rhyolitic rocks in the 1.25 Ma lake of Valles caldera, New Mexico, USA. Journal of Volcanology and Geothermal Research 178, 317-330.

Collinson, J.D., 1966. Antidune bedding in the Namurian of Derbyshire, England: Geologie en Mijnbouw 45, 262-264.

Collinson, J.D., Thompson, D.B., 1982 Sedimentary structures: London, Allen and Unwin, 194.

Condie, K.C., 2000. Episodic continental growth models: after thoughts and extensions. Tectonophysics 322, 153-162.

Condie, K.C., 2002. Continental growth during a 1.9-Ga superplume event. Journal of Geodynamics 34, 249-264.

Costa, J.B.S., Hasui, Y. 1997. Evolução geológica da Amazônia. In: M.L. Costa & R.S. Angélica (Ed.), Contribuições à geologia da Amazônia, 16-90.

Da Cruz, R.S., Fernandes, C.M.D., Villas, R.N.N., Juliani, C., Monteiro, L.V.S., Almeida, T.I.R., Lagler, B., Carneiro, C.C., Misas, C.M.E., 2015. A study of the hydrothermal alteration in Paleoproterozoic volcanic centers, São Felix do Xingu region, Amazonian Craton, Brazil, using short-wave infrared spectroscopy. J. Volc. Geoth. Res. 304, 324-335.

Dall'Agnol, R., Lafon, J.M., Macambira, M.J.B., 1994. Proterozoic anorogenic magmatism in the Central Amazonian Craton: geochronological and geochemical aspects. Mineral. Petrol. 50, 113-138.

Dall'Agnol, R., Costi, H.T., Leite, A.A.S., Magalhães, M.S., Teixeira, N.P., 1999. Rapakivi granites from Brazil and adjacent areas. Precambrian Research 95, 9-39.

Dall'Agnol, R., Teixeira, N.P., Rämö, O.T., Moura, C.A.V., Macambira, M.J.B., Oliveira, D.C., 2005. Petrogenesis of the paleoproterozoic, rapakivi, A-type granites of the Archean Carajás metallogenic province, Brazil. Lithos 80, 101-129.

Dall'Agnol, R., da Cunha, I.R.V., Guimarães, F.V., de Oliveira, D.C., Teixeira, M.F.B., Feio, G.R.L., Lamarão, C.N., 2017. Mineralogy, geochemistry, and petrology of Neoarchean ferroan to magnesian granites of Carajás province, Amazonian Craton: The origin of hydrated granites associated with charnockites. Lithos 277, 3-32.

Druitt, T.H., Sparks, R.S.J., 1984. On the formation of calderas during ignimbrite eruptions. Nature 310, 679-681.

Echeverri-Misas, C.M., 2010. Geologia e gênese do depósito de Au-(Cu) do Palito,

Formatted: Font: 12 pt, No underline, Font color: Auto

Formatted: Font: 12 pt, No underline, Font color: Auto

Formatted: Font: 12 pt, No underline, Font color: Auto

Formatted: Font: 12 pt, No underline, Font color: Auto

Formatted: Font: 12 pt, No underline, Font color: Auto

Província Aurífera do Tapajós. Dissertação de Mestrado, IG/USP.

Eriksson, P.G., Engelbrecht, J.P., Res,M., Harmer, R.E., 1994. The Bushy Bend lavas, a new volcanic member of the Pretoria Group, Transvaal Sequence. S. Afr. J. Geol. 97, 1-7.

Faraco, M.T.L., Carvalho, J.M.A., Klein, E.L., 1997. Carta metalogenética da Provéncia Auréfera do Tapajós, in: Costa, M.L.C., Ange´lica, R.S. (Eds.), Contribuic¸o˜es a` Geologia da Amazônia. Sociedade Brasileira de Geologia, Belém, Brazil 1, 423-437.

Fernandes, C.M.D., Juliani, C., Monteiro, L.V.S., Lagler, B., Misas, C.M.E., 2011. High-K calc-alkaline to A-type fissure-controlled volcano-plutonism of the São Félix do Xingu region, Amazonian craton, Brazil: Exclusively crustal sources or only mixed Nd model ages? Journal of South America Earth Science 32 (4), 351-368.

Ferrari, L., Orozco-Esquivel, T., Manea, V.C., Manea, M., 2012. The dynamic history of the Trans-Mexican Volcanic Belt and the Mexico subduction zone. Tectonophysics 522-523, 122-149.

Ferreira, A.L., Almeida, M.E., Brito, M.F.L., Monteiro, M.A.S., 2000. Projeto Especial Província Mineral do Tapajós. Geologia e recursos minerais da Folha Jacareacanga (SB.21-Y-B). Estados do Pará e Amazonas. Escala 1:250.000. Nota explicativa e mapas, CPRM, Brasília. [CD ROM].

Ferron, J.M.T.M., Bastos-Neto, A.C., Lima, E.F., Nardi, L.V.S., Costi, H.T., Pierosan, R., Prado, M., 2010. Petrology, geochemistry, and geochronology of Paleoproterozoic volcanic and granitic rocks (1.89–1.88 Ga) of the Pitinga Province, Amazonian Craton, Brazil. Journal of South American Earth Sciences 29, 483-497.

Fink, J., 1983. Structure and emplacement of a rhyolitic obsidian flow: little Glass Mountain, Medicine Highland, northern California. GSA Bull. 94, 362-380.

Fink, J.H., Manley, C.R., 1987. Origin of pumiceous and glassy textures in rhyolite flows and domes: Geological Society of America Special Paper 212, 77-88.

Fisher, R.V., 1961. Proposed classification of volcaniclastic sediments and rocks. Geological Society of America Bulletin 72, 1409-1414.

French, J.E., Heaman, L.M., Chacko, T., Srivastava, R.K., 2008. 1891–1883 Ma Southern Bastar–Cuddapah mafic igneous events, India: a newly recognized large igneous province. Precambrian Research 160, 308-322.

Giordano, D., La Felice, S., Arzilli, F., De Cristofaro, S.P., Masotta, M., Polo L. (2017). Il vulcanismo effusivo acido del Monte Amiata: stima delle condizioni pre- e sin-eruttive ed implicazioni vulcanologiche. Effusive acidic volcanism of Monte Amiata: estimates of pre- and syn-eruptive conditions and volcanological implications. Monografia Il Vulcano di Monte Amiata, ISBN 978-88-99742-32-4, 171-193.

Giordano, D., Nichols, A.R.L., Dingwell, D.B., 2005. Glass transition temperatures of natural hydrous melts: a relationship with shear viscosity and implications for the welding process. Jour. Volc Geoth. Res. 142, 105-118.

Giovanardi, T., Girardi, V.A.V., Correia, C.T., Sinigoi, S., Tassinari, C.C.G., Mazzucchelli, M., 2015. U-Pb zircons SHRIMP data from the Cana Brava Layered Complex: New constraints for the mafic-ultramafic intrusions of Northern Goiás, Brazil. Open Geosci 7, 197-206.

Goldfarb, R., Groves, D., Gardoll, S., 2001. Rotund versus skinny orogens: well-nourished or malnourished gold? Geology 29, 539-542.

Gutscher, M.A., Maury, R., Eissen, J.P., Bourdon, E., 2000. Can slab melting be caused by flat subduction? Geology 28, 535-538.

Hanson, R.E., Gose, W.A., Crowley, J.L., Ramezani, J., Bowring, S.A., Bullen, D.S., Hall, R.P., Pancake, J.A., Mukwakwami, J., 2004. Paleoproterozoic intraplate magmatism and basin development on the Kaapvaal Craton: age, paleomagnetism and geochemistry of ~1.93 to ~1.87 Ga post-Waterberg dolerites. South African Journal of Geology 107, 233-254.

Hasui, Y., Haraly, N.L.E., Schobbenhaus, C., 1993. Megaestruturação Pré-Cambriana do território brasileiro baseada em dados geofísicos e geológicos. Geociências 12, 7-31.

Heiken, G, Wohletz, K., 1987. Tephra deposits associated with silicic domes and lava flows. GSA Special Paper 212.

Heiken, G., Krier, D., McCormick, T., Snow, M.G., 2000. Intracaldera volcanism and sedimentation — Creede caldera, Colorado. In: Bethke, P.M., Hay, R.L. (Eds.), Ancient Lake Creede: Its volcano-tectonic setting, history of sedimentation, and relation to mineralization in the Creede Mining District. Geological Society of America Special Paper, 346. Boulder, Colorado, 127-157.

Hofmann, A.W., 1988. Chemical differentiation of the Earth: The relationship between mantle, continental crust and oceanic crust. EPSL 90, 297-314.

Hollocher, K., Robinson, P., Walsh, E., Roberts, D., 2012. Geochemistry of amphibolite-facies volcanics and gabbros of the Støren Nappe in extensions west and southwest of Trondheim, Western Gneiss Region, Norway: a key to correlations and paleotectonic settings. American Journal of Science 312, 357-416.

Juliani, C., 2002. Alteração hidrotermal e metalogênese em sistemas vulcano-plutônicos paleoproterozóicos na Província Aurífera do Tapaj, Cráton Sul Amazônico, Pará. Tese de Livre-Docência, IG/USP.

Juliani, C., Vasquez, M.L., Klein, E.L., Villas, R.N., Echeverri-Misas, C.M., Santiago, E.S.B., Monteiro, L.V.S., Carneiro, C.C., Fernandes, C.M.D., Usero, G., 2014. Metalogenia da Província Tapajós. In: Silva M.G.; Jost H.; Kuyumajian R.M. (Org.). Metalogênese das Províncias Tectônicas Brasileiras. 1 ed. : CPRM — Serviço Geológico do Brasil 1, 51-90.

Juliani, C., Rye, R.O., Nunes, C.M.D., Snee, L.W., Correa Silva, R.H., Monteiro, L.V.S., Bettencourt, J.S., Neumann, R., Neto, A.A., 2005. Paleoproterozoic high sulphidation mineralization in the Tapajós gold province, Amazonian Craton, Brazil: geology, mineralogy, alunite argon age, and stable-isotope constraints. Chemical Geology 215, 95-125.

Juliani, C., Fernandez C.M.D., 2010. Well-preserved Late Paleoproterozoic volcanic centers in the São Félix do Xingu region, Amazonian Craton, Brazil. Journal of Volcanology and Geothermal Research 191, 167-179.

Kay, S.M., Godoy, E., Kurtz, A., 2005. Episodic arc migration, crustal thickening, subduction erosion, and magmatism in the south_central Andes. Geological Society of America Bulletin 117, 67-88.

Klein, E.L., Almeida, M.E., and Costa, L.T.R., 2012. The 1.89-1.87 Ga Uatumã Silicic Large Igneous Province, northern South America: Large Igneous Provinces Commission: http://www.largeigneousprovinces.org/12nov (accessed 12 January 2012).

Klein, E.L., Santos, R.A., Fuzikawa, K., Angélica, R.S., 2001. Hydrothermal fluid evolution and structural control of the brittle-style Guarim lode-gold mineralisation, Tapajós Province, Amazonian Craton, Brazil. Miner. Depos. 36, 149-164.

Klein, E.L., Vasquez, M.L., Rosa-Costa, L.T., Carvalho, J.M.A., 2002. Geology of Paleoproterozoic gneiss- and granitoid-hosted gold mineralization in Southern

Tapajós Gold Province, Amazonian Craton, Brazil. Intern. Geol. Rev., 44, 544-558.

Klein, E.L., Rosa-Costa, L.T., Carvalho, J.M.A., 2004. Estudo de inclusões fluidas em veio de quartzo aurífero do prospecto Patinhas, Província Aurífera do Tapajós, Cráton Amazônico. RBG 34, 59-66.

Lagler, B., Juliani, C., Pessoa, F.F., Fernandes, C.M.D., 2011. Petrografia e geoquímica das sequências vulcânicas Paleoproterozóicas na região de Vila Tancredo, São Félix do Xingu (PA). In: SBGq, Congr. Bras. Geoquí., 13, e Simp. Países do Mercosul, 3, Gramado, RS. Anais, [CD-ROM].

Lamarão, C.N., Dall'Agnol, R., Lafon, J.M., Lima, E.F., 1999. As associações vulcânicas e plutônicas de Vila Riozinho e Morais Almeida, Província Aurífera do Tapajós, SW do estado do Pará. In: Simpósio sobre Vulcanismo e Ambientes Associados. 1, Gramado*/RS, Boletim de resumos, 93 (in Portuguese).

Lamarão, C.N., Dall'agnol, R., Lafon, J.M., Lima, E.F., 2002. Geology, geochemistry, and Pb-Pb zircon geochronology of the Paleoproterozoic magmatism of Vila Riozinho, Tapajós Gold Province, Amazonian craton, Brazil. Prec. Res. 119, 189-223.

Lamarão, C.N., Dall'agnol, R., Pimentel, M.M., 2005. Nd isotopic composition of Paleoproterozoic volcanic rocks of Vila Riozinho: Implications for the crustal evolution of the Tapajós gold province, Amazon craton. J. South Am. Earth Sci. 18, 277-292.

Legros, F., Kelfoun, K., 2000. On the ability of pyroclastic flows to scale topographic obstacles. J. Volcanol. Geotherm. Res. 98, 235-241.

Lenhardt, N., Hornung, J., Hinderer, M., Böhnel, H., Torres-Alvarado, I.S., Trauth, N., 2011. Build-up and depositional dynamics of an arc front volcaniclastic complex: the Miocene Tepoztlan Formation (Transmexican Volcanic Belt, Central Mexico). Sedimentology 58, 785-823.

Lenhardt, N., Eriksson, P., Catuneanu, O., Bumby, A.J., 2012. Nature of and controls on volcanism in the ca. 2.32-2.06 Ga Pretoria Group, Transvaal Supergroup, Kaapvaal Craton, South Africa. Precambrian Reasearch 214-215, 106-123.

Lenhardt, N., Masango S.M., Jolayemi, O.O., Lenhardt, S.Z., Peeters, G.J., Eriksson, P.G., 2017. The Palaeoproterozoic (~2.06 Ga) Rooiberg Group, South Africa: Dominated by extremely high-grade lava-like and rheomorphic ignimbrites? New observations and lithofacies analysis. Journal of African Earth Sciences 131, 213-

232.

Lesti, C., Porreca, M., Giordano, G., Mattei, M., Cas, R.A.F., Wright, H.M.N., Folkes, C.B., Viramonte, J., 2011. High-temperature emplacement of the Cerro Galán and Toconquis Group ignimbrites (Puna plateau, NW Argentina) determined by TRM analyses. Bull. Volcanol. 73, 1535-1565.

Lofgren, G., 1971. Spherulite textures in glassy and crystalline rocks. J. Geophys. Res. 76, 5635-5648.

Ludwig, K.R., 2009. Isoplot 4.1. A geochronological toolkit for Microsoft Excel. Berkeley Geochronology Center special publication 4, 76.

Macambira, E.M.B., 1997. Geologia e aspectos metalogenéticos dos elementos do grupo de platina no complexo máfico-ultramáfico da serra da Onça – sul do Pará. Tese de Mestrado, UFPA, Belém, Pará, Brasil.

Macambira, E.M.B., Vale, A.G., 1997. Programa Levantamentos Geológicos Básicos do Brasil. São Félix do Xingu. Folha SB-22-Y-B. Estado do Pará, CPRM, Brasília (in Portuguese).

Manea, V.C., Pérez-Gussinyé, M., Manea, M., 2012. Chilean flat-slab subduction controlled by overriding plate thickness and trench rollback. Geology 40 (1), 35-38.

Manville, V., Németh, K., Kano, K., 2009. Source to sink: A review of three decades of progresss in the understanding of volcaniclastic processes, deposits, and hazards. Sedimentary Geology 220, 136-161.

McPhie, J., Doyle, M., Allen, S.R., 1993. Volcanic textures: A guide to the interpretation of textures in volcanic rocks, Centre for Ore Deposit and Exploration Studies. University of Tasmania, 198.

Miall, A.D., 1996. The Geology of Fluvial Deposits: Sedimentary Facies, Basin Analysis, and Petroleum Geology. Springer-Verlag, New York. 582.

Minifie, M.J., Kerr, A.C., Ernst, R.E., Hastie, A.R., Ciborowski, T.J.R., Desharnais, G., Millar, I.L., 2013. The northern and southern sections of the western ca. 1880 Ma Circum-Superior Large Igneous Province, North America: the Pickle Crow dyke connection? Lithos 174, 217-235.

Monteiro, L.V.S., Xavier, R.P., de Carvalho, E.R., Hitzman, M.W., Johnson, C.A., de Souza Filho, C.R., Torresi, I., 2008. Spatial and temporal zoning of hydrothermal alteration and mineralization in the Sossego iron oxide-copper-gold deposit, Carajás Mineral Province, Brazil: paragenesis and stable isotope constraints.

Formatted: Normal, Left, Indent: Left: 0 cm, Hanging: 0.75 cm, Line spacing: 1.5 lines, No widow/orphan control, Don't adjust space between Latin and Asian text, Don't adjust space between Asian text and numbers

Miner Deposita 43, 129-159.

Mori, L., Gómez-Tuena, A., Cai, Y., Goldstein, S., 2007. Effects of prolonged flat subduction on the Miocene magmatic record of the central Trans-Mexican Volcanic Belt. Chemical Geology 244, 452-473.

Mori, P.E., Reeves, S., Correia, C.T., Haukka, M., 1999. Development of a fused glass disc XRF facility and comparison with the pressed powder pellet technique at Instituto de Geociências. Rev. Bras. Geociências, 29, 441-446.

Mueller, W.U., Concoran, P.L., 1998. Late-orogenic basins in the Archaean Superior Province, Canada: characteristics and inferences. Sedimentary Geology 120, 177-203.

Mueller, W.U., Chown, E.H., Thurston, P.C:, 2000a. Processes in physical volcanology and volcaniclastic sedimentation: modern and ancient. Precambrian Research 101, 81-85.

Navarro, M.S., Andrade, S., Ulbrich, H.H.G.J., Gomes, C.B., Girardi, V.A.V., 2008. The analysis of rare earth elements with ICP-MS in basaltic and related rocks: testing the efficiency of sample decomposition procedures. Geostand. Geoanal. Res. 32(2),167-180.

Németh, K., Cronin, S.J., Stewart, R.B., Charley, D., 2009. Intra- and extra- caldera volcaniclastic facies architecture of a frequently active mafic island-arc volcano, Ambryn Island, Vanuatu. Sedimentary Geology 220, 256-270.

Oberholzer, J.D., Eriksson, P.G., 2000. Subaerial volcanism in the Palaeoproterozoic Heekpoort Formation (Transvaal Supergroup), Kaapvaal craton. Precambrian Research 101, 193-210.

Pearce, J.A., Harris, N.B.W., and Tindle, A.G., 1984. Trace element discrimination diagrams for the tectonic interpretation of granitic rocks. Journal of Petrology 25, 956-983.

Pearce, 1996………………

Pessoa M.R., Santiago A.F., Andrade A.F., Barreto E.L., Nascimento J.O., Santos J.O.S., Oliveira J.R., Lopes R.C., Prazeres W.V. 1977. Projeto Jamanxim. CPRM/DNPM, 1-3, 614.

Pierosan, R., Lima, E.F., Nardi, L.V.S., Bastos Neto, A.C., Campos, C.P., Jarvis, K., Ferron, J.M.T.M., Prado, M., 2011. Geochemistry of Palaeoproterozoic volcanic rocks of the Iricoumé Group, Pitinga Mining District, Amazonian craton, Brazil: International Geology Review 53, 946-979.

Pinho, S.C.C., Fernandes, C.M.D., Teixeira, N.P., Paiva Jr., A.L., Cruz, V.L., Lamarão, C.N., Moura, C.A.V., 2006. O magmatismo paleoproterozóico da região de São Félix do Xingu, Província Estanífera do Sul do Pará: Petrografia e geocronologia. Revista Brasileira de Geociências 36, 793-802.

Pioli, L., Rosi, M., 2005. Rheomorphic structures in a high-grade ignimbrite: the Nuraxi tuff, Sulcis volcanic district (SW Sardinia, Italy). Journal of Volcanology and Geothermal Research 142, 11-28.

Polo, L.A., Giordano, D., Janasi, V., Freitas-Guimaraes, L., 2017(a). Effusive silicic volcanism in in the Paraná Magmatic Province, South Brazil: Physico-chemical conditions of storage and eruption and considerations on the rheological behaviour during emplacement. J. Volcanol. Geoth. Res. 355, 115-135.

Polo L.A., Janasi V., Giordano D., Lima E.F., Cañon-Tapia E., Roverato M., 2017(b). Effusive silicic volcanism in the Paraná Magmatic Province, South Brazil: Evidence for locally-fed lava flows and domes from detailed field work. J. Volcanol. Geoth. Res. 355, 204-218.

Quane, S. L., Russell, J. K., 2005. Welding: Insights from high-temperature analogue experiments. Journal of Volcanology and Geothermal Research 142 (1-2), 67-87.

Reis, N.R., Almeida, M.E., Ferreira, A.L., Riker, S.R., 2006. Geologia e Recursos Minerais do Estado do Amazonas. Sistema de Informações Geográficas 1:1.000.000. CPRM, Manaus, 144.

Rino, S., Tsuyoshi, K., Windley, B.F., Katayama, I., Motoki, A., Hirata, T., 2004. Major episodic increases of continental crustal growth determined from zircon ages of river sands; implications for mantle overturns in the Early Precambrian. Physics of the Earth and Planetary Interiors 146, 369-394.

Roverato, M., Capra, L., Sulpizio, R., Norini, G., 2011. Stratigraphic reconstruction of two debris avalanche deposits at Colima Volcano (Mexico): insights into pre-failure conditions and climate influence. J. Volc. Geoth. Res. 207 (1), 33-46.

Roverato, M., Cronin, S., Procter, J., Capra, L., 2014. Textural features as indicators of debris avalanche transport and emplacement, Taranaki volcano. Geol. Soc. Am. Bull. B30946-1

Roverato, M., 2016. The Montesbelos mass-flow (southern Amazonian craton, Brazil): a Paleoproterozoic volcanic debris avalanche deposit? Bull. Volcanol. 78, 49.

Roverato, M., Giordano, D., Echeverri-Misas, CM., Juliani, C., 2016. Paleoproterozoic felsic volcanism of the Tapajós Mineral Province, Southern

Amazon Craton, Brazil. Journal of Volcanology and Geothermal Research 310, 98-106.

Roverato, M., Juliani, C., Marcelo Dias-Fernandes, C., Capra, L., 2017. Paleoproterozoic andesitic volcanismin the southern Amazonian craton, the Sobreiro Formation: new insights from lithofacies analysis of the volcaniclastic sequences. Precambrian Research 289, 18-30.

Russell, J. K., Quane, S. L., 2005. Rheology of welding: Inversion of field constraints. Journal of Volcanology and Geothermal Research 142 (1-2), 173-191.

Santos, J.O.S., Hartmann, L.A., Gaudette, H.E., Groves, D.I., McNaughton, N.J., Fletcher, I.R., 2000. A new understanding of the provinces of the Amazon craton based on integration of field mapping and U_Pb and Sm_Nd geochronology. Gondwana Research 3, 453-488.

Santos, J.O.S., Groves D.I., Hartmann L.A., Moura M.A., McNaughton, N.J. 2001. Gold deposits of the Tapajós and Alta Floresta Domains, Tapajós-Parima orogenic belt, Amazon Craton, Brazil. Mineralium Deposita 36, 278-299.

Santos, J.O.S., 2003. Geotectônica dos Escudos da Guiana e Brasil Central. In: L.A. Bizzi, C. Schobbenhaus, R.M. Vidotti, J.H. Gonçalves (Eds.). Geologia, tectônica e recursos minerais do Brasil. Texto, mapas e SIG. CPRM - Serviço Geológico do Brasil, Brasília 169-226.

Santos, J.O.S., Van Breemen, O.B., Groves, D.I., Hartmann, L.A., Almeida, M.E., McNaughton, N.J., Fletcher, I.R., 2004. Timing and evolution of multiple Paleoproterozoic magmatic arcs in the Tapajós Domain, Amazon Craton: constraints from SHRIMP and TIMS zircon, baddeleyite and titanite U–Pb geochronology. Prec. Res. 13, 73-109.

Silva, F.S., Oliveira, D.C., Antonio, P.Y., D'Agrella-Filho, M., Lamarão, C.N., 2016. Bimodal magmatism of the Tucuma area, Carajás Province: U-Pb geochronology, classification and processes. J. S. Am. Earth Sci. 72, 95-114.

Simões, M.S., Lima, E.F., Sommer, C.A., Rossetti, L.M.M., 2017. Structures and lithofacies of inferred silicic conduits in the Paraná-Etendeka LIP, southernmost Brazil. Journal of Volcanology and Geothermal Research 355, 319-336.

Sulpizio, R., Mele, D., Dellino, P., La Volpe, L., 2007. Deposits and physical properties of pyroclastic density currents during complex Subplinian eruptions: the AD 472 (Pollena) eruption of Somma-Vesuvius, Italy. Sedimentology 54, 607-635.

Sumner, J.M., Branney, M.J. 2002. The emplacement history of a remarkable heterogeneous, chemically zoned, rheomorphic and locally lava-like ignimbrite: 'TL' on Gran Canaria. Journal of Volcanology and Geothermal Research 115, 109-138.

Tassinari, C.C.G., Macambira, M.J.B., 1999. Geochronological provinces of the Amazonian craton. Episodes 22, 174-182.

~~Teixeira, W., Tassinari, C.C.G., Cordani, U.G., Kawashita, K., 1989. A review of the geochronology of the Amazonian craton: tectonic implications. Precambrian Res. 42, 213-227.~~Teixeira, M.F.B., Dall'Agnol, R., Santos, J.O.S., Oliveira, D.C., Lamarão, C.N., McNaughton, N.J., 2018. Crystallization ages of Paleoproterozoic A-type granites of Carajás province, Amazon craton: Constraints from U-Pb geochronology of zircon and titanite. J. of South American Earth Sciences 88, 312-331.

Teixeira, N.P., Bettencourt, J.S., Moura, C.A.V., Dall'Agnol, R., Macambira, E.M.B., 2002. Archean crustal sources for Paleoproterozoic tin-mineralized granites in the Carajas Province, SSE Para, Brazil: Pb_Pb geochronology and Nd isotope geochemistry. Precambrian Research 119, 257-275.

Teixeira, W., Tassinari, C.C.G., Cordani, U.G., Kawashita, K., 1989. A review of the geochronology of the Amazonian craton: tectonic implications. Precambrian Res. 42, 213-227.

Teixeira, W., Nelson, J.R., Bettencourt, J.S., Klein, E.L., Oliveira, D.C., 2019. Intraplate Proterozoic magmatism in the Amazonian Craton reviewed: geochronology, crustal tectonics and global matches. In book: Dyke Swarms of the World: A Modern Perspective. DOI:10.1007/978-981-13-1666-1_4

Van Kranendonk, M.J., 2006. Volcanic degassing, hydrothermal circulation and the flourishing of early life on Earth: a review of the evidence from c. 3490-3240 Ma rocks of the Pilbara Supergroup, Pilbara Craton, Western Australia. Earth Science Rev. 74, 197-240.

Vasquez, M.L, Klein, E.L, Macambira, M.J.B., Santos, A., Bahia, R.B.C., Ricci, P., dos, S.F., Quadros, M.L.E.S., 2000. Geochronology of granitoids, mafic intrusions and mineralizations of the Tapajós Gold Province - Amazonian Craton - Brazil. In: Inter. Geol. Congr. 31, Abstracts, [CD-ROM].

Vasquez, M.L., Sousa, C.S., Carvalho, J.M.A., 2008. Mapa Geológico e de Recursos

Formatted: Font color: Auto

Formatted: Font: (Default) Times New Roman, 11 pt, No underline

Minerais do Estado do Pará, escala 1:1.000.000. Programa Geologia do Brasil, Belém, CPRM.

Vasquez, M.L., Dreher, A.M. 2011. Uma avaliação da estratigrafia dos eventos magmáticos de 1900-1860 Ma do Cráton Amazônico. In: SBG, Simp. Geol. Amaz. 12, Bol. Res. [CD ROM].

Walker, G.P.L., 1983. Ignimbrite types and ignimbrite problems. J. Volcanol. Geotherm. Res. 17, 65-88.

Went, D.J., 2016 Alluvial fan, braided river and shallow-marine turbidity current deposits in the Port Lazo and Roche Jagu formations, Northern Brittany: relationships to andesite emplacements and implications for age of the Plourivo-Plouézec Group. Geol. Mag. 1-24, Cambridge University Press 2016.

White, J.D.L., Houghton, B.F., 2006. Primary volcaniclastic rocks. Geological Society of America Bulletin 34, 677-680.

Willcock, M.A.W., Cas, R.A.F., Giordano, G., Morelli, C., 2013. The eruption, pyroclastic flow behaviour, and caldera in-filling processes of the extremely large volume (N1290 km3), intra- to extra-caldera, Permian Ora (Ignimbrite) Formation, Southern Alps, Italy. J. Volcanol. Geotherm. Res. 265, 102-126.

Williams, I,S., 1998. U-Th-Pb geochronology by ion microprobe. In: McKibben, M.A., Shanks, W.C.P., Ridley, W.I. (eds) Applications of Microanalytical Techniques to Understanding Mineralizing Processes, Rev Econ Geol vol 7. Soc. Econ. Geol, Littleton, 1-35.

Wolff, J.A., Wright, J.V., 1981. Rheomorphism of welded tuffs. Journal of Volcanology and Geothermal Research 10, 13-34.

Zanchetta, G., Sulpizio, R., Di Vito, M.A., 2004. The role of volcanic activity and climate in alluvial fan growth at volcanic areas: an example form southern Campania (Italy). Sedimenatry Geology 168, 249-280.

Zernack, A.V., Cronin, S.J., Neall, V.E., Procter, J.N., 2011. A medial to distal volcaniclastic record of an andesitic stratovolcano: detailed stratigraphy of the ring-plain succession of south-west Taranaki, New Zealand: International Journal of Earth Sciences 100, 1937-1966.

Zhao, G., Cawood, P.A., Wilde, S.A., Sun, M., 2002. Review of global 2.1–1.8 Ga orogens: implications for a pre-Rodinia supercontinent. Earth-Science Reviews 59, 125-162.

Zhao, G., Sun, M., Wilde, S.A., Li, S., 2004. A Paleo-Mesoproterozoic supercontinent:

assembly, growth and breakup. Earth-Science Reviews 67, 91-123.

Figure Captions

Figure 1: location map of the northern South America and the Amazonian C~~e~~raton ~~and~~ divided into several~~its~~ geochronological provinces and other domains according to Santos et al. (2000); TMP = Tapajós Mineral Province, SFX = São Felix do Xingú Region. ~~; G = Guyana, GF = French Guyana, S = Suriname.~~

Figure 2: distribution map of the outcrops analyzed during the field campaigns in both regions a) Tapajós Mineral Province (TMP) and b) São Felix do Xingú region (SFX); PW=distribution of the Santa Rosa formation inferred during the present work; F=distribution of the Santa Rosa formation inferred by Fernandes et al. (2011); BIF=Banded Iron Formation; red and white dot refers to primary andesitic deposits analyzed in Roverato et al. (2017).~~.~~ In both figures are reported the outcrops described in the paper.

Figure 3: massive and banded lavas and rheo-ignimbrite (?) deposits. a) Np173 (7º33'52.31" S, 55º10'58.80" W), b) Xu23 (6º41'08.65" S, 52º25'55.67" W), c) Xu101 (6º52'12.82" S, 52º09'16.12" W), d) Xu52 (6º28'19.32" S, 51º50'08.90" W), e), f), g) Np396 (6º32'41.06" S, 55º23'59.37" W); see Fig. 2 for the outcrops location. For the lithofacies description and more details see the text.

Figure 4: massive primary volcaniclastic rocks with different proportion of ash, lapilli and blocks. All the deposits are interpreted to be emplaced from pyroclastic density currents except (f) that is interpreted as a basal-breccia of a lava body. a) Xu104 (6º52'22.96" S, 52º08'15.91" W), -b) Np183 (7º32'04.13" S, 55º08'50.02" W), c) Np93 (6º44'16.60" S, 55º27'12.96" W), d) Xu29 (6º41'42.51" S, 52º01'23.06" W), e) Xu07 (6º41'56.36" S, 52º08'42.27" W) f) Xu192 (6º31'31.92" S, 53º02'36.60" W); see Fig. 2 for the outcrops location. For the lithofacies description see the text and Table 1.

Figure 5: microphotographs of different massive ash and lapilli ignimbrite deposits in

thin section: a) broken crystals suggesting the fragmental character of the rock; b) detail of a devitrified juvenile (?) fragment displaying axiolitic fabric; c) banded sub-millimetric to millimetric lithic fragments immersed in a devitrified groundmass.

Figure 6: reconstructed schematic stratigraphic column and associated photographs representing the evolution of ignimbrite deposits cropping out in the TMP (Np183; 7º32’04.13” S, 55º08’50.02” W); note the increase of welding from the base to the top.

Figure 7: schematic stratigraphic column and relative photographs of a >150 m thick felsic banded lava(s) cropping out in SFX (Xu192; 6º31’31.92” S, 53º02’36.60” W) overlying a basal breccia (Lf mLB) and an ignimbrite deposit characterized by a low grade of welding (Lf *l-gw*LA).

Formatted: Font: Not Italic, No underline

Figure 8: stratified primary volcaniclastic rocks, a) related to sedimentation by highly dilute ash-cloud (Np130; 6º54’16.09” S, 55º10’59.38” W) and, b) -attribute to pyroclastic surge-type depositional condition from dilute currents (XU162; 6º32’28.39” S, 52º25’26.07” W); see Fig. 2 for the outcrops location.. Relative thin section microphotographs (cb/d) showing micrometric shards. For the lithofacies description see the text and Table 1.

Figure 9: massive sedimentary rocks.. (a) -The alternation of lithofacies *csG* and *mS* indicates changes in energy conditions of sedimentation belonging to a subaqueous-subaerial fan-delta interface (Np146; 6º42’58.24” S, 55º28’53.49” W);. (b) dDetail of centimeters ripples of Lf *mS* (Np89; 6º54’39.36” S, 55º26’12.28 W);. (c) -Lf *csG* is also associated to Lf *xsSG* (see stratified rocks in section 6.2) (Np27; 8º08’18.43” S, 54º54’37.33” W).. (d) Np27, /e/f) e) Xu209 (6º13’55.26” S, 52º42’29.25” W), f) Np158 (7º03’33.79” S, 55º24’11.84” W); tThe rounded and clast supported character of these lithofacies is linked with fluvial/alluvial deposition by debris-flow dominated processes; see Fig. 2 for the outcrops location.. -For a more detailed lithofacies description see the text and Table 1.

Figure 10: stratified sedimentary rocks. (a) The quartzitic sandy cross-bedded lithofacies is interpreted as formed in fluvial channel or around margins of immature marine basins (?) (Xu 201; 6º16’12.95” S, 52º52’18.84” W);. (b) tThe cross-stratified

water reworked lithofacies is linked with stream-dominated fluvial/alluvial settings (Np82; 8º03’40.79” S, 54º50’43.52” W); ~~.~~ ~~(~~c)~~-~~ t~~T~~he silty sedimentation likely belong to a lacustrine environment characterized by small turbidities (Np158; 7º03’33.79” S, 55º24’11.84” W);~~.~~ ~~(~~d) ~~-~~t~~T~~he top of the photographs shows the Lf *bChs* interpreted as inorganic precipitation of silica (chert) in a closed lake basin; white arrows show fragments of the chert deposit eroded by low-energy sandy stream flows or local lacustrine turbidites (Np90; 6º49’50.20” S, 55º28’15.47” W); see Fig. 2 for the outcrops location.~~.~~ For a more detailed lithofacies description see the text and Table 1.

Figure 11: sketch of a wide (300 x 80 m) outcrop in the TMP (Np407; 6º40’35.21” S, 55º21’14.63” W). The stratigraphic sequence is tilted showing sub-vertical contacts of the different deposits. The sequence is interpreted displaying at the base banded (or rheo-ignimbrite) and massive lava flows passing to fragmental deposits to the top. ~~(~~a) ignimbrite medium-grade welded; b) the diffuse-stratified lithofacies indicates tractive processes usually attribute to pyroclastic surge-type depositional condition from dilute currents; c) sedimentary clast-supported deposit ~~(see descriptions in chapter 4.3)~~; d) non-welded lapilli to ash ignimbrite; e) banded lava o highly reomorphic ignimbrite (lava-like). For a more detailed lithofacies description see the text and Table 1.

Figure 12: classification diagrams for the Tapajos volcanics (TMP-V) and lava flow (TMP-LF). TAS diagram with limits of alkaline series from Kuno (1968), dashed line, and Irvine and Baragar (1971), solid line. AFM diagram with alkaline field from Irvine and Baragard (1971). SiO2 vs K2O classification diagram (Ewart, 1982). Literature values are from: VR (a) Vila Rozinho and MA (a) Moraes Almeida volcanic sequences from Lamarão et al. (2002); SF (b) Sobreiro Formation and~~,~~ SRF (b) Santa Rosa Formation from Fernandes et al. (2011).

Figure 13: REE and spider-diagrams of volcanics and lava flow rocks from the Tapajos region (TMP-V and TMP-LF). REE data are normalized to Chondrite I (CI; values from Ander and Ebihara, 1982) and trace elements are normalized to Mid Ocean Ridge Basalt (MORB; values from Hoffman, 1988). Literature values are from: VR (a) Vila Rozinho and MA (a) Moraes Almeida volcanic sequences are average values from Lamarão et al. (2002);~~,~~ SRF (b) Santa Rosa Formation from Fernandes et al. (2011)

divided in -V volcanoclastics and -LF lava flow. Due to the lack of literature data, comparison of VR (a) and MA (a) is reported only for REE diagram.

Figure 14: tectonic affinity discriminant diagrams for the Tapajos volcanics (TMP-V) and lava flow (TMP-LF). Zr+Nb+Ce+Y (ppm) vs FeO_{tot}/MgO (wt.%) diagram. Yb vs Ta diagram. La/Yb vs Nb/La diagram. Th-Ta-Hf/3 diagram. Literature values are from: VR (a) Vila Rozinho and MA (a) Moraes Almeida volcanic sequences from Lamarão et al. (2002);, SF (b) Sobreiro Formation and SRF (b) Santa Rosa Formation from Fernandes et al. (2011).

Figure 15: geochronological U-Pb data from Tapajos zircons. Average $^{206}Pb/^{207}Pb$ age (errors are calculated as 2σ) of the three samples. Probability density plot of $^{206}Pb/^{207}Pb$ ages. Calculated concordia age for sample NP396 (lava flow) and NP183 (ignimbrite).

Figure 16: geochronological U-Pb data from Xingu zircons. Calculated concordia age for ignimbrite sample XU-08. Probability density plot of $^{206}Pb/^{207}Pb$ ages.

Figure 17: peleogeographic reconstruction of the fissural and calderic volcanic activity during the Late-Paleoproterozoic in the southern part of the Amazonian craton. In the foreground is shown a section of a caldera and a post-caldera ignimbrite uplift that could facilitate the production of new sediments to be reworked and transported. The rising magma could form sporadic intra-caldera domes and volcanic centers as also shown in the background calderas. Reworked sediments can accumulate into volcano-tectonic depressions, which often collects intra-caldera lakes. In the background a fissure-fed volcanism is the responsible of the emission of lava flows and/or high-grade to rheomorphic ignimbrites. Fluvial deposits that occur throughout all successions represent periods of stream and river reworking. The area in punctuated by little scoria cones and maars that contribute to the amount of the fragmental products well represented in the study regions.

Tables

Table 1: Summary of the main characteristics of volcaniclastic lithofacies of the primary and secondary~~felsic~~ products analyzed and their interpretation.

Table 2: Major and trace element bulk rock composition of Tapajos samples. Class identify the lithological features of the rocks: VC: volcanoclastic; I: ignimbrite; R: rhyolite; Type identify the geochemical affinity according to the granite classification (Zr+Nb+Ce+Y (ppm) vs FeO_{tot}/MgO (wt.%) diagram, Fig. 14): I is for I-type granites and A is for A-type granites; b.d.l. is below detection limits; Mg# is calculated as Mg^{2+} / (Fe^{2+}_t + Mg^{2+}); (*) major elements analyses already published in Roverato et. (2016). ~~Table 2: Major and trace element bulk rock composition of Tapajos samples. VC: volcanoclastic; I: ignimbrite; R: rhyolite; b.d.l. is below detection limits; Mg# is calculated as Mg^{2+} / (Fe^{2+}_t + Mg^{2+}); (*) major elements analyses already published in Roverato et. (2016).~~

The 2.0-1.88 Ga Paleoproterozoic evolution of the southern Amazonian Craton (Brazil): an interpretation inferred by lithofaciological, geochemical and geochronological data.

Roverato*[1,2] M., Giordano[3,4] D., Giovanardi[5] T., Juliani[2] C., Polo[2] L.

1. YachayTech University, School of Geological Sciences and Engeneering, Hacienda San José, Urcuquí, Ecuador.
2. Instituto de Geociências (IGC), Universidade de São Paulo, INCT – Geociam, SP, 05508080, Brazil.
3. Universitá degli studi di Torino, Dipartimento di Scienze della Terra, via Valperga Caluso 35, 10125, Torino, Italy.
4. Centro Nazionale delle Ricerche (CNR), Istituto di Geoscienze e Georisorse (IGG), via G. Moruzzi 1, 56124, Pisa, Italy.
5. Universitá di Modena e Reggio Emilia, Dipartimento di Scienze Chimiche e Geologiche, 41125, Modena, via Campi 103, Italy.

*Corresponding author: matteoroverato1809@gmail.com

Keywords: Paleoproterozoic volcanism; Amazonian craton; Fissure eruption; Felsic volcanism; Lithofacies analyses

Abstract

The study of Paleoproterozoic rocks is crucial for understanding Earth's tectonic evolution during the time when most of the modern crust and ore deposits were formed. The rocks of the Brazilian Amazonian Craton record some of the most-complete and best-preserved Paleoproterozoic magmatic and volcanic episodes on Earth. Following previous investigations, we present new lithofaciological and stratigraphic records of the felsic rocks of the Tapajós Mineral Province (TMP) (~ 2-1.88 Ga) and the São Felix do Xingú region (SFX) (~ 1.88 Ga) which, combined with new petrological and geochronological data, help providing a more complete understanding of the tectonic, magmatic and volcanological evolution of the Amazonian Craton. This magmatism/volcanism is thought to be formed in a late-/post-orogenic to extentional regime confirmed by the new geochemical data presented here.

The transition from late-convergent to extensional tectonic setting could register the beginning of the taphrogenesis that marked the Amazonian Craton throughout the Mesoproterozoic. The volcanological approach of this contribution can serve as a strategy for the modelling of the evolution of Precambrian volcano-sedimentary basins around the world. The large amount of rocks analyzed are divided into primary and secondary volcaniclastic products depending on if they resulted from a direct volcanic activity (pyroclastic) or processes that reworked pyroclastic fragments. Furthermore, the deposits are subdivided into massive and stratified, depending on their primary mechanisms of transport and emplacement. By confirming the results from previous studies, our study permits to depict a more precise paleo-environmental picture of the processes that occurred in the Amazonian Craton during the Late-Paleoproterozoic. In particular, the presence of large regional-scale fissural systems and caldera collapses produced large silicic explosive volcanic eruptions, also accompanied by the emission of large volume effusive products. Although studies on the Amazonian Craton are still scarce and controversial, the present study provides new evidence that this volcanism may have formed one of the largest Silicic Large Igneous Provinces (SLIP) on earth. Our data also confirm that at least two major Paleoproterozoic periods of formation of volcanic rocks exist in the Amazonian craton. This point is of great relevance for any future interpretation of the geological evolution of this craton.

1. Introduction

The Proterozoic Eon (2500 – 541 Ma) is the longest and youngest part of the Precambrian Supereon. This Eon represents the time just before the proliferation of oxygen accumulation and complex life on Earth. This period was likely the most tectonically active in Earth's history. In fact, it is also the period during which the largest portion of the modern crust (43%) and mineral ores were produced (Condie, 2000). Studies by Condie (2000) and Rino et al. (2004) suggest that crust production took place episodically, forming predominantly granitoidal crust and secondary volcanic and metamorphic rocks, some of which are extraordinarily well preserved. The Amazonian Craton (AC) is one of the largest preserved Precambrian terrains in the world ($4.6x10^6$ km^2) (Almeida et al., 1981). It occupies approximately half of the Brazilian territory and it is the location of important mineral resources such as gold, iron, copper, and tin, among others (e.g. Faraco et al., 1997; Bahia and Quadros, 2000; Juliani, 2002; Klein et al., 2002, 2004; Reis et al., 2006; Klien and Carvalho, 2008;

Monteiro et al., 2008; Juliani et al., 2014, Dall'Agnol et al., 2017). Although the geological investigation of the AC has recently seen a renewed interest of the national and international scientific community, mainly because of the massive presence of ore deposits, a general consensus related to the interpretation of its complex Paleoproterozoic evolution is still missing. Ancient volcanic regions represent a challenge for the understanding of emplacement dynamics especially when the stratigraphic relationships are difficult to decipher or blurred by erosion or vegetation cover. The present work constitutes the natural prosecution of previous investigations, carried out by our research group (Juliani et al., 2005, 2010, 2014; Fernandes et al., 2011; da Cruz et al., 2015; Roverato, 2016; Roverato et al., 2016, 2017), which are devoted to characterize the dynamics of emplacement of Precambrian volcanic rocks and their relationships to sedimentary facies. The study area comprises of the Tapajós Mineral Province (TMP) and the São Felix do Xingú (SFX) region, Pará state, northern Brazil. This contribution provides a means to interpret the volcanic processes active in this region during the Precambrian, mainly based on field observation and detailed lithofacies analyses. In addition, new geochemical and geochronological data are provided. Our study demonstrates how powerful is the approach of rock structure and texture characterization to the interpretation of the eruptive processes that governed the emplacement of volcanic and volcaniclastic sequences. The detailed lithofacies characterization and the stratigraphic reconstruction are important in this area and constitute a powerful key-tool to appropriately interpret the evolution of Precambrian volcano-sedimentary basins. Such an approach would turn to be useful when employed to investigate ancient terrains associated both to the ancient Amazonian felsic volcanism and Precambrian terrains in general.

2. Geological evolution of the southern portion of the Amazonian craton

The AC (Almeida et al., 1981) is located in the northern part of South America and is divided into two Precambrian shields, the Central-Brazil (or Guaporé, southern portion) and Guiana Shields (northern portion), which are separated by the Phanerozoic Amazonian Sedimentary Basin (Fig. 1) (Almeida et al., 1981). The entire craton has become tectonically stable before the end of the Precambrian (Dall'Agnol et al., 1994).

It has also been considered (Amaral, 1974; Hasui et al., 1993; Costa and Hasui, 1997) as a large Archean platform that had been reworked and reactivated during the ca. 2100 Ma Trans-Amazonian event. Alternative proposals based on geochronological and isotopic data (Teixeira et al., 1989; Tassinari and Macambira, 1999; Santos et al., 2000) divided the craton into several, predominantly NW-oriented, geochronological provinces, which have been interpreted as successive continental accretionary events, followed by granitic magmatism and tectonic reworking (Santos, 2003; Vasquez et al., 2008).

In a recent review Teixeira et al. (2019) report that the AC is the host of four LIP-scale (or SLIP) magmatic events discriminated by the Orocaima, Uatumã, Avanavero and Rincón del Tigre events. The igneous rocks described in the present manuscript are widely attributed to the Uatumã event (Dall'Agnol et al., 1999; Lamarão et al., 1999). The studied region is located between TMP and SFX, which is considered to be related to a continental arc, with a NE-SW arc migration as suggested by Juliani and Fernandes (2010), Fernandes et al. (2011) and Roverato et al. (2017). According to these authors a migration from the Serra do Cachimbo graben (in TMP where the subduction trench is located) towards the SFX could be explained by a change in the subducting angle of the oceanic plate beneath the continental plate. This is in agreement with the flat-subduction plate settings proposed by previous authors in other parts of the world (Ferrari et al., 2012; Gutscher et al., 2000; Kay et al., 2005; Mori et al., 2007; Manea et al., 2012).

2.1. The TMP (Tapajós Mineral Province)

The TMP (Fig. 2a) is primarily situated in the Tapajós–Parima geochronological/tectonic province (Santos et al., 2000) with the eastern part belonging to the Amazonia Central geochronological/tectonic province (Fig. 1). Based on Sm–Nd data and U–Pb ages (2100–1870 Ma), Santos et al. (2001, 2004) and Vasquez et al. (2008), identified several different domains for the Tapajós–Parima geochronological province and consider the TMP as a sequence of continental magmatic arcs (Ferreira et al., 2000; Santos et al., 2000, 2004; Vasquez et al., 2000; Klein et al., 2001; Lamarão et al., 1999, 2002). Late Paleoproterozoic volcanism of the Tapajós domain is represented by the Vila Riozinho Formation, formed by ca. 2000-1990 Ma intermediate to acid volcanic rocks (Lamarão et al., 2002), and by the Iriri Group that can be divided into the Bom Jardim (Almeida et al., 2000), Salustiano (1870 ± 0.008 Ma; Juliani et al., 2005) and Aruri (Pessoa et al., 1977) formations.

The Bom Jardim Formation (1898 ± 5 Ma, Santos et al., 2001) consists of mafic to intermediate high-K to shoshonitic calc-alkaline rocks while the latter formations are characterized by rhyolites, dacites and their pyroclastic and epiclastic derivatives. Juliani et al. (2005) considered the Bom Jardim volcanism as a preliminary step of the Iriri event representing pre-caldera volcanism followed by the Salustiano and Aruri caldera-related felsic activity. Post-caldera volcanism is characterized by ring-felsic volcanic structures that produced A-type (Vasquez and Dreher, 2011) rhyolitic lavas and volcaniclastic deposits. Lamarão et al. (2002, 2005) described the felsic A-type Moraes Almeida volcanic sequence (1890 ± 6 Ma ryolite, 1875 ± 4 Ma ignimbite) represented by lavas and ignimbrites as part of the Iriri Group. Juliani et al. (2014) consider these last A-type rocks as similar in composition and age to the Santa Rosa Formation that crops out in the São Felix do Xingú region (SFX), which is considered to have formed by the same fissural-type volcanism (Juliani and Fernandes, 2010; Fernandes et al., 2011; Roverato et al., 2016). Preliminary data indicate that these rocks, for both TMP and SFX, display a very low grade of metamorphism, falling into the prehnite-pumpellyite field (Echeverri-Misas, 2010; Lagler et al., 2011; Fernandes et al., 2011).

2.2. The SFX (São Felix do Xingú region)

According to the work of Santos (2003) and Vasques et al. (2008) the SFX region belongs to the Amazonia Central province (Fig. 1). The study area (Fig. 2b) is located near to São Felix do Xingú city, which corresponds to the southern portion of the Carajás Province. The Paleoproterozoic volcanic sequences in the SFX comprise the basal Sobreiro and upper Santa Rosa formations (Macambira and Vale, 1997; Juliani and Fernades, 2010), which are crosscut by the Sn-bearing A-type granitoids of the Velho Guilherme Suite (Teixeira et al., 2002). Antonio et al. (2017) published the first U-Pb ages on zircons for the Santa Rosa Formation with 1877.4 ± 4.3 Ma for a rhyolite and 1895 ± 11 Ma for a dike. Recent geochronological data on a felsic porphyritic dike belonging to the Velho Guilherme suite yielded an age of 1857 ± 8.4 Ma (Shrimp U/Pb zircon analyses; Roverato, 2016). Other available geochronological data yielded ca. 1880 ± 6 Ma (TIMS Pb–Pb in zircon) for the Sobreiro Formation and ca. 1879 ±2 Ma (TIMS Pb–Pb in zircon) for the Santa Rosa Formation (Fernandes et al., 2011; Pinho et al., 2006; Teixeira et al., 2002). Despite their similar ages, their geochemical compositions, geological features and eruption styles point to their non-cogeneticity (Fernandes et al., 2011). The Sobreiro Formation (SF) comprises basaltic andesite, andesite and less dacite massive lava flows and volcanoclastic rocks with high-K calk-alkaline signature (Fernandes et al., 2011; Roverato et al., 2017). According to da Cruz et al. (2015) late- to post-magmatic hydrothermal alteration in these rocks is responsible for a secondary paragenesis characterized by epidote, chlorite, carbonate, clinozoisite, sericite, quartz, albite, hematite and pyrite. The Santa Rosa Formation (SRF) is described by Fernandes et al. (2011) as characterized by four lithological facies with A-type signature: (i) rhyolitic lava flow and thick dikes of banded rhyolite and ignimbrite; (ii) highly rheomorphic felsic ignimbrite associated with un-welded ash tuff; (iii) felsic crystal tuff, lapilli-tuff and co-ignimbritic breccias; (iv) granitic porphyry stocks and dikes and subordinate equigranular granitic intrusions.

3. Lithofacies analyses

Lithofaciological analyses were carried out in the course of this study in order to understand the geodynamic evolution of the study area. Here we report on the lithofacies analysis of rocks recognized during our field campaigns (and after in petrological thin section) at the TMP and SFX provinces. Within the study area (TMP and SFX), massive to banded lava flows and rheomorphic ignimbrites (Fig. 3) as well as felsic volcaniclastic rocks of various origin (Figs. 4-8, 11) are frequently found. Reworked (secondary) volcaniclastic rocks (Fig. 9,10) and sedimentary alluvial/coastal clastic deposits (epiclastic) are also widely distributed in both TMP and SFX areas. Primary volcaniclastic rocks are here defined as those fragmental products formed during a syn-eruptive explosion, which were deposited regardless of whether their transport occurs through air, water, granular debris or a combination of them (McPhie et al., 1993; White and Houghton, 2006, Manville et al., 2009; Roverato et al., 2017). On the other hand, all the units deposited as a consequence of a reworking process of pre-existing volcanic units are defined here as secondary volcaniclastic rocks. We also introduce into this group all those epiclatic products that constitute sediments that had been reworked before, independent of their source and composition. Table 1 shows a description and interpretation of the volcaniclastic lithofacies, both primary and secondary, for the deposits identified in the study areas.

4. Lava flows and rheo-ignimbrites

As already discussed by Roverato et al. (2016), the absence of unequivocal vitroclastic textures complicates the distinction between volcaniclastic and layered lava flows in general and, more in particular, for the ancient volcanic rocks investigated here. Lava flows found in the TMP and SFX provinces have both massive and banded structures (Fig. 3) while still maintaining, in some cases, glassy (obsidian) and aphanitic to porfiritic texture. Their composition varies from trachytic to rhyolitic with various content of alkalies (see section 8). The phenocryst assemblage consists mainly of plagioclase, quartz, Fe–Ti oxides and accessory-amount of zircon and apatite. Plagioclase and bipiramidal quartz crystals (Fig. 3a), with a maximum size of 3-4 mm, range from euhedral to anhedral, showing moderate to intense resorption. Plagioclase shows sieve texture indicating non-equilibrium conditions likely determined by magmatic transport. K-feldspar is also present as anhedral crystals in the groundmass often associated with sericite as alteration phase. Samples are generally affected by variable intensity of hydrothermal alteration. Plagioclase phenocrysts, in particular, present diffuse potassic and minor propylictic alterations. Abundant spherulites and lithophysaes of variable size, from millimetric to decimetric, were recognized in almost every sample and are thus common in these rocks (Fig. 3b, c). The spherulites (radiating fibers of K-feldspar and cristobalite), ranging from few millimeters to 2 cm, are typically associated with perlitic fractures. Their content can vary from 10 vol% to 70% in the investigated rocks. A large amount of the spherulites developed into lithophysae commonly reaching 10-12 cm as a consequence of cooling and degassing processes. In the obsidian-type lavas (Fig. 3c), the groundmass is characterized by a micro-granophiric-like devitrification texture characterized by crystallization of amorphous quartz and alkali feldspar, a process that occurred after the emplacement of lava bodies. Several rocks show textures that are not easy to be associated to either lava flows or flows of fragmented material which underwent rheomorphism (Fig. 3d-g). Both banded lavas and rheo-ignimbrites display folds (Fig. 3d-g, see also Fig. 11e) and sub-parallel bands on mm- to dm-scale, planar to wavy (Fig. 3e, see also Fig. 6 and 7) (parataxitic fabric), that deform and flattened around lithic fragments and crystals which alignment suggests the flow direction. In thin sections, the bands are characterized by extremely flattened vitroclastic textures with the former glass completely replaced by a mixture of quartz and feldspar (Roverato et al., 2016).

5. Primary volcaniclastic rocks

We consider primary volcaniclastic rocks those dense, scoriaceous and pumiceous products of fragmental character emplaced by explosive processes. With pyroclastic we refer to fragmental material generated by any kind of explosive volcanic activity and transported as ash-fall and pyroclastic density currents (Manville et al., 2009), which deposition occurs by suspension settling, from traction, by en masse freezing, or any combination of these (White and Houghton, 2006). Depending on the mechanism of transport and the eruptive style these clastic rocks were distinguished into two different categories, i.e. massive and stratified; and they can vary from well sorted, poorly sorted or unsorted. The rocks are predominantly rhyolitic in composition (Fernandes et al., 2011, Roverato et al., 2016) and there is no significant geochemical difference from the lava flows. Nine main lithofacies (Lf) have been recognized for the volcaniclastic rocks: six of them are massive and three are stratified.

5.1. Massive

Six massive lithofacies (mAL, mLA, mLB, *l-g*wLA, *m-g*wLA and *h-g*wLA) were recognized during our field campaign, three of them belong to the welded ignimbrites sub-group (Table 1). By using the granulometric classification proposed by Fisher (1961), ash is defined as any fragment with size <2 mm, lapilli are fragments with size between 2 to 64 mm and blocks (or bombs) have sizes > 64 mm. Massive lithofacies includes all those deposits that display a massive coherent structure. Outcrops of such kind of lithofacies are constituted by a high percentage of ash up to block-rich textures. Most of the observed samples appear to have been affected by devitrification processes of the juvenile pyroclastic fragments and matrix. The presence of juvenile material linked with other observed textures such as broken crystals (Best and Christiansen, 1997) and eutaxitic fabric allows us to confirm that the rocks belonging to lithofacies mAL, mLA, *l-g*wLA, *m-g*wLA and *h-g*wLA are fragmental and pyroclastic in origin. We discuss the meaning of Lf mLB below in section 5.1.2.

5.1.1. Lf mAL; mLA (massive Ash to Lapilli; massive Lapilli *and* Ash)

Description: the ash to lapilli (mAL) and lapilli *and* ash (mLA) deposits (Fig. 4a-e, Fig.6) are heterolithologic, matrix supported, containing angular to sub-rounded medium to coarse devitrified lapilli (displaying axiolitic fabric), banded fragments, occasional (or absent) lithics and angular-shaped broken crystals of plagioclase, bipiramidal quartz and rare oxides (Fig. 5). In mLA, clasts < 25 cm in size are randomly immersed in the groundmass (Fig 4d and 4e, 11d). Some of them are altered by carbonate minerals. Groundmass of mAL and mLA is formed by K-feldspar and quartz crystals, devitrified ash fragments and sericite crystals as phase of alteration (Fig. 5).

Interpretation: the general massive aspect and the poor sorting of mAL and mLA point to a laminar granular flow transport regime and the fine content suggests the deposition from a dilute fluid escape-dominated flow-boundary zone in which turbulent shear-induced tractional segregation is suppressed (Branney and Kokelaar, 2002; Sulpizio et al., 2007, Roverato et al., 2017). These lithofacies are interpreted as ash flow deposits suggesting the deposition from a pyroclastic density current (PDC) (Lenhardt et al., 2011; Sulpizio et al., 2014; Roverato et al., 2017). The coarser lithofacies mLA (fig. 4e) could be related to proximal co-ignimbritic breccias as result of deposition by denser pyroclastic granular flows (Branney and Kokelaar, 2002). The angular aspect of the clasts indicates short-period transport.

5.1.2. Lf mLB (massive Lapilli and Block)

Description: this lithofacies (fig. 4f, fig.7) represents monolithologic coarse-grained rocks having high-clast content (clast:matrix ratios up to 3:1). Angular/sub-angular coarse lapilli and blocks up to 50-60 cm of devitrified banded or massive lava fragments are immersed in a devitrified fine lapilli and coarse ash matrix.

Interpretation: the blocky and monolithologic coarse-grained aspect of the lithofacies mLB and its position underneath thick flow-deposits is attributed to the basal auto-brecciation of lava flows and/or rheo-ignimbrite flows. Despite the lithofacies is likely a consequence of an effusive volcanic activity (in the lava-flow case) it is considered anyway as part of the volcaniclastic group due to its fragmental character.

5.1.3. Lf *l*-*g*wLA; *m*-*g*wLA; *h*-*g*wLA (welded Ignimbrites)

Description: all massive deposits displaying welding characteristics have been grouped in the “welded ignimbrites” group (Table 1), following the idea of “grade of welding” (Walker, 1983) (i.e. the amount of welding and compaction exhibited by deposits). The rocks are matrix-supported with sub-rounded to angular lapilli and ash lithic clasts, euhedral, subhedral and broken crystals (plagioclase and less quartz) and deformed devitrified juvenile fragments (*fiamme*). Slightly- (low-grade, *l*-*g*wLA), medium- (medium-grade, *m*-*g*wLA), well-stretched (high-grade, *h*-*g*wLA) *fiamme*

(Fig. 6), as well as, devitrified shards define the eutaxitic fabric (Roverato et al., 2016). These fragments varying from millimetric to 3–4 cm in size are immersed in a homogeneous micro-granophiric-like devitrified groundmass (see Roverato et al., 2016 for details). Figure 6 shows a stratigraphic column representing a 35 m thick sequence of ignimbrite deposits found in the TMP, displaying very low-grade to high-grade welded fabric where the grade of welding increases toward the top of the succession. The very top of the sequence is characterized by columnar jointing.

Interpretation: the massive aspect and the poor sorting of the lithofacies *l-g*wLA, *m-g*wLA and *h-g*wLA point to a laminar granular flow transport regime, interpreted to be deposited from a pyroclastic density current (PDC). The welded character of these lithofacies is indicative of hot PDC emplacement and compaction that result into the low- up to high-grade eutaxitic fabric. This process is favored by loading-compaction, low-viscosity fragments, high temperature (i.e. > 900°C), cooling of gas-permeable fragments (pumices) and dissolved water (Branney and Kokelaar, 2002; Roverato et al., 2016 and references therein).

5.2. Stratified

These lithofacies, although commonly associated with ignimbrites, are not very spread in the studied areas. We also didn’t find any alternation between massive and stratified deposits even if this association is a common occurrence in PDC deposits (Sulpizio et al., 2014; Roverato et al., 2017), alternating dilute (stratified deposits resulting) and concentrated (massive deposits resulting) regimes during transport (Sulpizio et al., 2014). Just one example has been found in TMP and is reported in the stratigraphic reconstruction of fig.11.

5.2.1 Lf sA; xsA; dsAL (stratified Ash; cross-stratified Ash; diffusely stratified Ash to lapilli)

Description: the stratified samples and outcrops analyzed comprise well sorted very fine to fine ash organized in millimetric to sub-millimetric parallel (sA) or cross-stratified (xsA) layers, with sharp or gradational changes in grain size (Fig. 8). The fragments are represented by devitrified shards, crystals (plagioclase), and rare (or absent) lithics (fig. 8d) immersed in a devitrified groundmass. Diffuse-stratified lithofacies dsAL display a coarser character with coarse lithic and devitrified ash and lapilli fragments forming well developed parallel continuous meter-long stratification (or very-low angle cross-stratification) at centimeter scale (fig. 11b), with gradational changes in grain-size. The sorting varies from well to moderate.

Interpretation: the fine parallel layering of shards material displayed by lithofacies sA is interpreted here as being deposited under the product of sedimentation by the upper and highly dilute ash-cloud that accompany a pyroclastic-density current. We don’t exclude the direct sedimentation from tephra fall-out activity. Cross-stratified (Lf xsA) and diffuse-stratified (Lf dsAL) deposits indicate tractive processes usually attribute to pyroclastic surge-type depositional condition from dilute currents (Cas and Wright 1987; Lenhardt et al., 2011; Roverato et al., 2017). We interpreted these as pyroclastic surge deposits although Lf dsAL could also be the product of coarse ash fall-out processes. Pyroclastic surge deposits usually display small volume and rarely reach more than 10 km from their source (Lenhardt et al., 2011). Conversely, fall-out deposits could emplace tens of kilometers from their source.

6. Secondary volcaniclastic/epiclastic rocks

The nomenclature of Fisher et al. (1961) is applied also for the secondary volcaniclastic rocks as follow: silt (2<>64μm), sand (64μm<>2 mm), gravel (2<>64 mm), cobble (64<>256mm). These rocks are considered as the product of reworking and erosive processes. The clasts belonging to this group show a wide range of composition, size and shape variations. Based on their component, texture and fabric, we recognized five massive, both matrix- and clast-supported, and four stratified lithofacies (fig. 9).

6.1. Massive

6.1.1. Lf mS (massive Sand)

Description: this lithofacies consists of reddish moderately to well-sorted, massive, fine- to medium grained sand forming parallel strata intercalated to clast-supported conglomerate deposits (Lf csG) (fig. 9a). The sandstone strata extend tens of meters and present thinness between 0.4-0.8 m. Lf mS is predominantly composed of quartz, feldspar and minor rock fragments. Contacts between mS and csG are sharp with rare slightly erosional surfaces. The tops of the sandstone are characterized by the presence of centimeters ripples (fig. 9b).

Interpretation: the massive sand (mS) and the small ripples found at the top of the strata indicate low energy under tractional currents in shallow water conditions

(Collison and Thompson, 1982; Lenhardt et al., 2011). The alternation of Lf csG and mS indicates changes in energy conditions of sedimentation. We interpret these oscillations as belonging to a subaqueous-subaerial fan-delta interface setting where continental supply of material alternates to under-water sand accumulation (Lf mS).

6.1.2. Lf csG (clast supported Gravel)

Description: this lithofacies (Fig. 9a, c, d) is massive, clast to matrix supported, with heterolithologic felsic rounded high-spherical coarse gravel with a sandy inter-clast matrix. Clasts are mainly characterized by massive and banded medium- to coarse-size felsic lava fragments (and rare quartz; size does not exceed 5 cm) and present rounded with low- to high-sphericity. We found lithofacies csG also associated to xsSG (see below section 6.2.2.) (Fig. 9c, 10b).

Interpretation: lithofacies csG is dominated by water flow processes where matrix plays a secondary role. The clast-supported character and less matrix content indicates that water removed the finer particles during transport and deposition. Lf csG display rounded clasts and well-sorting indicative of good selection during transport and emplacement. The rounded character of csG and the presence of matrix in the deposits suggest a laminar debris-flow regime in medial reaches of stream-dominated fluvial/alluvial fans (Mueller and Corcoran, 1998).

6.1.3. Lf csGS (clast supported Gravel to Sand)

Description: Lf csGS (Fig. 9e, 11c) is massive, moderately well-sorted and clast-supported. Clasts (gravel to sand) present sub-rounded to sub-angular with low/medium sphericity with maximum size of 2-3 cm. The rocks belonging to this lithofacies are mainly formed by massive felsic lava fragments with different color and crystallinity.

Interpretation: Lf csGS is dominated by water flow processes where matrix plays a secondary role. The clast-supported character and less matrix content indicates that water removed the finer particles during transport and deposition. This lithofacies represents deposition within a debris-flow dominated fluvial/alluvial environment. Poor sorting, clast-supported and sub-angular clasts point to deposition by localized laminar hyperconcetrated-flows in volcanic fans fringing flanks of volcanic edifices. Single cross-beds are usually ca. 1 cm thick

6.1.4. Lf csGC (clast supported Gravel and Cobble)

Description: Lithofacies csGC (Fig. 9f) is massive, low-sorted and clast-supported. The clast population is characterized by sub-rounded, low/medium sphericity, massive felsic porfiritic fragments with maximum size up to 20 cm. This lithofacies has an interstitial matrix characterized by medium to coarse sand.

Interpretation: Lf csGC is dominated by water flow processes where matrix plays a secondary role. The clast-supported character and less matrix content indicates that water removed the finer particles during transport and deposition. This lithofacies represents deposition within a debris-flow dominated alluvial environment. Poor sorting, clast-supported and sub-angular clasts likely points to deposition by localized non-cohesive debris-flows.

6.2. Stratified

6.2.1 Lf xsS (cross-stratified Sand)

Description: lithofacies cross-stratified Sand (Fig. 10a) consist of white to brownish low-angle cross-stratified coarse quartzitic sandstone. The sandstones are characterized by lobe to sheet-shaped bodies. Major bedsets are recognized ranging in thickness from 0.5 to 1.5 m, composed of fine-grained sandstone dominated by medium-angle cross strata (18-20º). Single cross-beds are usually 0.7-1cm thick. The outcrops displaying this lithofacies extend tens of meters with sharp upper and lower contact.

Interpretation: the cross-stratification of xsS is interpreted as formed in fluvial channels attesting the deposition from crested dune bed-forms that formed under condition of lower flow regime (Collinson, 1996; Miall, 1996; Capuzzo and Wetzel, 2004; Went, 2016). The deposition of medium-angle cross-bedding within large-scale examples of beds indicates that these larger beds are likely a product of bar migration. The beds are interpreted as channel-fill deposits (Lenhardt et al., 2017) related to a fluvial environment likely associated to meandering or braided rivers. Shoreline deposition developed around margins of immature marine basins is also considered.

6.2.2. Lf xsSG (cross-stratified Sand and Gravel)

Description: Lf xsSG (Fig. 10b) is characterized by crystal-lithic fine to coarse sand and fine gravel (max 5-6 mm in size) organized in cross-bedded stratification. Clasts display medium roundness and sphericity and are mostly composed by felsic fragments. Stratification is defined by alternating of well to poorly sorted, fine to coarse millimeters-thick strata. The finer black layers are formed by sub-millimetric hematite sand.

Interpretation: Lf xsSG correspond to cross-stratified water reworked deposits. The cross-stratified thicker fine gravelly strata, alternated with sandy layers laterally discontinuous, were interpreted as different pulses as the result of rapid deposition from hyperconcentrated flows (Zanchetta et al., 2004) in a stream-dominated fluvial/alluvial setting. Alternation with csG (Fig. 9c) represents difference of energy condition.

6.2.3. Lf dsSt (diffusely layered Silt)

Description: this lithofacies consists of parallel, lenticular, truncated, and locally low-angle cross-stratified multicolor millimetric well-sorted fine- to very fine-grained sand and silt strata (Fig. 10c). Within the sandy bedset, a thinning- and fining-upward trend may be distinguished. Small and straight groove marks have been detected and reduced tiny slump folding is also presence in some parts.

Interpretation: lithofacies dsSt displays diffuse fine stratification with tiny ripples, suggesting transport and sedimentation in shallow water. The thin sheet-shaped is interpreted as flood sediments (Lenhardt et al., 2011). These deposits are interpreted to have been formed in low energy lacustrine environment or ponds (Collinson, 1996; Roverato et al., 2017) characterized by small turbidities successions affected by scouring and tiny deformations (slumps) of the sediments.

6.2.4. Lf bChS (bedded Chert and Sand)

Description: the bedded chert lithofacies (with sand) (bChS) (Fig. 10d) crops out in both regions and it is characterized by outcrops that can be traced on strike for hundreds of meters. The facies consist of thin laminated pinkish chert (layers < 1mm in thickness) with darker laminae intercalated, formed predominantly by hematite (Lenhardt et al., 2017). The layers are composed by microcrystalline quartz. In some portions, these lithofacies are associated with fine to medium sand composed mainly by quartz and less volcanic fragments.

Interpretation: this lithofacies is interpreted as inorganic precipitation of silica in a closed lake basin mainly due to its association with volcanic rocks and fine sandstone (Blatt et al., 1980; Eriksson et al., 1994). The picture in figure 10d shows elongated ripped-up millimetric fragments of chert immersed in the sandstone eroded by low-energy stream flow or local lacustrine turbidites. As suggests by Lenhardt et al. (2017) the chert may have formed during repeated pulses of hydrothermal fluids that circulated into the lake water during hiatuses in the volcanism (Van Kranendonk, 2006).

7. Analytical methods for geochemistry and geochronology

A total of 19 new samples (9 volcaniclastics and 10 lava flows) from the Tapajós region (associated with the data published in Roverato et al., 2016; Table 2) were analysed for bulk rock major and trace elements. Major element bulk rock analyses were performed by X-ray fluorescence, using a wavelength dispersive Philips PW 2400 spectrometry, using fused glass disks according to procedures described by Mori et al. (1999). Accuracy was greater than 2%. Trace element analyses in selected samples were performed by Inductively Coupled Plasma-Mass Spectrometry (ICP-MS) using the procedure described by Navarro et al. (2008). Accuracy, determined with respect to the reference standards BHVO-2 and BR, was 0.5–2%.

Zircon grains were examined with a FEI-QUANTA 250 scanning electron microscope equipped with secondary-electron and cathodoluminescence (CL) detectors at the Instituto de Geociências - Centro de Pesquisas Geocronologicas - Universidade de São Paulo (IGc-CPGeo-USP); the most common conditions used in CL analysis were 60 μA of emission current, 15.0 kV of accelerating voltage, 7 μm of beam diameter, 200 μs of acquisition time, and a resolution of 2048x1887 pixels and 345 dpi. Selected samples were analyzed for U-Pb isotopes using a SHRIMP-IIe also at IGc-CPGeo-USP, following the analytical procedures of Williams (1998) as reported by Giovanardi et al. (2015). Correction for common Pb is based on the measured ^{204}Pb, and the typical error for the ^{206}Pb/^{238}U ratio is less than 2%; U abundance and U-Pb ratios were calibrated against the TEMORA-II standard. The dataset consists of 56 new U-Pb SHRIMP-II analyses and is reported in Table 3. Thirty-five analyses were performed on zircon grains from the Tapajós region as follow: 11 analyses on sample NP380-C, 11 analyses on sample NP183 and 13 analyses on sample NP396-B. Eleven analyses were performed on zircon grains from Xingú sample XU08. For all samples, ^{207}Pb/^{235}U and ^{206}Pb/^{238}U concordia ages (with 95% of confidence level and 2σ error) are calculated using Isoplot 4.1 software (Ludwig, 2009).

8. Geochemistry of the TMP samples

Independently of their nature (lavas or volcaniclastic), the rocks of the TMP follow a typical calc-alkaline trend (Fig. 12). They are mostly rhyolitic in composition (Table 2), with four exceptions which fall in the trachytic field. In addition, their low LOI values (0.32-3.51%) and the low FeO content (0.78 – 3.26%) together with the negative correlation FeO vs SiO_2 appears to indicate that the investigated volcanic rocks neither underwent significant alteration processes nor they belong to sedimentary suites which commonly contain water rich clay minerals. TMP volcaniclastic and lava flows show similar negative correlation between TiO_2, Al_2O_3, MgO, FeOt, CaO, Na_2O and P_2O_5 with SiO_2. A negative correlation between K_2O and SiO2 also exists for the volcanoclastic, but not for the lava flows. The similar trends observed suggest that both these kind of rocks are originated by similar magmatic sources. Such a conclusion is supported by similar variation paths, although with different values, of minor and trace elements (Fig. 13). In particular, TMP lava flows show LREE enrichment ($(La/Yb)_N$=10.68-21.45; normalization to Chrondrite I from Anders & Ebihara, 1982) and a negative Eu anomaly which increases from trachytes ($(Eu/Eu^*)_N$=0.89-0.78) to rhyolites ($(Eu/Eu^*)_N$=0.69-0.31) (Fig. 13). The Eu negative anomaly, shown from all the samples, is expression of feldspar fractionation. On the other hand, volcaniclastics rocks show similar LREE enrichment ($(La/Yb)_N$=11.12-28.10) and negative Eu anomaly ($(Eu/Eu^*)_N$=0.97-0.37) (Fig. 13). In addition, volcaniclastics have higher LREE abundances with respect to lavas (La between 35.5-91.3 ppm and between 40.5-71.9 ppm, respectively) while they have similar MREE and HREE contents (Yb between 1.56-3.43 ppm and between 1.83-4.11 ppm, respectively). Volcaniclastics commonly show higher Rb (121-272.9 ppm) and Pb (4.5-137.1 ppm) with respect to lavas (Rb=96.1-232 ppm and Pb=2.7-45.8 ppm). Volcaniclastics are enriched in LILE, Th and U with respect to MORB (Fig. 13; normalization to MORB from Hoffman, 1988), with the exception of Sr, which commonly show a pronounced negative anomaly ($(Sr/Sr^*)_N$=0.55-0.05). The Sr negative anomaly is consistent with feldspar fractionation. Negative anomalies are also present for Nb and Ta, while Ba and Pb are commonly enriched (Fig. 13). Lavas show a similar trace pattern, but higher values dispersion (Fig. 13). The Ba enrichment is less pronounced with respect to volcaniclastics (Ba between 75-1965 ppm and 310-2245 ppm, respectively) and the Nb/Ta ratio show higher dispersion (3.29-14.63 and 6.73-13.9, respectively), indicating more limited fractionation of feldspar. Geochemical affinity of Tapajós volcaniclastics and lava flows suggests that the magmatism occurred in active continental setting (Fig. 14). Using the tectonic discriminant diagrams of Zr+Nb+Ce+Y (ppm) vs FeOtot/MgO (wt.%), Yb vs Ta and Th-Ta-Hf/3 (Wahlen et al., 1987; Pearce et al., 1984; Wood, 1980), the magmatism in the Tapajos region appears related to a syn- to post-collisional setting with few samples falling into the intraplate field (Fig. 14). According to the refined diagram Nb+Y vs Rb of Pearce (1996), all the Tapajos volcanics, together with the majority of volcanic rocks from the Sobreiro formation (Fernandes et al., 2011) are consistent with a late- to post-collisional setting (Fig. 14).

9. U-Pb zircon Geochronology

Zircons from Tapajos samples are colorless, sometimes fractured and euhedral to sub-euhedral. They can contain inclusions of apatite or spinel and display commonly low emission in Cathodoluminescence (CL). All crystals show magmatic oscillatory zoning and commonly a dark core which, in most cases, appears to be homogenous. Nonetheless, in few cases an inner core with discordant and partially reabsorbed domains is recognized. Some of the zircons also show a bright CL rim with transgressive or sub-concordant contacts with the inner oscillatory zoning. Zircons from sample XU08 from the Xingu region are colourless, rarely fractured and sub-euhedral. Inclusions of apatite or spinel are also observed sometimes. Crystals are medium in CL emissions and commonly show a homogeneous core and a concordant magmatic oscillatory zoning. Few zircons show a core with discordant zoning. No transgressive bright CL rims were recognized. Analyses were carried out on zircons that do not show transgressive or resorption features and discordant inner cores. Zircons from sample NP183 (Ignimbrite) provide 4 discordant and 7 concordant analyses that provide an upper intercept at 1984 ±8.5 Ma (95% confident decay-const. errs included, MSWD 1.09) and a concordia age at 1986 ±8.2 Ma (2σ, decay-const. errs included, MSWD 1.08, Probability of concordance = 0.30; Fig. 15). Single spot $^{206}Pb/^{207}Pb$ ages range between 2010 ±17 Ma and 1909 ±53 Ma with an average age of 1985 ±11 Ma (95% confident decay-const. errs included, MSWD 1.6, Probability of concordance = 0.15; Fig. 15). Zircons from sample NP380 (Ignimbrite) show slightly older single spot $^{206}Pb/^{207}Pb$ ages between 2023 ±31 Ma and 1981 ±24 Ma with an average age of 1998 ±5.9 Ma (95% confident decay-const. errs included, MSWD 0.74, Probability of concordance = 0.68; Fig. 15). Analyses are slightly discordant (up to 4%) providing an upper intercept at 1998 ±7.7 Ma (95% confident decay-const. errs included, MSWD 0.74). Zircons from sample NP396 (Banded lava) provide 5 discordant ages and 8 concordant analyses, which provide an upper intercept at 1994 ±8.2 Ma (95% confident decay-const. errs included, MSWD 1.40) and a concordia age at 1997 ±7.0 Ma (2σ, decay-const. errs included, MSWD 5.70, Probability of concordance = 0.02; Fig. 15). Single spot $^{206}Pb/^{207}Pb$ ages range between 2014 ±14 Ma and 1973 ±8 Ma with an average age of 1994 ±8.7 Ma (95% confident decay-const. errs included, MSWD 1.6, Probability of concordance = 0.12; Fig. 15). Pooling together the analyses of the Tapajós samples provides an average age of 1991 ±12 Ma (2σ, MSWD 1.50, Probability of concordance = 0.06). Zircons from sample XU08 (Lava flow) provide a concordia age at 1882 ±6.4 Ma (2σ, decay-const. errs included, MSWD 2.70, Probability of concordance = 0.10; Fig. 16). Single spot $^{206}Pb/^{207}Pb$ ages range between 1899 ±10 Ma and 1875 ±13 Ma, with an average at 1884 ±5.2 Ma (95% confident decay-const. errs included, MSWD 0.60, Probability of concordance = 0.82).

10. Discussion

10.1. Subduction-related to extensional setting

The geochemistry of the TMP samples presented in this work display a high-K calc-alkaline signature (Fig. 12); they mainly fall into the A-type intra-plate granite field and tectonic discriminant diagrams suggest a late- to post-collisional setting for the TMP volcanism (Fig. 14). This interpretation is also supported by enrichment in LILE, Th, U and LREE of our samples, which suggest a strong crustal component in the parent melt consistent with a subduction/post orogenetic geodynamic setting (Figs. 12, 13, 14), and the high HSFE which shifted the TMP volcanics composition in the A-type granites showing however FeO/MgO which are low and comparable with I- and S-types granites (Fig. 14). Similar features are reported in previous works (Lamarão et al., 1999; Lamarão et al., 2002) for volcanics in the Tapajós region, which are grouped into the Vila Riozinho (VR) and Maraes Aldeida (MA) formations, respectively. The VR rocks are intermediate to felsic in composition (Lamarão et al., 2002) with a calc-alkaline signature, while the rhyolites and ignimbrites of MA are slightly enriched in silica compared to the rhyolites of VR and are geochemically similar to evolved A-type granites (Lamarão et al., 2002). Our results show similarities with these data, suggesting that our specimens could be part of the VR and/or MA formations. The identification of two volcanic series has important implications for the understanding of the magmatic evolution of the Amazonian craton in late Paleoproterozoic. A model for the evolution of the TMP involves a first stage of subduction-related magmatism followed by an intracontinental magmatism related to a distensional event (Lamarão et al., 2002). Geochronological analyses by Lamarão et al. (2002) yielded ages of ca. 2 Ga for the VR and ca. 1.88-1.87 Ga for the MA volcanisms. The three new U-Pb geocronological analyses reported in this study yielded ages of ca. 2000 Ma (fig. 15) are concordant with the ages presented by Lamarão et al. (2002) for the VR magmatism, thus suggesting that the TMP rocks could be part of the VR volcanic sequence. However, TMP rocks are geochemically more evolved with respect to VR in terms of SiO_2 (63.8-76.6 wt.% and 54.4-71.8 wt.%, respectively), K_2O (2.3-7.1 wt.% and 2.1-5.8 wt.%, respectively) and REE abundances and are more similar to MA rocks (Figs. 11, 12 and 13). In particular, REE patterns of the TMP samples are comparable with the rocks of the MA formation (Fig. 12) while they are more enriched in REE with respect to VR rocks. Conversely, TMP rocks are enriched in Ba (Fig. 12), while MA are depleted, and have compositions for Rb/Zr ratio and Nb, considered as a proxy for arc maturity (Brown et al., 1984), similar to VR and different from MA (Rb/Zr between 0.3-1.1 in TMP, 0.2-0.7 in VR and 0.2-1.7 in MA; Lamarão et al., 2002). Thus, according to geochronological and petrological data, we proposed that the TMP rocks in this study must be ascribed to the VR formation. Geochemical differences in our rocks and VR volcanics could be explained by a more evolved character of the TMP rocks. The evidences of plagioclase fractionation from the parent melts of the TMP (negative Eu and Sr anomalies, Fig. 12) and their absence in less evolved VR rocks reinforce this interpretation, and suggest fractional crystallization as the prominent process controlling the VR magmatism evolution. However, we want to point out that due to the large area covered by the presented investigation (Fig. 2), together with the VR area, the geochemical variations between our rocks (TMP) and VR could be the result of local/regional heterogeneities in the magmatism. This hypothesis is supported by the intermediate characteristics of the TMP samples with respect to the VR and MA volcanoclastic material (Figs 11, 12 and 13).

Recently, new authors (Juliani et al., 2014) suggest the geochemical and geocronological signature of the MA formation could be correlated to the felsic Santa Rosa formation (SRF) cropping out in the SFX region. Our new U-Pb geocronological analyses on one rock sample from the SRF yielded an average age of 1884 ±5.2 Ma (Fig. 16) that is consistent with previous Pb-Pb ages on other locations. Juliani and Fernandes (2010) published two Pb-Pb ages on zircons of 1879 ± 2 Ma and 1884 ± 1.7 for a rhyolite and an ash tuff, respectively. Recently Antonio et al. (2017) publishes the first U-Pb ages on zircons for the Santa Rosa Formation with 1877.4 ± 4.3 Ma for a rhyolite and 1895 ± 11 Ma for a dike. All geochronological results support a ca. 1880 Ma age for the emplacement of these rocks.

The southern Amazonian craton, as well as other Precambrian terrains worldwide (Condie, 2002; Hoffman, 1988; Zhao et al., 2002), are considered to be characterized by a series of orogenic to post-orogenic events from 2.0 up to 1.88 Ga. The amalgamation of cratonic blocks worldwide established connections between South America and West Africa and other cratonic terrains such as Western Australia and South Africa, Laurentia and Baltica, Siberia and Laurentia, Laurentia and Central Australia, etc (Zhao et al., 2002). These late-Paleoproterozoic collisional processes likely formed the controversial supercontinent Columbia (Zhao et al., 2004). This period also coincides with a major peak in orogenic gold resources (Goldfarb et al., 2001; Juliani et al., 2014) and understanding the geodynamic of this period is crucial for economic interests. Antonio et al. (2017) highlight that for the period 1.88 Ga, many cratonic terrains have been characterized by extensive magmatism. These authors report as examples the 1880 Ma NE-trending Ghost dike swarm and the 1880 Ma Circum-Superior LIP in the Canadian shield (Minifie et al., 2013), the 1880 Ma Southern Bastar- Cuddapah LIP in India (French et al., 2008), the Mashonaland sills and the Post-Waterberg dolerites in Kalahari craton (Hanson et al., 2004), an extensive A-type magmatism in Baltica and in Siberia. The A-type affinity of the 1.88 Ga rocks is widely described by other authors in different regions into the Amazonian craton (Ferron et al., 2010; Pierosan et al., 2011; Fernandes et al., 2011; Klein et al., 2012; Barreto et al., 2014; Teixeira et al., 2018). Currently, the significance of the 1.88 Ga A-type magmatism in the AC is still matter of debate, also due to the extremely large aerial cover which interested several different domains with different basements and geologic evolutions. For example, studies on the Carajas region suggest that the 1.88 Ga anorogenic magmatism in this domain was provoked by delamination and fusion of the Archean basement by a mantle plume which originated an extensional setting (Dell'Agnol et al., 2005; Silva et al., 2016; Teixeira et al., 2018; Teixeira et al., 2019).

Conversely, the geochemical features of the TMP and SFX magmatism presented in this work and in literature (Lamarão et al., 2002, 2005; Fernandes et al., 2011) mainly support an extensional regime of these regions related to a late- to post-collisional event, being possibly related to the end of the subduction process. The transition from convergent (late-/post-orogenic) to extensional tectonic setting could register the beginning of the taphrogenesis that marked the Amazonian Craton throughout the Mesoproterozoic (Brito Neves, 1999; Lamarão et al., 2002). The ca. 1.88 Ga felsic magmatism in different provinces of the Amazonian craton could represent the oldest magmatism related to this event.

It should be mentioned that in term of textural features, the products emitted during the transition between the late-/post-collisional to extensive events don't display substantial variations. In other words, the lithofaciological signature of the volcanic and volcaniclastic rocks that characterized the 2 Ga VR event (subduction related) is similar for those products erupted during the 1.88-1.87 Ga extensional volcanism that characterized the MA and SRF events. Moreover, the post-orogenic to extensional setting emphasizes the continental setting where the studied volcanic products have been emitted. Following the idea of Roverato et al. (2017) for the Late-Paleoproterozoic andesitic Sobreiro Formation, we stress the lack of any evidences in favour of subaqueous eruptions for the emitted felsic products such as pillow lavas as well as hyaloclastites. This suggests the subaerial character of the volcanism and its emitted products acted in both regions.

10.2. Eruptive style and emplacement

The study areas are widely characterized by volcanic deposits whose eruptive style is hard to differentiate. Distinguishing between banded lavas and high grade ignimbrites is, sometime, extremely challenging (Henry and Wolff, 1992; Manley, 1995). This is made even more complicated when the investigated deposits are ancient and the outcrops intensely eroded, such as those Precambrian terrains investigated here (Lenhardt et al., 2012; Roverato et al., 2016; Lenhardt et al., 2017). Evidences in the field show that a great volume of the volcanic activity is represented by the emission of lava flows and/or high-grade to rheomorphic ignimbrites, although an important amount of other fragmental products of different type (Lf mAL, mLA, *l-g/m-g/h-g*wAL) are also well represented in both regions. High-grade welded and rheomorphic (up to lava-like) ignimbrites share similar features with lavas, displaying banding and ductile folds formed by the elongation of fiamme and vesicles (Schmincke and Swanson, 1967; Chapin and Lowell, 1979; Wolff and Wright, 1981; Branney et al., 1992; Sumner and Branney, 2002; Pioli and Rosi, 2005; Andrews and Branney, 2011; Brown and Bell, 2013). Although the ignimbrites investigated here have a fragmental derivation their origin largely differ from those characteristic of fallout deposits that form by a sustained column explosive-driven eruption. High-grade welded and rheomorphic ignimbrites are correlated with highly explosive plinian-type eruptions which produce, during their column collapse stage, large PDC. In addition, high-grade rheomorphism of silicic products, either deriving from an explosive or effusive eruption, are favored by high temperature low-viscosity emplacement conditions and the presence of some residual water. The high temperatures condition of our deposits is also confirmed by the pervasive presence of spherulites and lithophysae formed during the slow-cooling regimes of large silica-rich lavas and welded ignimbrites (Lofgren, 1971; Breitkreuz, 2013). The eruptive scenario showed in figure 17 giving origin to the frequent eruption of large volume and high discharge rate lava flows and ignimbrites was likely characterized by fissure-fed and caldera collapses systems as those described by previous authors (Legros et al., 2000; Aguirre et al., 2003; Cas et al., 2011; Lesti et al., 2011; Lenhardt et al., 2012; Willcock et al., 2013). Eruptions fed by extensive fissures of large size, in fact, appear to be the most favourable volcanic systems to minimize cooling during emplacement and produce an alternance of low-height sustained column eruptions feeding PDC and eruptions characterized by the effusion of low viscosity lava flows, coulees and domes, while maintaining high discharge rates (e.g. Bachmann et al., 2000; Aguirrez-Diaz & Labarthe-Hernandez, 2003; Polo et al., 2018a, b; Simões et al., 2017). The sustained fountaining and entrainment of air in the eruptive jet is strongly influenced by the geometry of the conduit (Legros et a., 2000) as well as the transition from sustained to collapsing eruptive column. A wide-geometry conduit would impede much air entrainment into the pyroclastic fountain and, at the same time, would favors magmatic escape of volcanic gases, favoring the low fountaining and promoting a “boil-over” style eruption (Branney and Kokelaar, 1992, 2002; Lenhardt et al., 2017) with high discharge rate. Moreover, the low air injection would inhibit the dilution of the eruptive material making it thermodynamically isolated from the surrounding environment (Lesti et al., 2011), preserving the high temperatures and enhancing the agglutination of fragments (welding) (Quane and Russell, 2004; Russell and Quane

2005; Giordano et al., 2005). When the low-altitude pyroclastic fountaining or the emission of high temperature lavas would be maintained for long time the high flow-mobility is ensured (Sulpizio et al., 2014). If the material supply from the vent continues for long time and with high discharge rate, the mobility could be maintained even on very low slope angles (Sulpizio et al., 2014; Giordano et al., 2017; Kolzenburg et al., 2017), and flowing various kilometers up to hundreds of kilometers far from the vent (Aguirre-Diaz et al., 2008; Cas et al., 2011; Giordano et al., 2017). This could explain the presence of large silicic volcanic areas characteristic of the ancient Amazonian volcanism (Roverato et al., 2016). Although, volcaniclastic rocks seem to be volumetrically less important in the study areas than the lava flows and/or rheomorphic ignimbrites the recognition of fragmental rocks during our field campaigns is important to understand their significance into our paleogeographic reconstruction (Fig. 17). An idealized deposit sequence of a caldera forming eruption displays an air-fall deposit overlain by an ignimbrite (Druitt and Sparks, 1984) and the transition from the sustained column phase to the pyroclastic flow phase is often accompanied by a strong increase in the discharge rate (Bursik and Woods, 1996). The stratigraphic sequence of figure 11 shows this association of a possible air-fall deposit (Lf dsAL) linked with pyroclastic flow-dominated deposits (Lf mAL and *m*-*g*wLA). In some cases, pyroclastic eruptions commonly precede lava emplacement (Fink 1983; Heiken and Wohletz 1987). The sequence presented in figure 7 shows a low-grade welded ignimbrite deposit (Lf *l*-*g*wAL) overlaid by a thick banded body that we are interpreting here as a lava flow. At the base of the banded lava is a breccia (Lf mLB) consisting of clasts of a mix of lava textural types, including massive, vesicular, flow banded and flow-folded, glassy, pumiceous and devitrified. Autobrecciation in lavas or rheomorphic ignimbrites occurs when more rigid layers and the external parts are broken in response to the applied shear stress locally exceeding the tensile strength (Fink and Manley; 1987). Some polymictic breccia deposits (Lf mLA) are characterized by lithic angular clasts and devitrified fragments that could point to co-ignimbritic breccias with short transport of the emitted material. These deposits could be also related to collapse-caldera-breccias falling down into the caldera ring during the roof subsidence. Air-fall (sA) and dilute pyroclastic flow (xsA) deposits (surge type) crop out in both regions. These, linked with the glassy and lithic pyroclastic material described above, are evidence of intense explosive phases from more sustained column eruptions of smaller intra-caldera volcanic centers and/or associated to events of caldera collapse (Fig. 17).

10.2.1 The sedimentary response

Sets of small basins intra-calderas and probable relatively immature shallow marine deposits are interpreted as forming part of a tectonically unstable setting of a young extensional environment that characterized the southern Amazonian craton during the Paleoproterozoic. Reworked sediments can accumulate into volcano-tectonic depressions created by the eruption, which often collects an intra-caldera lake (Heiken et al., 2000 Németh et al., 2009, Manville et al., 2009). The sedimentation into intra-volcano shallow-water lacustrine basins would have be facilitated (Fig. 17). The alternation of subaerial to shallow-water sedimentation displayed by the alternation of Lf mS and csG is indicative of this volcano-tectonic depressions, which could be also interpreted as immature marine depressions. Subaerial and subaqueous talus coarse-grained up to finer grained turbidites (dsSt) and suspension deposits formed during quiescent periods into lakes or pounds is also inferred (Bacon et al., 2002). Silica-rich accumulations into shallow water basins (Chipera et al., 2008; Manville et al., 2009) deriving from hydrothermal activity in a dynamic volcanic context is also thought to be responsible for the formation of chert accumulation (Lf bChS). Post caldera uplifting (Fig. 17), resurgence or central volcanism could also contribute to produce new sediments to be reworked and transported. Fluvial erosion and reworking of primary deposits produced wide range of different sediments from localized cross-bedded, well-sorted sand (Lf xsS) and gravel (Lf xsSG) beds to massive clast-supported sand and gravel (Lf csGS, csG) and cobble (Lf csGC) deposits. Fluvial deposits occur throughout all successions, representing periods of stream and river reworking and re-establishment after an eruptive phase (Zernack et al., 2011; Roverato et al., 2017). Debris-flows, hyperconcentrated flows, sheet-floods and active sandy braided river systems existed and the absence of vegetation during the Precambrian (Oberholzer and Eriksson, 2000; Roverato et al., 2017) permitted that copious rainfalls easily reworked the available sediments.

11. Conclusion

This study is the result of the lithofaciological analysis carried out during the 2013, 2014 and 2015 field campaigns in the Amazon Craton in the TMP and SFX regions and the successive geochemical and geochronological analysis of samples collected in the field. This work constitutes a further step ahead toward the comprehension of significance, chronostratigraphic distribution and the dynamic of eruption and emplacement of felsic volcanic products in the region. Our results complete previous studies and confirm that products present in the Amazonia Craton could be related either to caldera-type systems (e.g. Lamarão et al., 2002; Juliani et al., 2005; Lamarão et al., 2005; Pierosan et al., 2011) and to fissure-fed eruptive environment following the model proposed by Aguirre-Diaz and Labarthe-Hernandez (2003) for the “Sierra Madre Occidental” formation and by Juliani and Fernandes (2010) for the Xingu region. The two models are in fact very similar only differing for the size of the hypothesized magma chambers and the shape of the fissural vents. The described volcano-sedimentary sequences that were characterized by the emission of large volcanic felsic products were likely formed in a late-/post-orogenic (~ 2 Ga) to extensional regimes (~ 1.88 Ga).

Acknowledgments

This work was supported by the project CAPES/CNPq 402564/2012-0 (Programa Ciências sem Fronteiras) to Caetano Juliani and Matteo Roverato. M. Roverato acknowledges the grant of the Brasilian CAPES/ CNPq Programa Ciências Sem Fronteiras, Atração de Jovem Talento 402564/2012-0. We acknowledge the CNPq/CT-Mineral (Proc. 550.342/ 2011-7) and the INCT-Geociam (573733/2008-2) — (CNPq/MCT/ FAPESPA/PETROBRAS). Furthermore, the first author would like to thank Jeovaci Jr. Martins da Rocha, Diego Felipe Gomez Gutierrez, Lucas Villela Cassini for the help in the field and Carlos Marcelo Diaz Fernandez for the help and very useful discussions. Dr. Giordano acknowledges the financial support for this research from the CAPES project (proposal 302827) of the Ciências Sem Fronteiras program (Brazil) and the local research funds (2012, 2013, 2014) of the University of Turin (Ex60-2015). We are indebted to Nils Lenhardt and Roberto Dall’Agnol for the dedication in reviewing this manuscript and important comments and reviews, which improved considerably this work.

References

Aguirre-Diaz, G.J., Labarthe-Hernández, G., 2003. Fissure ignimbrites: fissure-source origin for voluminous ignimbrites of the Sierra Madre Occidental and its relationship with Basin and Range faulting. Geology 31, 773-776.

Aguirre-Diaz, G.J., Labarthe-Hernàndez, G., Tristàn-Gonzàlez, M., Nieto-Obregòn, J., Isaac Gutiérrez-Palomares, I., 2008. The ignimbrite flare-up and graben calderas of the Sierra Madre Occidental, Mexico. In: Martí, J., Gottsman, J. (Eds.), Caldera Volcanism: Analysis, Modelling and Response. Developments in Volcanology 10, 143-180.

Almeida, F.F.M., Hasui, Y., Brito Neves, B.B., Fuck, R.A., 1981. Brazilian structural provinces: an introduction. Earth Science Reviews 17, 1-29.

Almeida, M.E., Brito, M.F.L., Ferreira, A.L., Monteiro, M.A.S., 2000. Projeto Especial Província Mineral do Tapajós. Geologia e recursos minerais da Folha Vila Mamãe Anã (SB.21-V-D). Estados do Pará e Amazonas. CPRM, Brasília. [CD-ROM].

Amaral, G., 1974. Geologia Pré-Cambriana da Região Amazônica. Tese de Livre Docência, IG/USP (212 pp.).

Anders, E., Ebihara, M., 1982. Solar system aboundances of the elements. Geochim. Cosmochim. Ac. 46, 2363-2380.

Andrews, G.D.M., Branney, M.J., 2011. Emplacement and rheomorphic deformation of a large, lava-like rhyolitic ignimbrite: Grey’s Landing, southern Idaho. Geological Society of America Bulletin 123, 725-743.

Antonio, P., D'Agrella-Filho, M.S., Trindade, R.I.F., Nédélec, A., de Oliveira, D.C., da Silva, F.F., Roverato M., Lana, C., 2017. Turmoil before the boring billion: Paleomagnetism of the 1880–1860 Ma Uatumã event in the Amazonian craton. Gondwana Research 49, 106-129.

Araújo, O.J.B., Maia, R.G.N., Jorge, João, X.S., Costa, J.B.S., 1988. A megaestruturação arqueana da folha Serra dos Carajás. In: SBG (Ed.), Congresso Latinoamericano de Geologia, seventh ed. Belém. 324-333.

Bacon, C.R., Gardner, J.V., Mayer, L.A., Buktenica, M.W., Dartnell, P., Ramsey, D.W., Robinson, J.E., 2002. Morphology, volcanism, and mass wasting in Crater Lake, Oregon. Geological Society of America bulletin 114, 675-692.

Bahia, R.B.C., Quadros, M.L.E.S., 2000. Geologia e recursos minerais da Folha Caracol SB.21-X-C. Estados do Pará e Amazonas. Escala 1:250.000. Brasília: CPRM, 2000. 1 CD ROM.

Barreto, C.J.S., Lafonb, J.M., da Rosa Costac L.T., Fernandes-Limad, E., 2014. Palaeoproterozoic (~1.89 Ga) felsic volcanism of the Iricoumé Group, Guyana

Shield, South America: geochemical and Sm-Nd isotopic constraints on sources and tectonic environment. International Geology Review, 2014. http://dx.doi.org/10.1080/00206814.2014.930800

Best, M.G., Christiansen, E.H., 1997. Origin of broken phenocrysts in ash-flow tuffs. GSA Bulletin, 109 (1), 63-73.

Blatt, H., Middleton, G., Murray, R., 1980. Origin of Sedimentary Rocks. Prentice-Hall, Englewood Cliffs, 634.

Branney, M.J., Kokelaar, B.P., 1992. A reappraisal of ignimbrite emplacement: progressive aggradation and changes from particulate to non-particulate flow during emplacement of high-grade ignimbrite. Bull. Volcanol. 54, 504-520.

Breitkreuz, C., 2013. Spherulites and lithophysae—200 years of investigation on high temperature crystallization domains in silica-rich volcanic rocks. Bull. Volcanol. 75:705.

Brito-Neves, B.B., 2011. The Paleoproterozoic in the South-American continent: Diversity in the geologic time. Journal of South American Earth Sciences 32, 270-286.

Brown, D.J., Bell, B.R., 2013. The emplacement of a large, chemically zoned, rheomorphic, lava-like ignimbrite: the Sgurr of Eigg Pitchstone, NW Scotland. Journal of the Geological Society 170, 753-767.

Brown, G.C., Thorpe, R.S., Webb, P.C., 1984. The geochemical characteristics of granitoids in contrasting arcs and comments on magma sources. Journal of the Geological society 141, 413-426.

Bursik, M.I., Woods, A.W., 1996. The dynamics and thermodynamics of large ash flows. Bull. Volcanol. 58, 175-193.

Capuzzo, N., Wetzel, A., 2004. Facies and basin architectural of the Late Carboniferous Salvan-Dorénaz continental basin (Western Alps, Switzerland/France). Sedimentology 51, 675-697.

Cas, R.A.F., Wright, J.V., 1987. Volcanic Successions, Modern and Ancient. Unwin Hyman, Boston. 528.

Cas, R.A.F., Wright, H.M.N., Folkes, C.B., Lesti, C., Porreca, M., Giordano, G., Viramonte, J.G., 2011. The flow dynamics of an extremely large volume pyroclastic flow, the 2.08-Ma Cerro Galán Ignimbrite, NW Argentina, and comparison with other flow types. Bull. Volcanol. 73, 1583-1609.

Chipera, S.J., Goff, F., Goff, C.J., Fittipaldo, M., 2008. Zeolitization of intracaldera sediments and rhyolitic rocks in the 1.25 Ma lake of Valles caldera, New Mexico, USA. Journal of Volcanology and Geothermal Research 178, 317-330.

Collinson, J.D., 1966. Antidune bedding in the Namurian of Derbyshire, England: Geologie en Mijnbouw 45, 262-264.

Collinson, J.D., Thompson, D.B., 1982 Sedimentary structures: London, Allen and Unwin, 194.

Condie, K.C., 2000. Episodic continental growth models: after thoughts and extensions. Tectonophysics 322, 153-162.

Condie, K.C., 2002. Continental growth during a 1.9-Ga superplume event. Journal of Geodynamics 34, 249-264.

Costa, J.B.S., Hasui, Y. 1997. Evolução geológica da Amazônia. In: M.L. Costa & R.S. Angélica (Ed.), Contribuições à geologia da Amazônia, 16-90.

Da Cruz, R.S., Fernandes, C.M.D., Villas, R.N.N., Juliani, C., Monteiro, L.V.S., Almeida, T.I.R., Lagler, B., Carneiro, C.C., Misas, C.M.E., 2015. A study of the hydrothermal alteration in Paleoproterozoic volcanic centers, São Felix do Xingu region, Amazonian Craton, Brazil, using short-wave infrared spectroscopy. J. Volc. Geoth. Res. 304, 324-335.

Dall'Agnol, R., Lafon, J.M., Macambira, M.J.B., 1994. Proterozoic anorogenic magmatism in the Central Amazonian Craton: geochronological and geochemical aspects. Mineral. Petrol. 50, 113-138.

Dall'Agnol, R., Costi, H.T., Leite, A.A.S., Magalhães, M.S., Teixeira, N.P., 1999. Rapakivi granites from Brazil and adjacent areas. Precambrian Research 95, 9-39.

Dall'Agnol, R., Teixeira, N.P., Rämö, O.T., Moura, C.A.V., Macambira, M.J.B., Oliveira, D.C., 2005. Petrogenesis of the paleproterozoic, rapakivi, A-type granites of the Archean Carajás metallogenic province, Brazil. Lithos 80, 101-129.

Dall'Agnol, R., da Cunha, I.R.V., Guimarães, F.V., de Oliveira, D.C., Teixeira, M.F.B., Feio, G.R.L., Lamarão, C.N., 2017. Mineralogy, geochemistry, and petrology of Neoarchean ferroan to magnesian granites of Carajás province, Amazonian Craton: The origin of hydrated granites associated with charnockites. Lithos 277, 3-32.

Druitt, T.H., Sparks, R.S.J., 1984. On the formation of calderas during ignimbrite eruptions. Nature 310, 679-681.

Echeverri-Misas, C.M., 2010. Geologia e gênese do depósito de Au-(Cu) do Palito, Província Aurífera do Tapajós. Dissertação de Mestrado, IG/USP.

Eriksson, P.G., Engelbrecht, J.P., Res,M., Harmer, R.E., 1994. The Bushy Bend lavas, a new volcanic member of the Pretoria Group, Transvaal Sequence. S. Afr. J. Geol. 97, 1-7.

Faraco, M.T.L., Carvalho, J.M.A., Klein, E.L., 1997. Carta metalogenética da Provéncia Auréfera do Tapajós, in: Costa, M.L.C., Ange´lica, R.S. (Eds.), Contribuic¸o˜es a` Geologia da Amazônia. Sociedade Brasileira de Geologia, Belém, Brazil 1, 423-437.

Fernandes, C.M.D., Juliani, C., Monteiro, L.V.S., Lagler, B., Misas, C.M.E., 2011. High-K calc-alkaline to A-type fissure-controlled volcano-plutonism of the São Félix do Xingu region, Amazonian craton, Brazil: Exclusively crustal sources or only mixed Nd model ages? Journal of South America Earth Science 32 (4), 351-368.

Ferrari, L., Orozco-Esquivel, T., Manea, V.C., Manea, M., 2012. The dynamic history of the Trans-Mexican Volcanic Belt and the Mexico subduction zone. Tectonophysics 522-523, 122-149.

Ferreira, A.L., Almeida, M.E., Brito, M.F.L., Monteiro, M.A.S., 2000. Projeto Especial Província Mineral do Tapajós. Geologia e recursos minerais da Folha Jacareacanga (SB.21-Y-B). Estados do Pará e Amazonas. Escala 1:250.000. Nota explicativa e mapas, CPRM, Brasília. [CD ROM].

Ferron, J.M.T.M., Bastos-Neto, A.C., Lima, E.F., Nardi, L.V.S., Costi, H.T., Pierosan, R., Prado, M., 2010. Petrology, geochemistry, and geochronology of Paleoproterozoic volcanic and granitic rocks (1.89–1.88 Ga) of the Pitinga Province, Amazonian Craton, Brazil. Journal of South American Earth Sciences 29, 483-497.

Fink, J., 1983. Structure and emplacement of a rhyolitic obsidian flow: little Glass Mountain, Medicine Highland, northern California. GSA Bull. 94, 362-380.

Fink, J.H., Manley, C.R., 1987. Origin of pumiceous and glassy textures in rhyolite flows and domes: Geological Society of America Special Paper 212, 77-88.

Fisher, R.V., 1961. Proposed classification of volcaniclastic sediments and rocks. Geological Society of America Bulletin 72, 1409-1414.

French, J.E., Heaman, L.M., Chacko, T., Srivastava, R.K., 2008. 1891–1883 Ma Southern Bastar–Cuddapah mafic igneous events, India: a newly recognized large igneous province. Precambrian Research 160, 308-322.

Giordano, D., La Felice, S., Arzilli, F., De Cristofaro, S.P., Masotta, M., Polo L. (2017). Il vulcanismo effusivo acido del Monte Amiata: stima delle condizioni pre- e sin-eruttive ed implicazioni vulcanologiche. Effusive acidic volcanism of Monte Amiata: estimates of pre- and syn-eruptive conditions and volcanological implications. Monografia Il Vulcano di Monte Amiata, ISBN 978-88-99742-32-4, 171-193.

Giordano, D., Nichols, A.R.L., Dingwell, D.B., 2005. Glass transition temperatures of natural hydrous melts: a relationship with shear viscosity and implications for the welding process. Jour. Volc Geoth. Res. 142, 105-118.

Giovanardi, T., Girardi, V.A.V., Correia, C.T., Sinigoi, S., Tassinari, C.C.G., Mazzucchelli, M., 2015. U-Pb zircons SHRIMP data from the Cana Brava Layered Complex: New constraints for the mafic-ultramafic intrusions of Northern Goiás, Brazil. Open Geosci 7, 197-206.

Goldfarb, R., Groves, D., Gardoll, S., 2001. Rotund versus skinny orogens: well-nourished or malnourished gold? Geology 29, 539-542.

Gutscher, M.A., Maury, R., Eissen, J.P., Bourdon, E., 2000. Can slab melting be caused by flat subduction? Geology 28, 535-538.

Hanson, R.E., Gose, W.A., Crowley, J.L., Ramezani, J., Bowring, S.A., Bullen, D.S., Hall, R.P., Pancake, J.A., Mukwakwami, J., 2004. Paleoproterozoic intraplate magmatism and basin development on the Kaapvaal Craton: age, paleomagnetism and geochemistry of ~1.93 to ~1.87 Ga post-Waterberg dolerites. South African Journal of Geology 107, 233-254.

Hasui, Y., Haraly, N.L.E., Schobbenhaus, C., 1993. Megaestruturação Pré-Cambriana do território brasileiro baseada em dados geofísicos e geológicos. Geociências 12, 7-31.

Heiken, G, Wohletz, K., 1987. Tephra deposits associated with silicic domes and lava flows. GSA Special Paper 212.

Heiken, G., Krier, D., McCormick, T., Snow, M.G., 2000. Intracaldera volcanism and sedimentation — Creede caldera, Colorado. In: Bethke, P.M., Hay, R.L. (Eds.), Ancient Lake Creede: Its volcano-tectonic setting, history of sedimentation, and relation to mineralization in the Creede Mining District. Geological Society of America Special Paper, 346. Boulder, Colorado, 127-157.

Hofmann, A.W., 1988. Chemical differentiation of the Earth: The relationship between mantle, continental crust and oceanic crust. EPSL 90, 297-314.

Hollocher, K., Robinson, P., Walsh, E., Roberts, D., 2012. Geochemistry of amphibolite-facies volcanics and gabbros of the Støren Nappe in extensions west and southwest of Trondheim, Western Gneiss Region, Norway: a key to correlations and paleotectonic settings. American Journal of Science 312, 357-416.

Juliani, C., 2002. Alteração hidrotermal e metalogênese em sistemas vulcano-plutônicos paleoproterozóicos na Província Aurífera do Tapaj, Cráton Sul Amazônico, Pará. Tese de Livre-Docência, IG/USP.

Juliani, C., Vasquez, M.L., Klein, E.L., Villas, R.N., Echeverri-Misas, C.M., Santiago, E.S.B., Monteiro, L.V.S., Carneiro, C.C., Fernandes, C.M.D., Usero, G., 2014. Metalogenia da Província Tapajós. In: Silva M.G.; Jost H.; Kuyumajian R.M. (Org.). Metalogênese das Províncias Tectônicas Brasileiras. 1 ed. : CPRM — Serviço Geológico do Brasil 1, 51-90.

Juliani, C., Rye, R.O., Nunes, C.M.D., Snee, L.W., Correa Silva, R.H., Monteiro, L.V.S., Bettencourt, J.S., Neumann, R., Neto, A.A., 2005. Paleoproterozoic high sulphidation mineralization in the Tapajós gold province, Amazonian Craton, Brazil: geology, mineralogy, alunite argon age, and stable-isotope constraints. Chemical Geology 215, 95-125.

Juliani, C., Fernandez C.M.D., 2010. Well-preserved Late Paleoproterozoic volcanic centers in the São Félix do Xingu region, Amazonian Craton, Brazil. Journal of Volcanology and Geothermal Research 191, 167-179.

Kay, S.M., Godoy, E., Kurtz, A., 2005. Episodic arc migration, crustal thickening, subduction erosion, and magmatism in the south_central Andes. Geological Society of America Bulletin 117, 67-88.

Klein, E.L., Almeida, M.E., and Costa, L.T.R., 2012. The 1.89-1.87 Ga Uatumã Silicic Large Igneous Province, northern South America: Large Igneous Provinces Commission: http://www.largeigneousprovinces.org/12nov (accessed 12 January 2012).

Klein, E.L., Santos, R.A., Fuzikawa, K., Angélica, R.S., 2001. Hydrothermal fluid evolution and structural control of the brittle-style Guarim lode-gold mineralisation, Tapajós Province, Amazonian Craton, Brazil. Miner. Depos. 36, 149-164.

Klein, E.L., Vasquez, M.L., Rosa-Costa, L.T., Carvalho, J.M.A., 2002. Geology of Paleoproterozoic gneiss- and granitoid-hosted gold mineralization in Southern

Tapajós Gold Province, Amazonian Craton, Brazil. Intern. Geol. Rev., 44, 544-558.

Klein, E.L., Rosa-Costa, L.T., Carvalho, J.M.A., 2004. Estudo de inclusões fluidas em veio de quartzo aurífero do prospecto Patinhas, Província Aurífera do Tapajós, Cráton Amazônico. RBG 34, 59-66.

Lagler, B., Juliani, C., Pessoa, F.F., Fernandes, C.M.D., 2011. Petrografia e geoquímica das sequências vulcânicas Paleoproterozóicas na região de Vila Tancredo, São Félix do Xingu (PA). In: SBGq, Congr. Bras. Geoquí., 13, e Simp. Países do Mercosul, 3, Gramado, RS. Anais, [CD-ROM].

Lamarão, C.N., Dall'Agnol, R., Lafon, J.M., Lima, E.F., 1999. As associações vulcânicas e plutônicas de Vila Riozinho e Morais Almeida, Província Aurífera do Tapajós, SW do estado do Pará. In: Simpósio sobre Vulcanismo e Ambientes Associados. 1, Gramado*/RS, Boletim de resumos, 93 (in Portuguese).

Lamarão, C.N., Dall'agnol, R., Lafon, J.M., Lima, E.F., 2002. Geology, geochemistry, and Pb-Pb zircon geochronology of the Paleoproterozoic magmatism of Vila Riozinho, Tapajós Gold Province, Amazonian craton, Brazil. Prec. Res. 119, 189-223.

Lamarão, C.N., Dall'agnol, R., Pimentel, M.M., 2005. Nd isotopic composition of Paleoproterozoic volcanic rocks of Vila Riozinho: Implications for the crustal evolution of the Tapajós gold province, Amazon craton. J. South Am. Earth Sci. 18, 277-292.

Legros, F., Kelfoun, K., 2000. On the ability of pyroclastic flows to scale topographic obstacles. J. Volcanol. Geotherm. Res. 98, 235-241.

Lenhardt, N., Hornung, J., Hinderer, M., Böhnel, H., Torres-Alvarado, I.S., Trauth, N., 2011. Build-up and depositional dynamics of an arc front volcaniclastic complex: the Miocene Tepoztlan Formation (Transmexican Volcanic Belt, Central Mexico). Sedimentology 58, 785-823.

Lenhardt, N., Eriksson, P., Catuneanu, O., Bumby, A.J., 2012. Nature of and controls on volcanism in the ca. 2.32-2.06 Ga Pretoria Group, Transvaal Supergroup, Kaapvaal Craton, South Africa. Precambrian Reasearch 214-215, 106-123.

Lenhardt, N., Masango S.M., Jolayemi, O.O., Lenhardt, S.Z., Peeters, G.J., Eriksson, P.G., 2017. The Palaeoproterozoic (~2.06 Ga) Rooiberg Group, South Africa: Dominated by extremely high-grade lava-like and rheomorphic ignimbrites? New observations and lithofacies analysis. Journal of African Earth Sciences 131, 213-

232.

Lesti, C., Porreca, M., Giordano, G., Mattei, M., Cas, R.A.F., Wright, H.M.N., Folkes, C.B., Viramonte, J., 2011. High-temperature emplacement of the Cerro Galán and Toconquis Group ignimbrites (Puna plateau, NW Argentina) determined by TRM analyses. Bull. Volcanol. 73, 1535-1565.

Lofgren, G., 1971. Spherulite textures in glassy and crystalline rocks. J. Geophys. Res. 76, 5635-5648.

Ludwig, K.R., 2009. Isoplot 4.1. A geochronological toolkit for Microsoft Excel. Berkeley Geochronology Center special publication 4, 76.

Macambira, E.M.B., 1997. Geologia e aspectos metalogenéticos dos elementos do grupo de platina no complexo máfico-ultramáfico da serra da Onça – sul do Pará. Tese de Mestrado, UFPA, Belém, Pará, Brasil.

Macambira, E.M.B., Vale, A.G., 1997. Programa Levantamentos Geológicos Básicos do Brasil. São Félix do Xingu. Folha SB-22-Y-B. Estado do Pará, CPRM, Brasília (in Portuguese).

Manea, V.C., Pérez-Gussinyé, M., Manea, M., 2012. Chilean flat-slab subduction controlled by overriding plate thickness and trench rollback. Geology 40 (1), 35-38.

Manville, V., Németh, K., Kano, K., 2009. Source to sink: A review of three decades of progresss in the understanding of volcaniclastic processes, deposits, and hazards. Sedimentary Geology 220, 136-161.

McPhie, J., Doyle, M., Allen, S.R., 1993. Volcanic textures: A guide to the interpretation of textures in volcanic rocks, Centre for Ore Deposit and Exploration Studies. University of Tasmania, 198.

Miall, A.D., 1996. The Geology of Fluvial Deposits: Sedimentary Facies, Basin Analysis, and Petroleum Geology. Springer-Verlag, New York. 582.

Minifie, M.J., Kerr, A.C., Ernst, R.E., Hastie, A.R., Ciborowski, T.J.R., Desharnais, G., Millar, I.L., 2013. The northern and southern sections of the western ca. 1880 Ma Circum-Superior Large Igneous Province, North America: the Pickle Crow dyke connection? Lithos 174, 217-235.

Monteiro, L.V.S., Xavier, R.P., de Carvalho, E.R., Hitzman, M.W., Johnson, C.A., de Souza Filho, C.R., Torresi, I., 2008. Spatial and temporal zoning of hydrothermal alteration and mineralization in the Sossego iron oxide-copper-gold deposit, Carajás Mineral Province, Brazil: paragenesis and stable isotope constraints.

Miner Deposita 43, 129-159.

Mori, L., Gómez-Tuena, A., Cai, Y., Goldstein, S., 2007. Effects of prolonged flat subduction on the Miocene magmatic record of the central Trans-Mexican Volcanic Belt. Chemical Geology 244, 452-473.

Mori, P.E., Reeves, S., Correia, C.T., Haukka, M., 1999. Development of a fused glass disc XRF facility and comparison with the pressed powder pellet technique at Instituto de Geociências. Rev. Bras. Geociências, 29, 441-446.

Mueller, W.U., Concoran, P.L., 1998. Late-orogenic basins in the Archaean Superior Province, Canada: characteristics and inferences. Sedimentary Geology 120, 177-203.

Mueller, W.U., Chown, E.H., Thurston, P.C:, 2000a. Processes in physical volcanology and volcaniclastic sedimentation: modern and ancient. Precambrian Research 101, 81-85.

Navarro, M.S., Andrade, S., Ulbrich, H.H.G.J., Gomes, C.B., Girardi, V.A.V., 2008. The analysis of rare earth elements with ICP-MS in basaltic and related rocks: testing the efficiency of sample decomposition procedures. Geostand. Geoanal. Res. 32(2),167-180.

Németh, K., Cronin, S.J., Stewart, R.B., Charley, D., 2009. Intra- and extra- caldera volcaniclastic facies architecture of a frequently active mafic island-arc volcano, Ambryn Island, Vanuatu. Sedimentary Geology 220, 256-270.

Oberholzer, J.D., Eriksson, P.G., 2000. Subaerial volcanism in the Palaeoproterozoic Heekpoort Formation (Transvaal Supergroup), Kaapvaal craton. Precambrian Research 101, 193-210.

Pearce, J.A., Harris, N.B.W., and Tindle, A.G., 1984. Trace element discrimination diagrams for the tectonic interpretation of granitic rocks. Journal of Petrology 25, 956-983.

Pearce, J.A., 1996. Sources and settings of granitic rocks. Episodes 19 (4), 120-125.

Pessoa M.R., Santiago A.F., Andrade A.F., Barreto E.L., Nascimento J.O., Santos J.O.S., Oliveira J.R., Lopes R.C., Prazeres W.V. 1977. Projeto Jamanxim. CPRM/DNPM, 1-3, 614.

Pierosan, R., Lima, E.F., Nardi, L.V.S., Bastos Neto, A.C., Campos, C.P., Jarvis, K., Ferron, J.M.T.M., Prado, M., 2011. Geochemistry of Palaeoproterozoic volcanic rocks of the Iricoumé Group, Pitinga Mining District, Amazonian craton, Brazil: International Geology Review 53, 946-979.

Pinho, S.C.C., Fernandes, C.M.D., Teixeira, N.P., Paiva Jr., A.L., Cruz, V.L., Lamarão, C.N., Moura, C.A.V., 2006. O magmatismo paleoproterozóico da região de São Félix do Xingu, Província Estanífera do Sul do Pará: Petrografia e geocronologia. Revista Brasileira de Geociências 36, 793-802.

Pioli, L., Rosi, M., 2005. Rheomorphic structures in a high-grade ignimbrite: the Nuraxi tuff, Sulcis volcanic district (SW Sardinia, Italy). Journal of Volcanology and Geothermal Research 142, 11-28.

Polo, L.A., Giordano, D., Janasi, V., Freitas-Guimaraes, L., 2017(a). Effusive silicic volcanism in in the Paraná Magmatic Province, South Brazil: Physico-chemical conditions of storage and eruption and considerations on the rheological behaviour during emplacement. J. Volcanol. Geoth. Res. 355, 115-135.

Polo L.A., Janasi V., Giordano D., Lima E.F., Cañon-Tapia E., Roverato M., 2017(b). Effusive silicic volcanism in the Paraná Magmatic Province, South Brazil: Evidence for locally-fed lava flows and domes from detailed field work. J. Volcanol. Geoth. Res. 355, 204-218.

Quane, S. L., Russell, J. K., 2005. Welding: Insights from high-temperature analogue experiments. Journal of Volcanology and Geothermal Research 142 (1-2), 67-87.

Reis, N.R., Almeida, M.E., Ferreira, A.L., Riker, S.R., 2006. Geologia e Recursos Minerais do Estado do Amazonas. Sistema de Informações Geográficas 1:1.000.000. CPRM, Manaus, 144.

Rino, S., Tsuyoshi, K., Windley, B.F., Katayama, I., Motoki, A., Hirata, T., 2004. Major episodic increases of continental crustal growth determined from zircon ages of river sands; implications for mantle overturns in the Early Precambrian. Physics of the Earth and Planetary Interiors 146, 369-394.

Roverato, M., Capra, L., Sulpizio, R., Norini, G., 2011. Stratigraphic reconstruction of two debris avalanche deposits at Colima Volcano (Mexico): insights into pre-failure conditions and climate influence. J. Volc. Geoth. Res. 207 (1), 33-46.

Roverato, M., Cronin, S., Procter, J., Capra, L., 2014. Textural features as indicators of debris avalanche transport and emplacement, Taranaki volcano. Geol. Soc. Am. Bull. B30946-1

Roverato, M., 2016. The Montesbelos mass-flow (southern Amazonian craton, Brazil): a Paleoproterozoic volcanic debris avalanche deposit? Bull. Volcanol. 78, 49.

Roverato, M., Giordano, D., Echeverri-Misas, CM., Juliani, C., 2016. Paleoproterozoic felsic volcanism of the Tapajós Mineral Province, Southern

Amazon Craton, Brazil. Journal of Volcanology and Geothermal Research 310, 98-106.

Roverato, M., Juliani, C., Marcelo Dias-Fernandes, C., Capra, L., 2017. Paleoproterozoic andesitic volcanismin the southern Amazonian craton, the Sobreiro Formation: new insights from lithofacies analysis of the volcaniclastic sequences. Precambrian Research 289, 18-30.

Russell, J. K., Quane, S. L., 2005. Rheology of welding: Inversion of field constraints. Journal of Volcanology and Geothermal Research 142 (1-2), 173-191.

Santos, J.O.S., Hartmann, L.A., Gaudette, H.E., Groves, D.I., McNaughton, N.J., Fletcher, I.R., 2000. A new understanding of the provinces of the Amazon craton based on integration of field mapping and U_Pb and Sm_Nd geochronology. Gondwana Research 3, 453-488.

Santos, J.O.S., Groves D.I., Hartmann L.A., Moura M.A., McNaughton, N.J. 2001. Gold deposits of the Tapajós and Alta Floresta Domains, Tapajós-Parima orogenic belt, Amazon Craton, Brazil. Mineralium Deposita 36, 278-299.

Santos, J.O.S., 2003. Geotectônica dos Escudos da Guiana e Brasil Central. In: L.A. Bizzi, C. Schobbenhaus, R.M. Vidotti, J.H. Gonçalves (Eds.). Geologia, tectônica e recursos minerais do Brasil. Texto, mapas e SIG. CPRM - Serviço Geológico do Brasil, Brasília 169-226.

Santos, J.O.S., Van Breemen, O.B., Groves, D.I., Hartmann, L.A., Almeida, M.E., McNaughton, N.J., Fletcher, I.R., 2004. Timing and evolution of multiple Paleoproterozoic magmatic arcs in the Tapajós Domain, Amazon Craton: constraints from SHRIMP and TIMS zircon, baddeleyite and titanite U–Pb geochronology. Prec. Res. 13, 73-109.

Silva, F.S., Oliveira, D.C., Antonio, P.Y., D'Agrella-Filho, M., Lamarão, C.N., 2016. Bimodal magmatism of the Tucuma area, Carajás Province: U-Pb geochronology, classification and processes. J. S. Am. Earth Sci. 72, 95-114.

Simões, M.S., Lima, E.F., Sommer, C.A., Rossetti, L.M.M., 2017. Structures and lithofacies of inferred silicic conduits in the Paraná-Etendeka LIP, southernmost Brazil. Journal of Volcanology and Geothermal Research 355, 319-336.

Sulpizio, R., Mele, D., Dellino, P., La Volpe, L., 2007. Deposits and physical properties of pyroclastic density currents during complex Subplinian eruptions: the AD 472 (Pollena) eruption of Somma-Vesuvius, Italy. Sedimentology 54, 607-635.

Sumner, J.M., Branney, M.J. 2002. The emplacement history of a remarkable heterogeneous, chemically zoned, rheomorphic and locally lava-like ignimbrite: 'TL' on Gran Canaria. Journal of Volcanology and Geothermal Research 115, 109-138.

Tassinari, C.C.G., Macambira, M.J.B., 1999. Geochronological provinces of the Amazonian craton. Episodes 22, 174-182.

Teixeira, M.F.B., Dall'Agnol, R., Santos, J.O.S., Oliveira, D.C., Lamarão, C.N., McNaughton, N.J., 2018. Crystallization ages of Paleoproterozoic A-type granites of Carajás province, Amazon craton: Constraints from U-Pb geochronology of zircon and titanite. J. of South American Earth Sciences 88, 312-331.

Teixeira, N.P., Bettencourt, J.S., Moura, C.A.V., Dall'Agnol, R., Macambira, E.M.B., 2002. Archean crustal sources for Paleoproterozoic tin-mineralized granites in the Carajas Province, SSE Para, Brazil: Pb_Pb geochronology and Nd isotope geochemistry. Precambrian Research 119, 257-275.

Teixeira, W., Tassinari, C.C.G., Cordani, U.G., Kawashita, K., 1989. A review of the geochronology of the Amazonian craton: tectonic implications. Precambrian Res. 42, 213-227.

Teixeira, W., Nelson, J.R., Bettencourt, J.S., Klein, E.L., Oliveira, D.C., 2019. Intraplate Proterozoic magmatism in the Amazonian Craton reviewed: geochronology, crustal tectonics and global matches. In book: Dyke Swarms of the World: A Modern Perspective. DOI:10.1007/978-981-13-1666-1_4

Van Kranendonk, M.J., 2006. Volcanic degassing, hydrothermal circulation and the flourishing of early life on Earth: a review of the evidence from c. 3490-3240 Ma rocks of the Pilbara Supergroup, Pilbara Craton, Western Australia. Earth Science Rev. 74, 197-240.

Vasquez, M.L, Klein, E.L, Macambira, M.J.B., Santos, A., Bahia, R.B.C., Ricci, P., dos, S.F., Quadros, M.L.E.S., 2000. Geochronology of granitoids, mafic intrusions and mineralizations of the Tapajós Gold Province - Amazonian Craton - Brazil. In: Inter. Geol. Congr. 31, Abstracts, [CD-ROM].

Vasquez, M.L., Sousa, C.S., Carvalho, J.M.A., 2008. Mapa Geológico e de Recursos Minerais do Estado do Pará, escala 1:1.000.000. Programa Geologia do Brasil, Belém, CPRM.

Vasquez, M.L., Dreher, A.M. 2011. Uma avaliação da estratigrafia dos eventos magmáticos de 1900-1860 Ma do Cráton Amazônico. In: SBG, Simp. Geol.

Amaz. 12, Bol. Res. [CD ROM].

Walker, G.P.L., 1983. Ignimbrite types and ignimbrite problems. J. Volcanol. Geotherm. Res. 17, 65-88.

Went, D.J., 2016 Alluvial fan, braided river and shallow-marine turbidity current deposits in the Port Lazo and Roche Jagu formations, Northern Brittany: relationships to andesite emplacements and implications for age of the Plourivo-Plouézec Group. Geol. Mag. 1-24, Cambridge University Press 2016.

White, J.D.L., Houghton, B.F., 2006. Primary volcaniclastic rocks. Geological Society of America Bulletin 34, 677-680.

Willcock, M.A.W., Cas, R.A.F., Giordano, G., Morelli, C., 2013. The eruption, pyroclastic flow behaviour, and caldera in-filling processes of the extremely large volume (N1290 km3), intra- to extra-caldera, Permian Ora (Ignimbrite) Formation, Southern Alps, Italy. J. Volcanol. Geotherm. Res. 265, 102-126.

Williams, I,S., 1998. U-Th-Pb geochronology by ion microprobe. In: McKibben, M.A., Shanks, W.C.P., Ridley, W.I. (eds) Applications of Microanalytical Techniques to Understanding Mineralizing Processes, Rev Econ Geol vol 7. Soc. Econ. Geol, Littleton, 1-35.

Wolff, J.A., Wright, J.V., 1981. Rheomorphism of welded tuffs. Journal of Volcanology and Geothermal Research 10, 13-34.

Zanchetta, G., Sulpizio, R., Di Vito, M.A., 2004. The role of volcanic activity and climate in alluvial fan growth at volcanic areas: an example form southern Campania (Italy). Sedimenatry Geology 168, 249-280.

Zernack, A.V., Cronin, S.J., Neall, V.E., Procter, J.N., 2011. A medial to distal volcaniclastic record of an andesitic stratovolcano: detailed stratigraphy of the ring-plain succession of south-west Taranaki, New Zealand: International Journal of Earth Sciences 100, 1937-1966.

Zhao, G., Cawood, P.A., Wilde, S.A., Sun, M., 2002. Review of global 2.1–1.8 Ga orogens: implications for a pre-Rodinia supercontinent. Earth-Science Reviews 59, 125-162.

Zhao, G., Sun, M., Wilde, S.A., Li, S., 2004. A Paleo-Mesoproterozoic supercontinent: assembly, growth and breakup. Earth-Science Reviews 67, 91-123.

Figure Captions

Figure 1: location map of the northern South America and the Amazonian Craton divided into several geochronological provinces and other domains according to Santos et al. (2000); TMP = Tapajós Mineral Province, SFX = São Felix do Xingú Region.

Figure 2: distribution map of the outcrops analyzed during the field campaigns in both regions a) Tapajós Mineral Province (TMP) and b) São Felix do Xingú region (SFX); PW=distribution of the Santa Rosa formation inferred during the present work; F=distribution of the Santa Rosa formation inferred by Fernandes et al. (2011); BIF=Banded Iron Formation; red and white dot refers to primary andesitic deposits analyzed in Roverato et al. (2017). In both figures are reported the outcrops described in the paper.

Figure 3: massive and banded lavas and rheo-ignimbrite (?) deposits. a) Np173 (7º33’52.31” S, 55º10’58.80” W), b) Xu23 (6º41’08.65” S, 52º25’55.67” W), c) Xu101 (6º52’12.82” S, 52º09’16.12” W), d) Xu52 (6º28’19.32” S, 51º50’08.90” W), e), f), g) Np396 (6º32’41.06” S, 55º23’59.37” W); see Fig. 2 for the outcrops location. For the lithofacies description and more details see the text.

Figure 4: massive primary volcaniclastic rocks with different proportion of ash, lapilli and blocks. All the deposits are interpreted to be emplaced from pyroclastic density currents except (f) that is interpreted as a basal-breccia of a lava body. a) Xu104 (6º52’22.96” S, 52º08’15.91” W), b) Np183 (7º32’04.13” S, 55º08’50.02” W), c) Np93 (6º44’16.60” S, 55º27’12.96” W), d) Xu29 (6º41’42.51” S, 52º01’23.06” W), e) Xu07 (6º41’56.36” S, 52º08’42.27” W) f) Xu192 (6º31’31.92” S, 53º02’36.60” W); see Fig. 2 for the outcrops location. For the lithofacies description see the text and Table 1.

Figure 5: microphotographs of different massive ash and lapilli ignimbrite deposits in thin section: a) broken crystals suggesting the fragmental character of the rock; b) detail of a devitrified juvenile fragment displaying axiolitic fabric; c) banded sub-millimetric to millimetric lithic fragments immersed in a devitrified groundmass.

Figure 6: reconstructed schematic stratigraphic column and associated photographs

representing the evolution of ignimbrite deposits cropping out in the TMP (Np183; 7º32’04.13” S, 55º08’50.02” W); note the increase of welding from the base to the top.

Figure 7: schematic stratigraphic column and relative photographs of a >150 m thick felsic banded lava(s) cropping out in SFX (Xu192; 6º31’31.92” S, 53º02’36.60” W) overlying a basal breccia (Lf mLB) and an ignimbrite deposit characterized by a low grade of welding (Lf *l-gw*LA).

Figure 8: stratified primary volcaniclastic rocks, a) related to sedimentation by highly dilute ash-cloud (Np130; 6º54’16.09” S, 55º10’59.38” W) and, b) attribute to pyroclastic surge-type depositional condition from dilute currents (XU162; 6º32’28.39” S, 52º25’26.07” W); see Fig. 2 for the outcrops location. Relative thin section microphotographs (c/d) showing micrometric shards. For the lithofacies description see the text and Table 1.

Figure 9: massive sedimentary rocks. a) The alternation of lithofacies *csG* and *mS* indicates changes in energy conditions of sedimentation belonging to a subaqueous-subaerial fan-delta interface (Np146; 6º42’58.24” S, 55º28’53.49” W); b) detail of centimeters ripples of Lf *mS* (Np89; 6º54’39.36” S, 55º26’12.28 W); c) Lf *csG* is also associated to Lf *xsSG* (see stratified rocks in section 6.2) (Np27; 8º08’18.43” S, 54º54’37.33” W). d) Np27, e) Xu209 (6º13’55.26” S, 52º42’29.25” W), f) Np158 (7º03’33.79” S, 55º24’11.84” W); the rounded and clast supported character of these lithofacies is linked with fluvial/alluvial deposition by debris-flow dominated processes; see Fig. 2 for the outcrops location. For a more detailed lithofacies description see the text and Table 1.

Figure 10: stratified sedimentary rocks. a) The quartzitic sandy cross-bedded lithofacies is interpreted as formed in fluvial channel or around margins of immature marine basins (?) (Xu 201; 6º16’12.95” S, 52º52’18.84” W); b) the cross-stratified water reworked lithofacies is linked with stream-dominated fluvial/alluvial settings (Np82; 8º03’40.79” S, 54º50’43.52” W); c) the silty sedimentation likely belong to a lacustrine environment characterized by small turbidities (Np158; 7º03’33.79” S, 55º24’11.84” W); d) the top of the photographs shows the Lf *bChs* interpreted as inorganic precipitation of silica (chert) in a closed lake basin; white arrows show

fragments of the chert deposit eroded by low-energy sandy stream flows or local lacustrine turbidites (Np90; 6º49’50.20” S, 55º28’15.47” W); see Fig. 2 for the outcrops location. For a more detailed lithofacies description see the text and Table 1.

Figure 11: sketch of a wide (300 x 80 m) outcrop in the TMP (Np407; 6º40’35.21” S, 55º21’14.63” W). The stratigraphic sequence is tilted showing sub-vertical contacts of the different deposits. The sequence is interpreted displaying at the base banded (or rheo-ignimbrite) and massive lava flows passing to fragmental deposits to the top. a) ignimbrite medium-grade welded; b) the diffuse-stratified lithofacies indicates tractive processes usually attribute to pyroclastic surge-type depositional condition from dilute currents; c) sedimentary clast-supported deposit ; d) non-welded lapilli to ash ignimbrite; e) banded lava o highly reomorphic ignimbrite (lava-like). For a more detailed lithofacies description see the text and Table 1.

Figure 12: classification diagrams for the Tapajos volcanics (TMP-V) and lava flow (TMP-LF). TAS diagram with limits of alkaline series from Kuno (1968), dashed line, and Irvine and Baragar (1971), solid line. AFM diagram with alkaline field from Irvine and Baragard (1971). SiO2 vs K2O classification diagram (Ewart, 1982). Literature values are from: VR (a) Vila Rozinho and MA (a) Moraes Almeida volcanic sequences from Lamarão et al. (2002); SF (b) Sobreiro Formation and SRF (b) Santa Rosa Formation from Fernandes et al. (2011).

Figure 13: REE and spider-diagrams of volcanics and lava flow rocks from the Tapajos region (TMP-V and TMP-LF). REE data are normalized to Chondrite I (CI; values from Ander and Ebihara, 1982) and trace elements are normalized to Mid Ocean Ridge Basalt (MORB; values from Hoffman, 1988). Literature values are from: VR (a) Vila Rozinho and MA (a) Moraes Almeida volcanic sequences are average values from Lamarão et al. (2002); SRF (b) Santa Rosa Formation from Fernandes et al. (2011) divided in -V volcanoclastics and -LF lava flow. Due to the lack of literature data, comparison of VR (a) and MA (a) is reported only for REE diagram.

Figure 14: tectonic affinity discriminant diagrams for the Tapajos volcanics (TMP-V) and lava flow (TMP-LF). Zr+Nb+Ce+Y (ppm) vs FeO_{tot}/MgO (wt.%) diagram. Yb vs

Ta diagram. La/Yb vs Nb/La diagram. Th-Ta-Hf/3 diagram. Literature values are from: VR (a) Vila Rozinho and MA (a) Moraes Almeida volcanic sequences from Lamarão et al. (2002); SF (b) Sobreiro Formation and SRF (b) Santa Rosa Formation from Fernandes et al. (2011).

Figure 15: geochronological U-Pb data from Tapajos zircons. Average $^{206}Pb/^{207}Pb$ age (errors are calculated as 2σ) of the three samples. Probability density plot of $^{206}Pb/^{207}Pb$ ages. Calculated concordia age for sample NP396 (lava flow) and NP183 (ignimbrite).

Figure 16: geochronological U-Pb data from Xingu zircons. Calculated concordia age for ignimbrite sample XU-08. Probability density plot of $^{206}Pb/^{207}Pb$ ages.

Figure 17: peleogeographic reconstruction of the fissural and calderic volcanic activity during the Late-Paleoproterozoic in the southern part of the Amazonian craton. In the foreground is shown a section of a caldera and a post-caldera ignimbrite uplift that could facilitate the production of new sediments to be reworked and transported. The rising magma could form sporadic intra-caldera domes and volcanic centers as also shown in the background calderas. Reworked sediments can accumulate into volcano-tectonic depressions, which often collects intra-caldera lakes. In the background a fissure-fed volcanism is the responsible of the emission of lava flows and/or high-grade to rheomorphic ignimbrites. Fluvial deposits that occur throughout all successions represent periods of stream and river reworking. The area in punctuated by little scoria cones and maars that contribute to the amount of the fragmental products well represented in the study regions.

Tables

Table 1: Summary of the main characteristics of volcaniclastic lithofacies of the primary and secondary products analyzed and their interpretation.

Table 2: Major and trace element bulk rock composition of Tapajos samples. Class identify the lithological features of the rocks: VC: volcanoclastic; I: ignimbrite; R: rhyolite; Type identify the geochemical affinity according to the granite classification (Zr+Nb+Ce+Y (ppm) vs FeO_{tot}/MgO (wt.%) diagram, Fig. 14): I is for I-type granites and A is for A-type granites; b.d.l. is below detection limits; Mg# is calculated as Mg^{2+} / (Fe^{2+}_{t} + Mg^{2+}); (*) major elements analyses already published in Roverato et. (2016).

Figure 1

Click here to download high resolution image

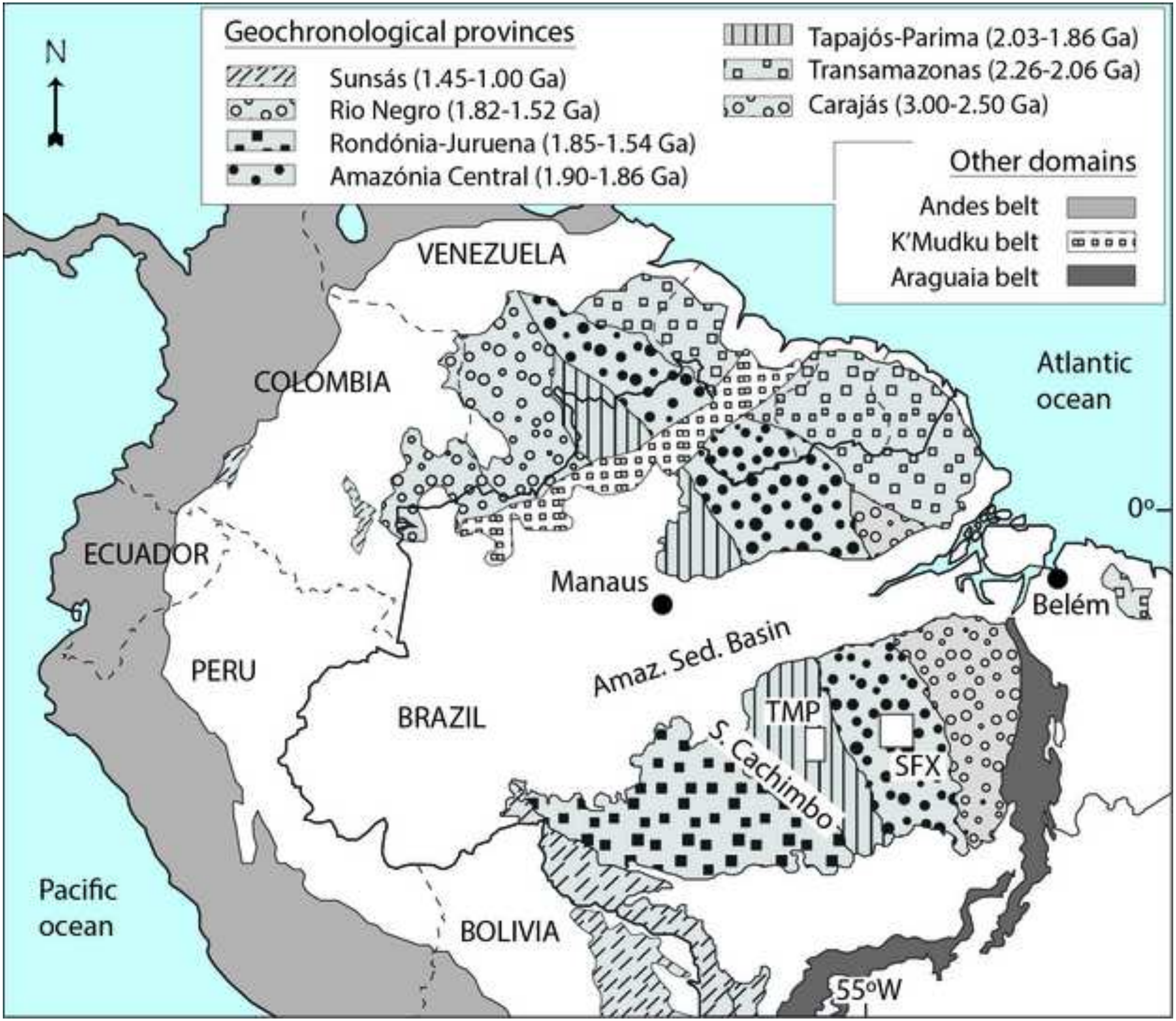

Figure 2
Click here to download high resolution image

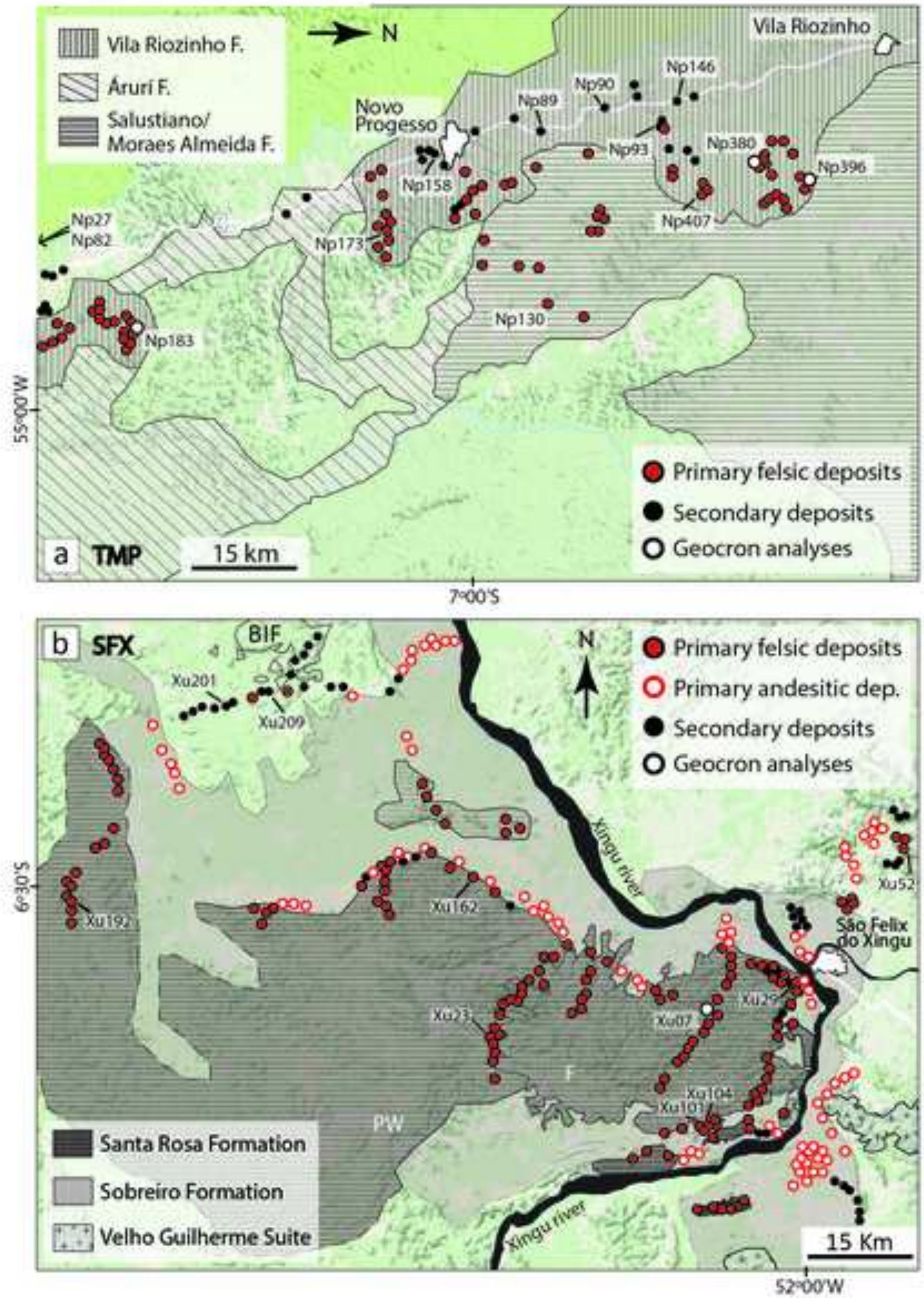

Figure 3

Click here to download high resolution image

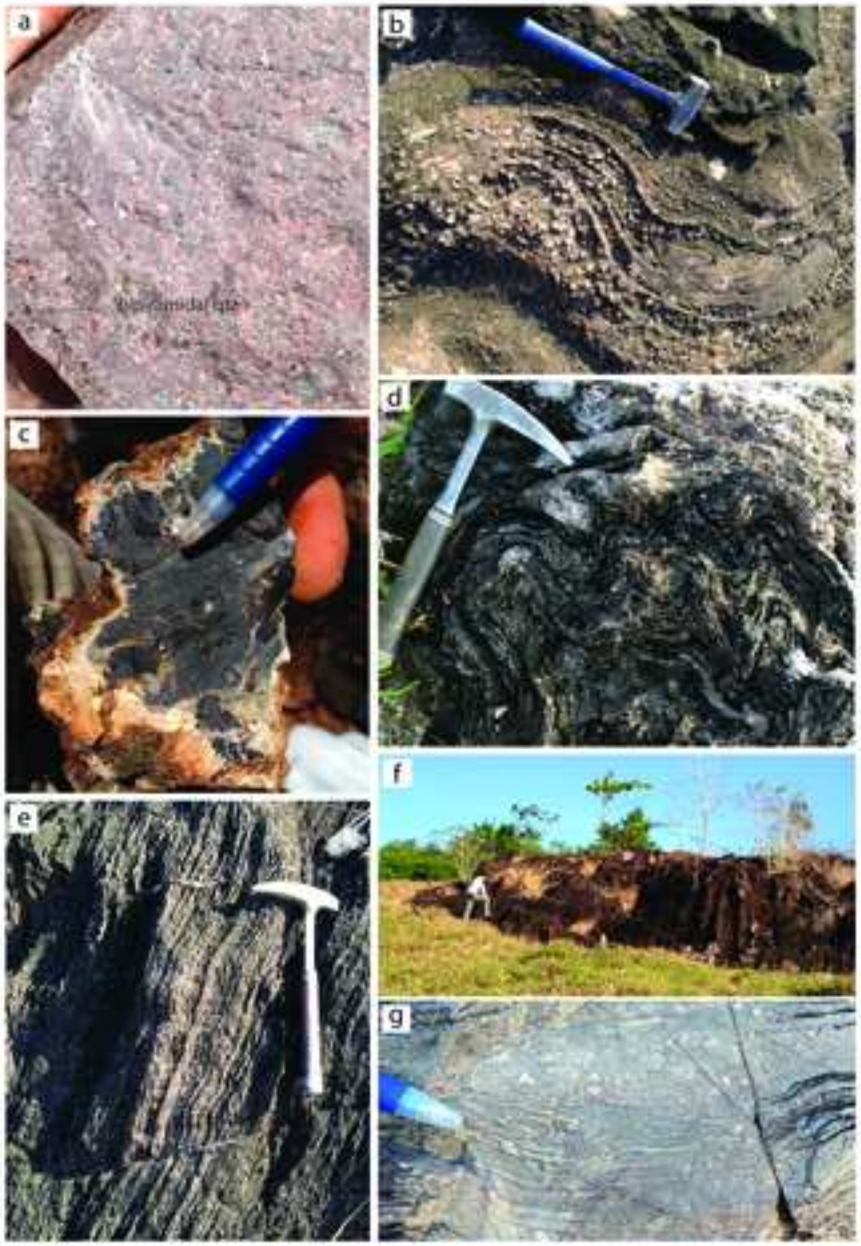

Figure 4
Click here to download high resolution image

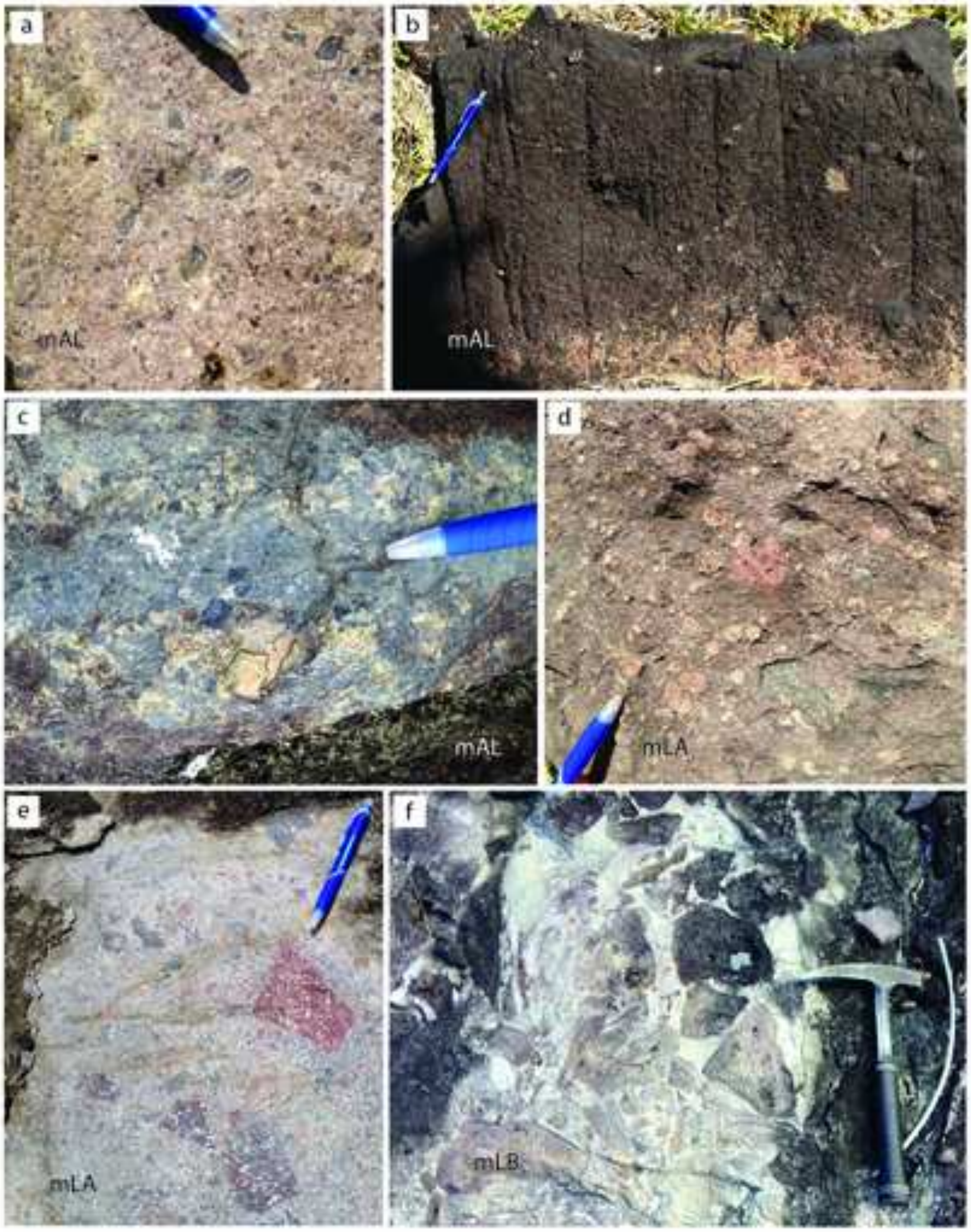

Figure 5

Click here to download high resolution image

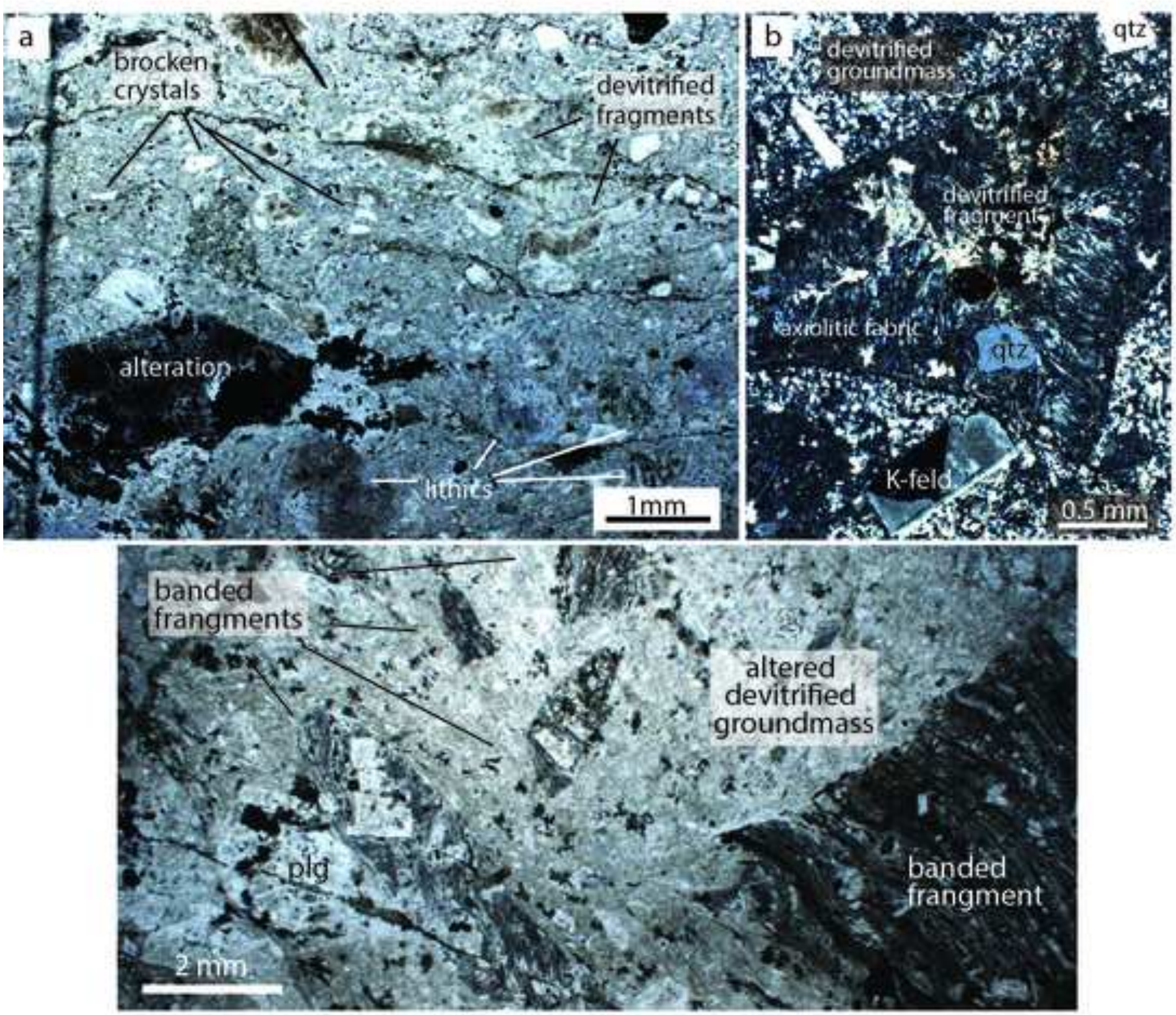

Figure 6
Click here to download high resolution image

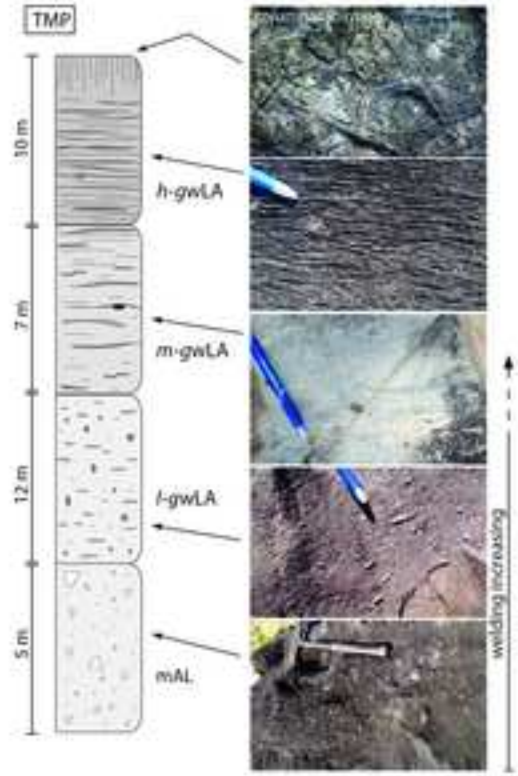

Figure 7
Click here to download high resolution image

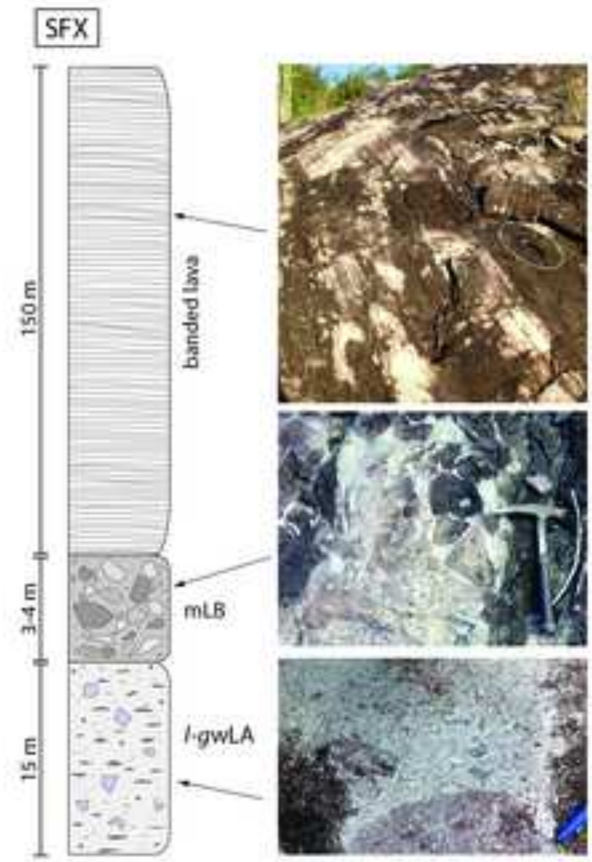

Figure 8
Click here to download high resolution image

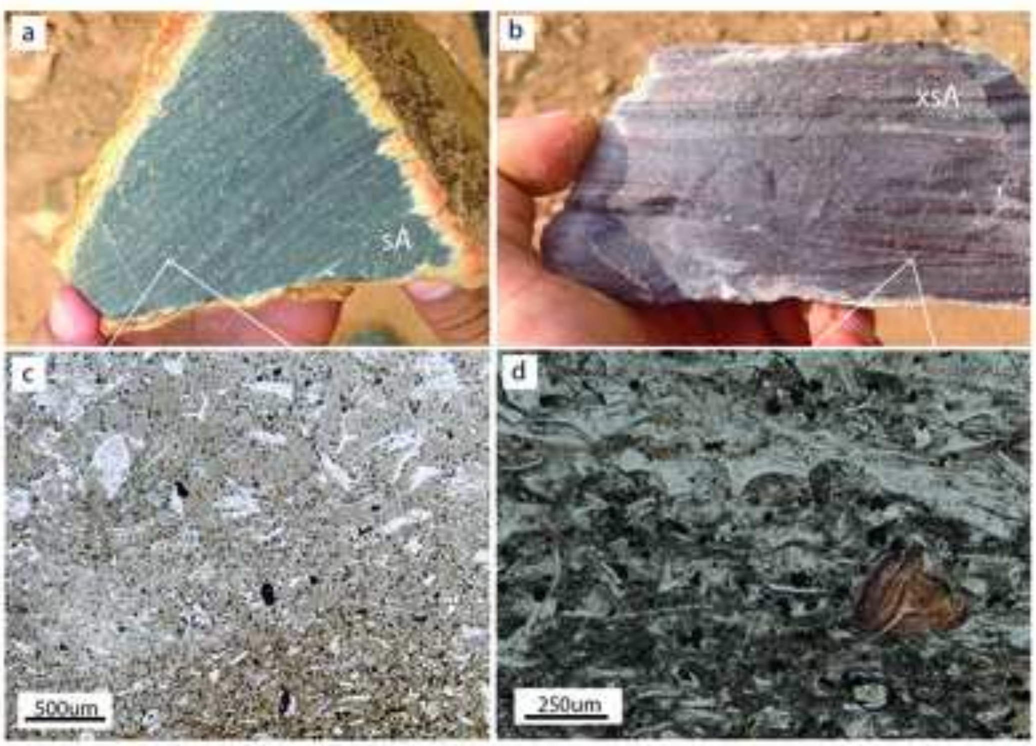

Figure 9
Click here to download high resolution image

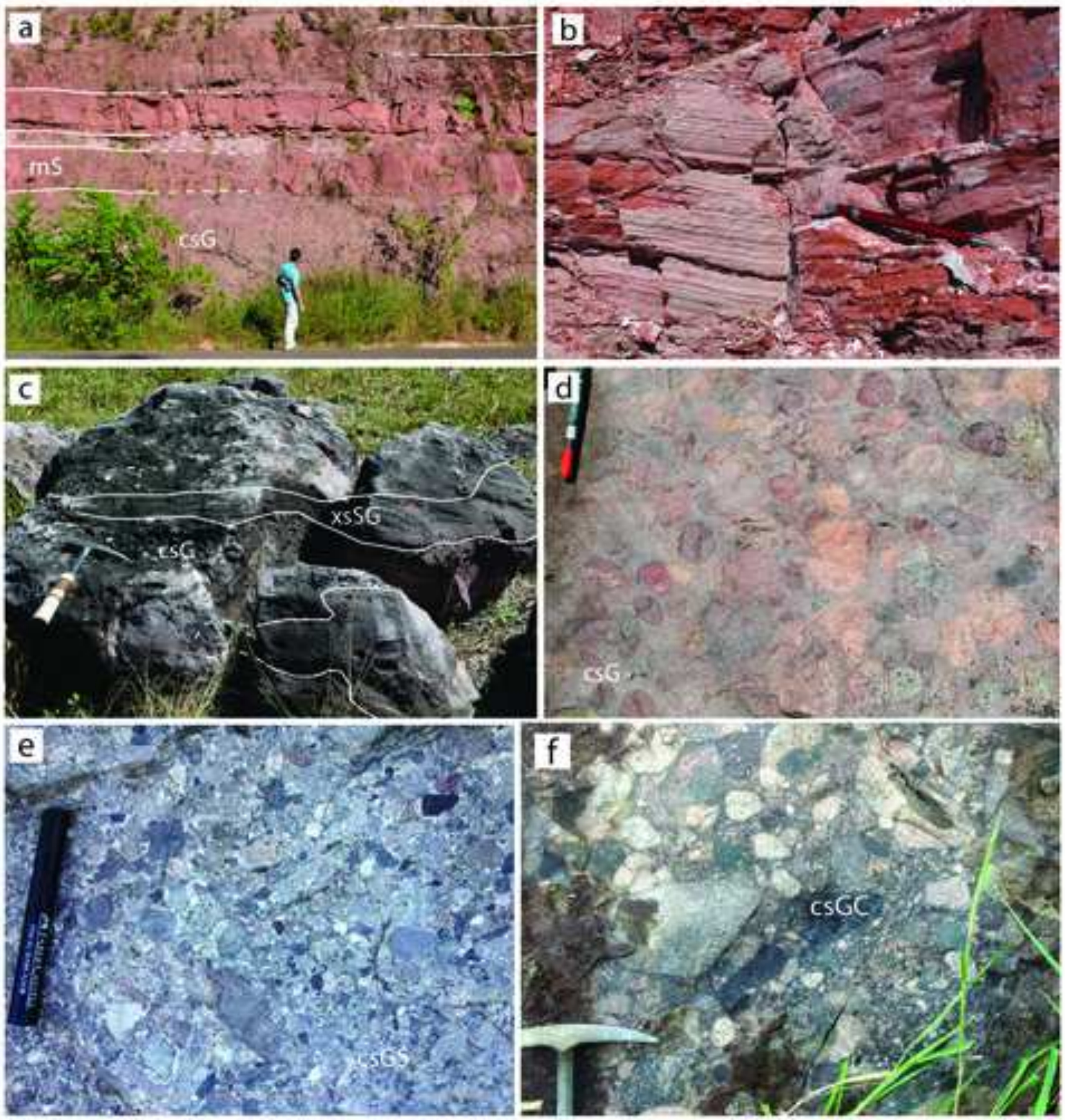

Figure 10
Click here to download high resolution image

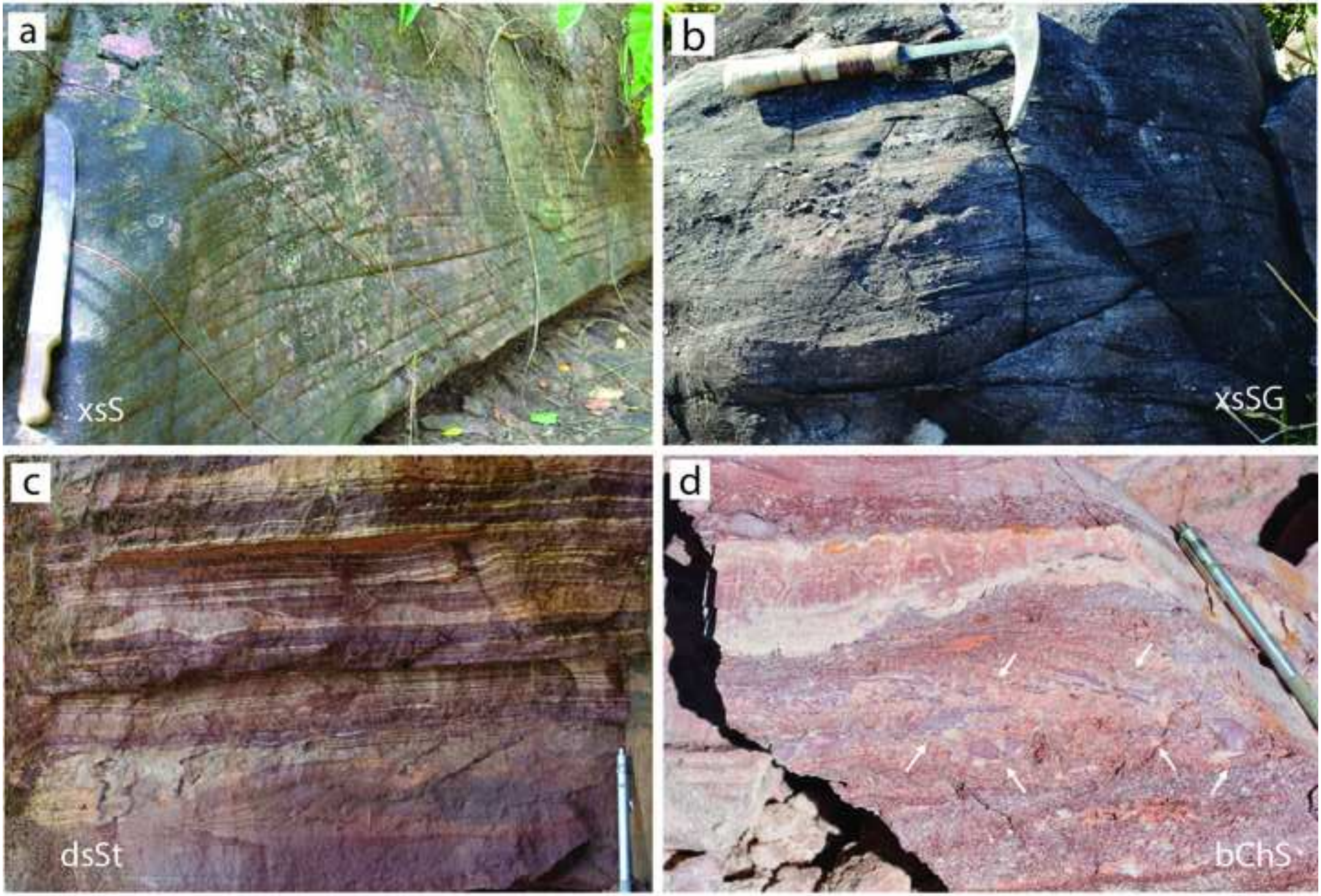

Figure 11
Click here to download high resolution image

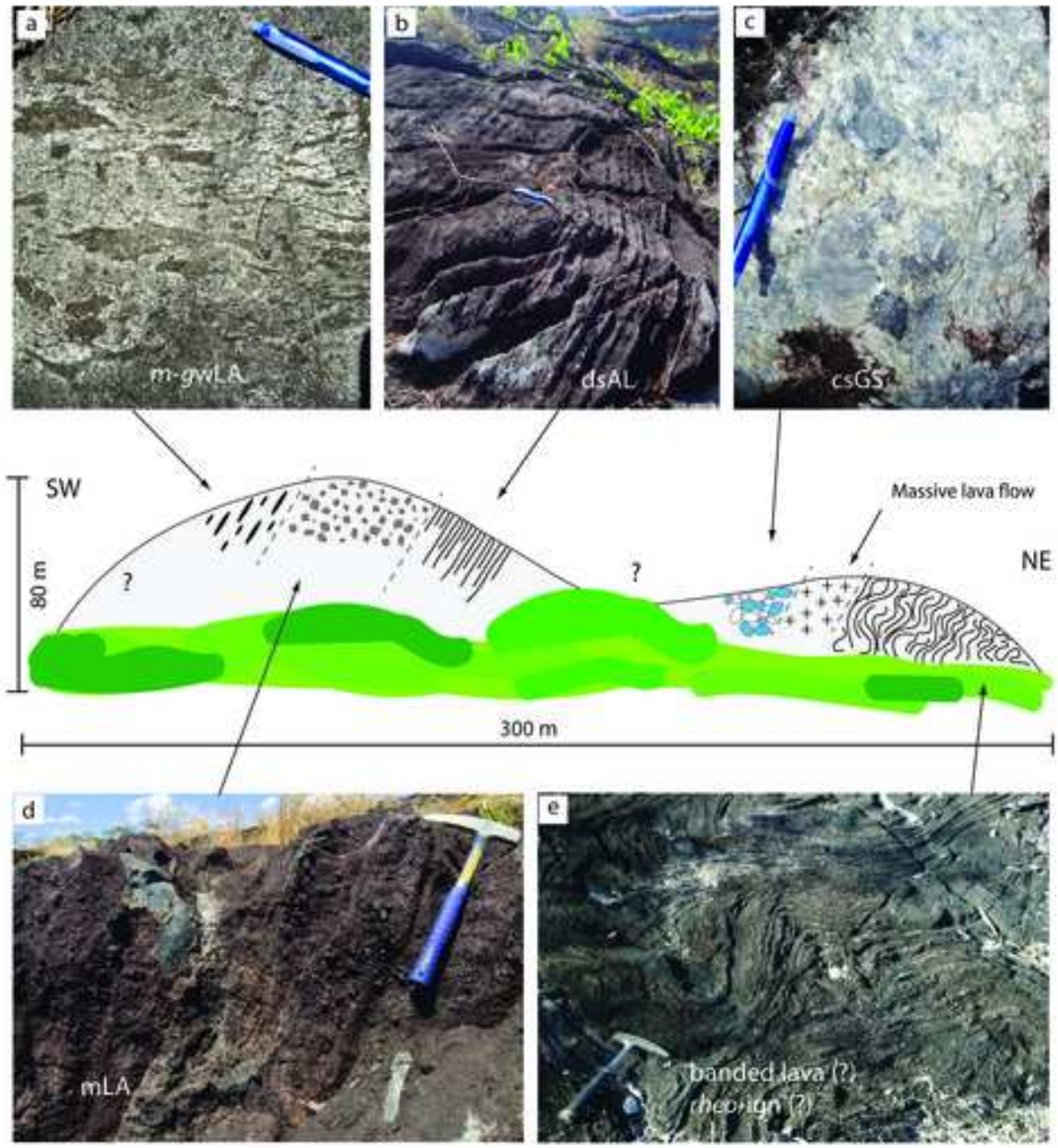

Figure 12

Click here to download high resolution image

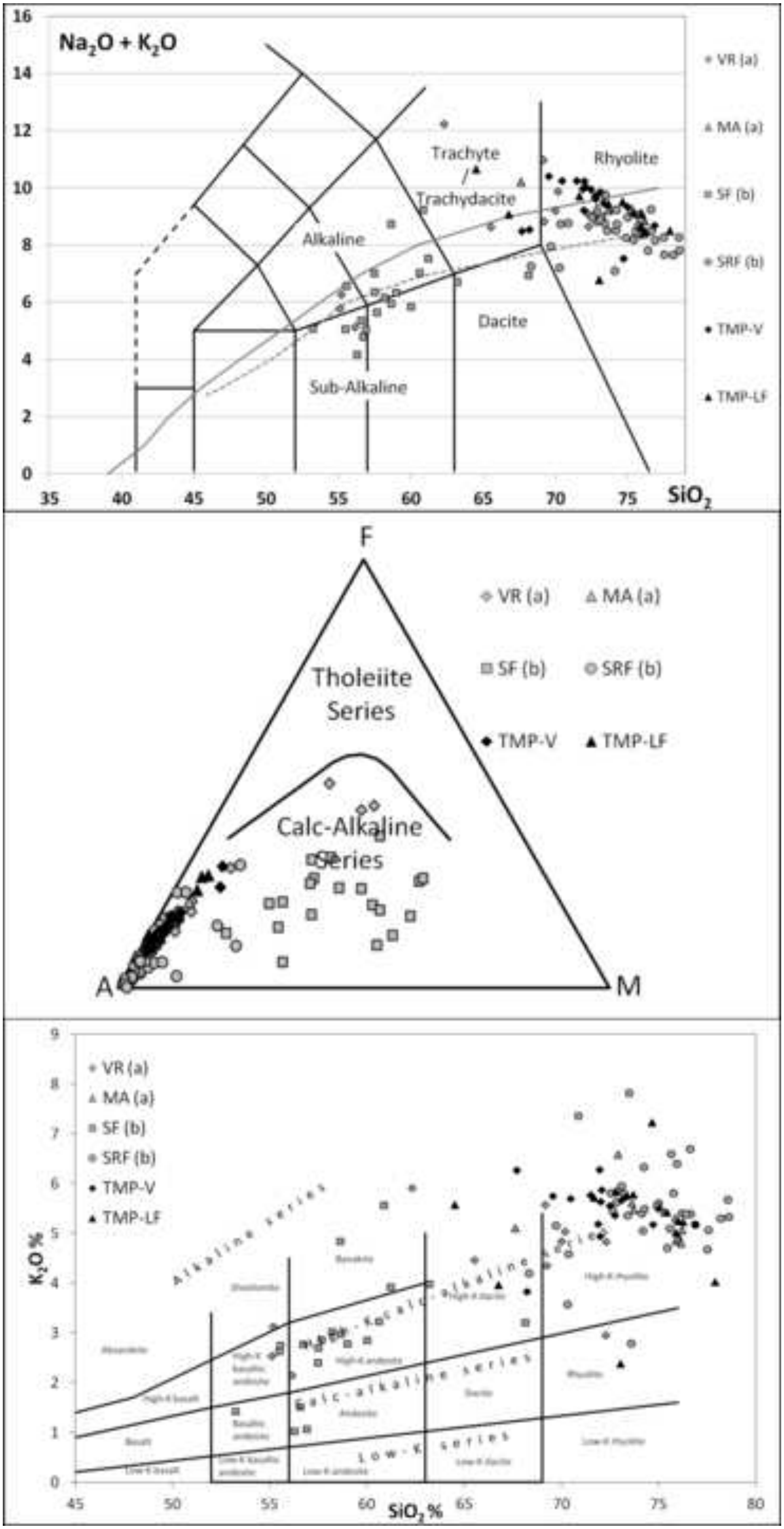

Figure 13
Click here to download high resolution image

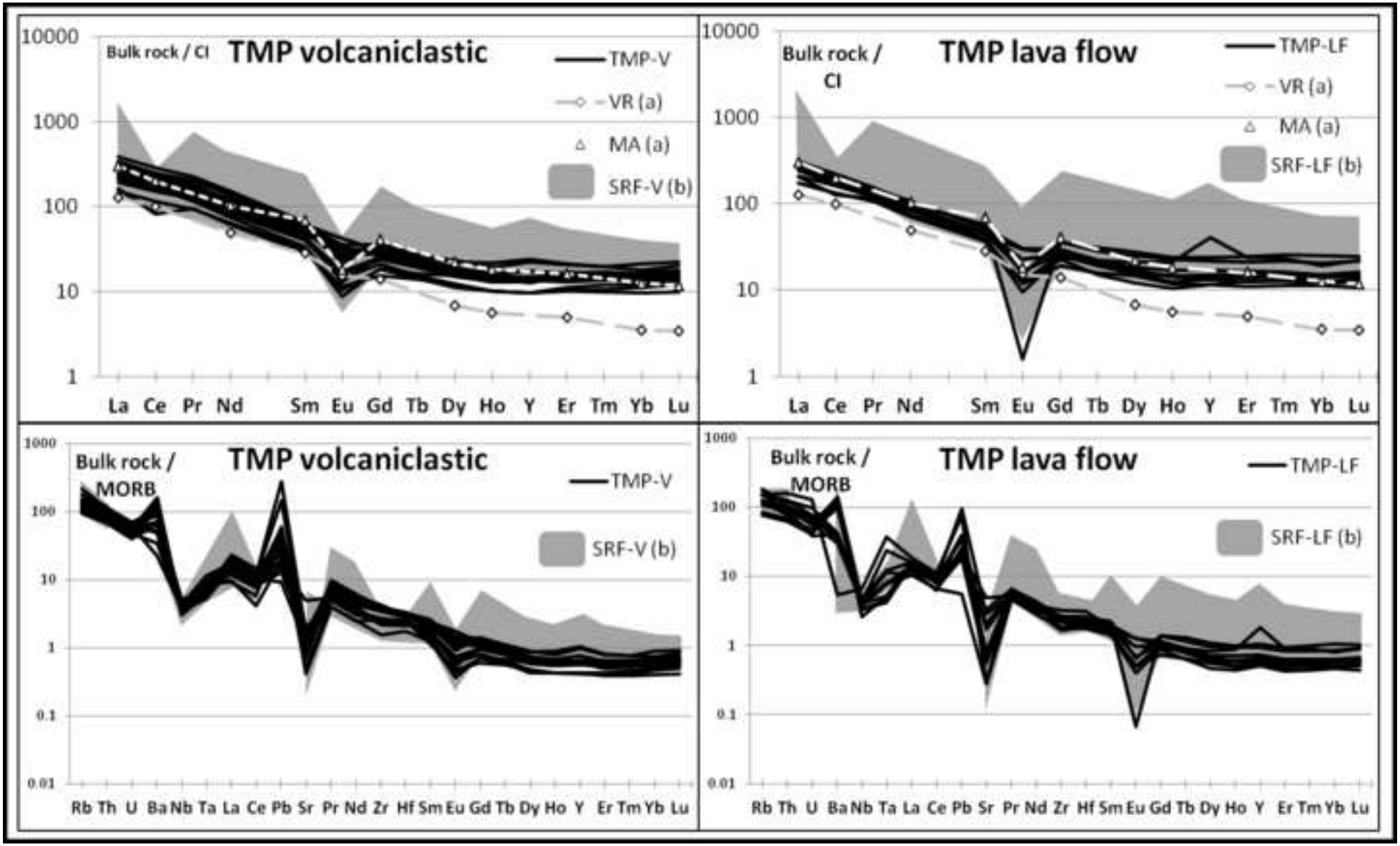

Figure 14

Click here to download high resolution image

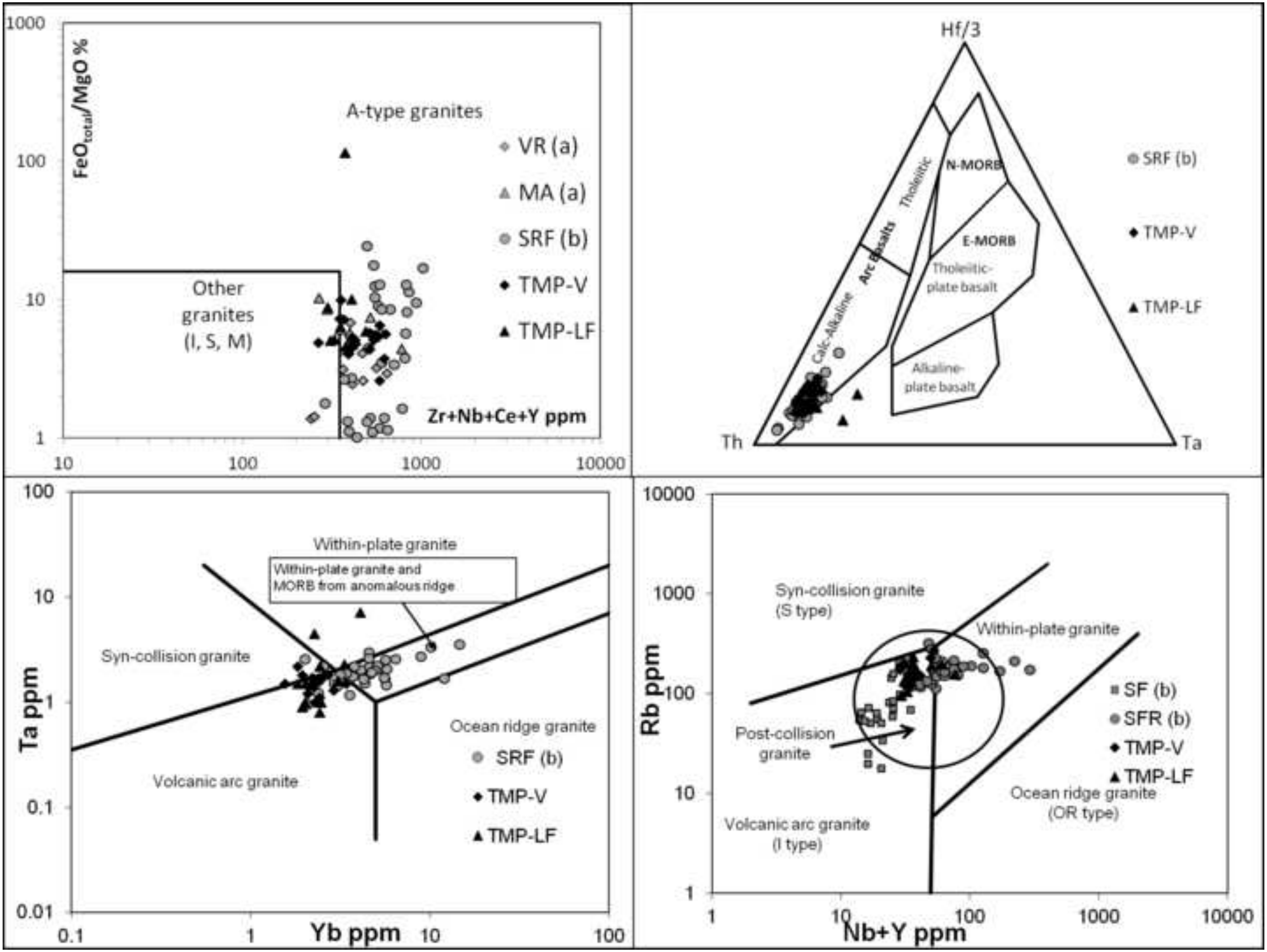

Figure 15

Click here to download high resolution image

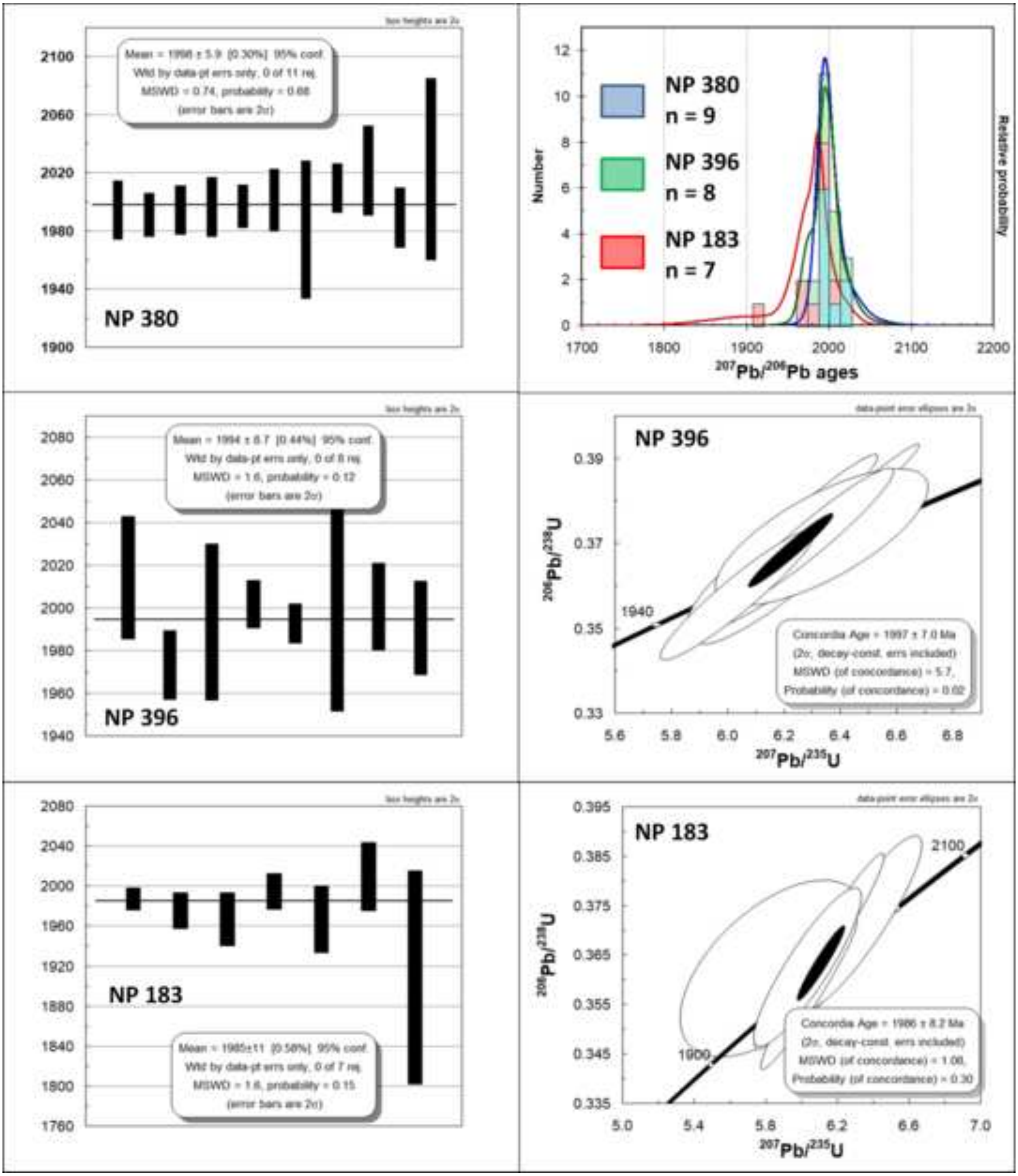

Figure 16
Click here to download high resolution image

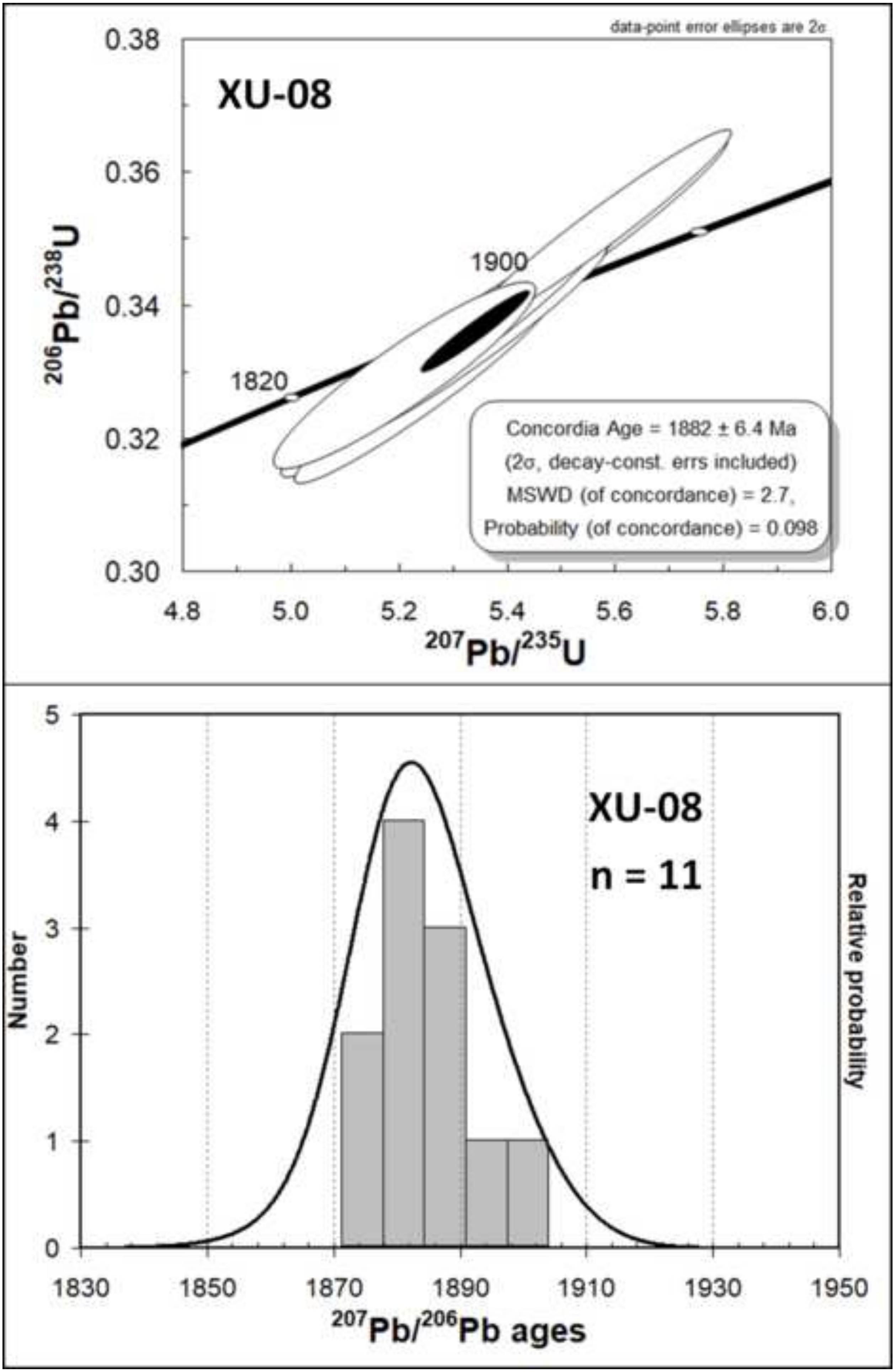

Figure 17
Click here to download high resolution image

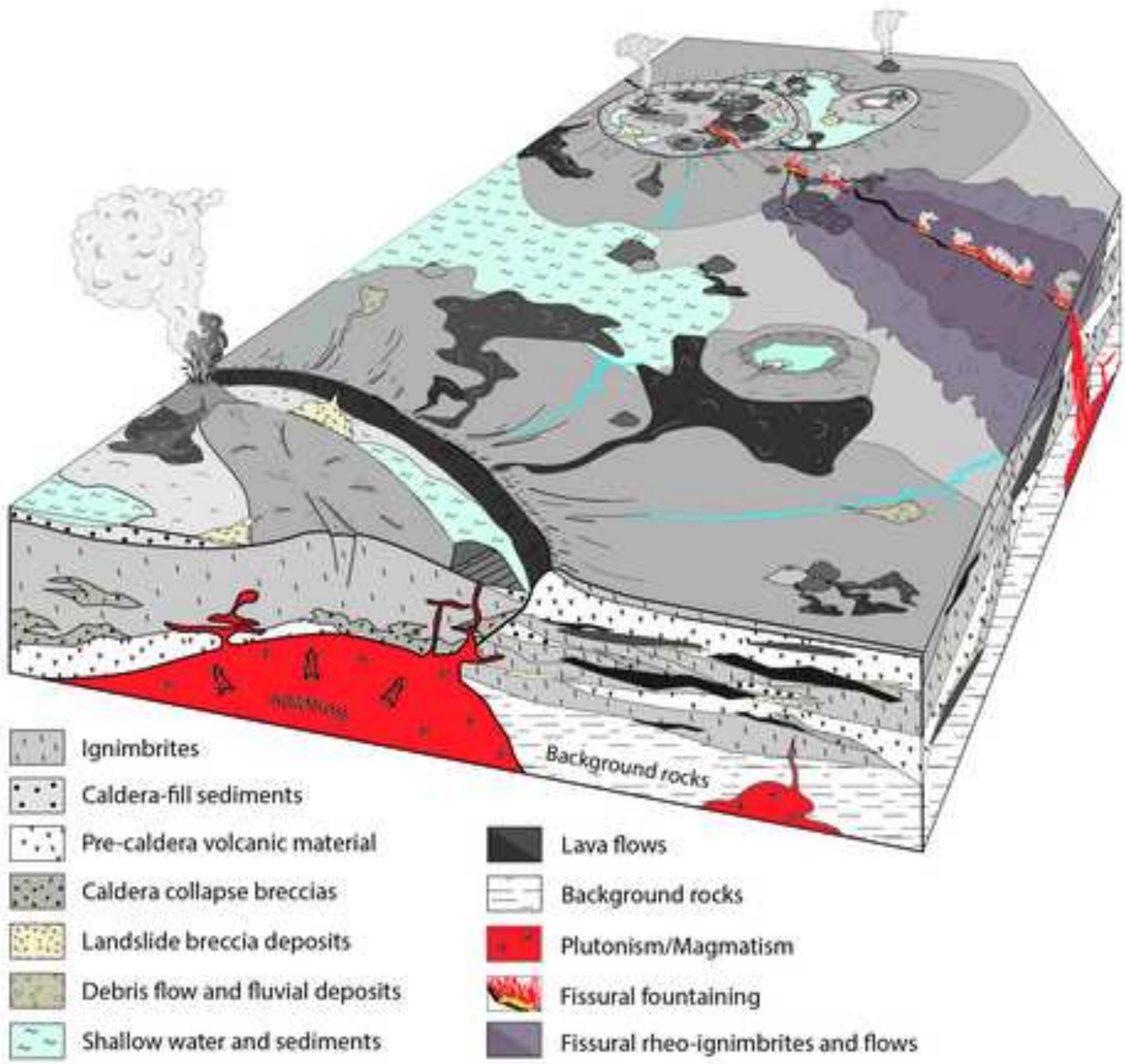

Table 1

			Lithofacies	Description	Interpretation
Primary volcaniclastic rocks	Massive		**mAL** Massive Ash to Lapilli	Massive fine and coarse ash and variable fine to coarse lithic lapilli content. Devitrified fragments immersed. Brocken crystal (plg/prx) content. Moderate to bed sorting.	The massive fine aspect suggests deposition from a dilute pyroclastic density current (PDC). Brocken crystals confirm the fragmental character. Granular flow regime.
			mLA Massive Lapilli and Ash	Massive, fine, fine to coarse and coarse devitrified lapilli immerse in ash matrix, less blocks immersed, maximum size 20-25 cm. Moderate sorting.	The massive aspect suggests deposition from a dilute PDC. The coarser character could be also related to proximal co-ignimbritic breccias as result of deposition by denser pyroclastic granular flows.
			mLB, Massive Lapilli and Block	Massive, monolithologic, angular coarse lapilli and blocks (50-60 cm) immersed in lapilli matrix. Moderate sorting.	Basal auto-brecciation of lava flows and/or rheo-ignimbrite flows
		Welded ignimbrites	*l-g***wLA**, *m-g***wLA**, *h-g***wLA** low-, medium-, high-grade welded Lapilli and Ash	Massive, fine to coarse, moderately to strongly flattened devitrified lapilli (*fiamme*) varying from millimetric to 3–4 cm in size and lithic lapilli and ash. Crystal content. Clasts are immersed in a homogeneous ashy matrix. Low- to high-grade welded deposits. Eutaxitic texture. Moderate sorting.	The massive aspect suggests deposition from a pyroclastic density current. Welding is the result of post-depositional loading and are favored by low-viscosity pyroclasts that are promoted by high emplacement temperature, porosity and dissolved water.
	Banded		rheo-**ign** Rheoignimbrite (lava -like)	Layering of thin, dark and light bands and boudinaged fiamme. Parataxitic fabric displays subhorizontal bands and intricate small-scale intrafolial folds are present. The bands are deformed and flattened around lithic fragments and crystals.	The vitric fragments immersed in the welded ignimbrite distort and stretch up to the volcaniclastic flow becomes banded and starts to flow viscously.
	Stratified		**sA** Stratified Ash	Stratification of millimetric fine, devitrified, angular, sharply ash fragments.	The stratification is due to the bedding of shards fragments from a fall-out activity or from a dilute ignimbrite cloud.
			dsAL Diffusely stratified Ash to Lapilli	Diffusely stratified lithic and devitrified coarse ash and lapilli. Thickness of individual bedding surfaces ranges between few to several centimeters. Moderate sorting.	The diffuse stratification could indicates a flow boundary which is influenced by traction processes such as for pyroclastic density currents. Fall-out deposit (?).

		xsA Cross-stratified Ash	Cross-stratified fine ash formed by angular and sharply devitrified fragments (shards). Cross stratification is discontinuous over decimeters in macro-scale and as well as over millimeters in microscopic scale. Well to moderate sorted.	The internal cross-stratification indicates a grain by grain deposition process from a turbulent current with a flow boundary zone dominated by traction mechanism. Pyroclastic density currents (surge).
Secondary volcaniclastic/epiclastic rocks	Massive	**mS** Massive Sand	Massive quartzitic sand, good sorting. No internal structures. centimeter ripples at the top of the strata.	Continental supply in a shallow, low energy, water sedimentary setting. Subaerial to sub-aqueous transition.
		csG Clast supported Gravel	Clast supported polimictic gravel with rounded clasts, good sphericity and sorting. Clasts are mainly characterized by massive and banded felsic lava fragments.	Clast-supported with minor matrix content is indicative of water flow. Shallow water to subaerial. Laminar debris-flow regime in a medial reaches of stream-dominated fluvial/alluvial fans.
		csGS Clast supported Gravel to Sand	Clast supported polimictic, gravel to coarse sand with sub-rounded/sub-angular fragments, low-medium shericity.	Clast-supported with minor matrix content is indicative of water flow. Deposition within a debris-flow dominated fluvial/alluvial environment.
		csGC Clast supported Gravel and Cobble	Clast supported polimictic, gravel and cobble with sub-rounded fragments (<20 cm), low-medium shericity, low-sorted.	Water removed the finer particles during transport and deposition. Deposition within a debris-flow dominated alluvial environment.
	Stratified	**xsS** Cross-stratified Sand	Low angle cross-stratified quartzitic sand, good sorting. Layers ranges between millimeters to centimeters.	Wave-induce structure in a coastal sub-aqueous marine-basin environment or fluvial channels environment in low energy regime.
		xsSG Cross-stratified Sand and Gravel	Fine to coarse sand and fine crystal-lithic gravel, poor sorting, layers ranges between millimeters to centimeters.	Low to medium energy processes. Hyperconcentrated flood in stream reworking setting.
		dsSt Diffusely layered Silt	Diffusely millimetric layered silt. Presence of ripples and low energy wave structures, good sorting.	Shallow water basin, sedimentation in lacustrine basin and/or ponds. Some turbidite sedimentation.
		bChS Bedded Chert (and Sand)	Bedded chert with local sand contribution. Thinly multicolor laminated deposit with < 1 mm microcrystalline quartz-dominate layers.	Precipitation of silica particles in closed lake basins in association with volcanic rocks and sandstone.

Table 1

Table 2

Region	Tapajos										
Sample	NP – 079*	NP269a	Np380b	Np411c	NP- CO67*	NP - 080C	NP – 084A*	NP – 101*	NP - 123	NP - 156B*	NP - 159B
Class	VC	I	I	I	I	I	I	I	I	I	I
Type	A	A	A	A	A	A	A	A	A	A	A
XRF(%)											
SiO_2	71.80	68.78	72.20	66.36	70.81	70.80	68.15	72.22	72.80	71.59	65.48
TiO_2	0.34	0.32	0.35	0.72	0.40	0.40	0.48	0.32	0.31	0.36	0.58
Al_2O_3	14.16	15.37	14.24	15.57	14.76	14.52	15.43	14.28	13.59	14.27	18.22
Cr_2O_3	b.d.l.	b.d.l.	b.d.l.	b.d.l.	b.d.l.	b.d.l.	b.d.l.	b.d.l.	b.d.l.	b.d.l.	b.d.l.
FeOt	1.41	1.81	1.48	3.64	1.53	1.59	2.02	1.34	1.64	1.39	2.86
MnO	0.04	0.02	0.05	0.07	0.09	0.07	0.09	0.04	0.06	0.04	0.04
MgO	0.32	0.25	0.29	0.90	0.35	0.31	0.54	0.25	0.37	0.19	1.10
CaO	1.04	0.15	0.94	1.49	0.91	0.63	0.98	0.59	1.29	0.50	0.14
Na_2O	3.75	2.80	4.31	4.57	4.42	4.07	4.56	4.12	2.28	3.63	2.14
K_2O	5.73	6.00	5.32	3.73	5.71	5.77	5.63	5.60	5.04	5.60	6.06
P_2O_5	0.04	0.06	0.05	0.22	0.07	0.06	0.09	0.04	0.06	0.04	0.10
LOI	0.99	3.51	0.32	1.30	1.03	1.48	1.34	0.82	2.59	1.28	3.42
Tot	99.62	99.07	99.55	98.57	100.08	99.70	99.31	99.62	100.03	98.89	100.14
Mg#	0.29	0.20	0.26	0.31	0.29	0.26	0.32	0.25	0.29	0.20	0.41
ppm											
V	20	11	11	34	14	17	29	13	28	10	38
Co	34	38	2	15	17	31	29	43	25	32	12
Ni	1.20	2.50	0.50	0.50	0.40	0.70	0.90	0.80	0.60	0.60	2.80
Zn	28	33	45	71	55	50	55	36	33	27	55
Rb	185	194	179	121	155	144	122	191	230	174	273
Sr	221	188	209	557	141	124	187	174	172	148	127
Y	15	15	22	23	21	22	21	22	37	15	35
Zr	267	241	277	245	361	371	440	276	224	272	401
Nb	13	15	14	12	12	13	11	14	13	14	18
Cs	2.10	1.20	2.30	3.0	2.70	2.10	2.80	2.60	15	2.10	7.1
Ba	673	945	1425	1536	2185	1813	2245	1365	898	1362	1202
La	53	67	56	57	64	72	79	51	70	38	72
Ce	100	98	111	110	117	136	149	99	126	50	129
Pr	10	12	11	11	13	16	18	11	13	8.4	16
Nd	34	40	39	42	47	53	63	37	45	28	54
Sm	4.9	5.8	6.4	6.9	7.3	7.9	9.0	6.0	8.0	4.3	8.2
Eu	0.58	0.80	0.98	1.52	1.83	1.58	2.36	0.90	1.23	0.64	1.67
Gd	3.6	4.1	5.0	5.4	5.4	5.4	6.1	4.8	7.2	3.0	6.7
Tb	0.52	0.56	0.73	0.76	0.73	0.78	0.76	0.69	0.99	0.50	0.97
Dy	2.69	3.0	3.9	4.1	3.8	4.0	3.9	3.6	5.4	2.92	5.6
Ho	0.57	0.57	0.74	0.76	0.78	0.75	0.77	0.73	1.21	0.57	1.06
Er	1.61	1.65	2.19	2.17	2.08	2.33	2.19	2.21	3.3	1.77	3.3
Tm	0.24	0.26	0.35	0.36	0.33	0.34	0.34	0.36	0.48	0.29	0.48
Yb	1.56	1.83	2.38	2.22	2.30	2.12	2.08	2.41	3.43	1.95	2.90
Lu	0.24	0.29	0.38	0.35	0.36	0.36	0.34	0.36	0.54	0.33	0.49
Hf	7.7	7.0	7.3	6.4	8.4	8.5	8.9	7.2	6.3	7.6	9.8
Ta	1.50	2.20	1.00	1.50	1.00	1.40	1.20	1.70	1.50	1.80	1.30
Pb	23	6.3	13	7.3	24	73	20	10	26	9.2	4.5
Th	21	21	19	13	15	17	14	20	22	20	21
U	4.9	3.4	5.0	2.90	3.3	3.6	2.90	4.0	2.90	4.6	4.8

Table 2: continued

Region	Tapajos										
Sample	NP - 175A	NP – 176*	NP - 178B*	NP – 179*	NP – 180*	NP – 183A*	NP – 184*	NP - 093	NP - 094	Np272a	Np393A
Class	I	I	I	I	I	I	I	VC	VC	R	R
Type	A	I	A	A	A	A	A	A	A	A	A
XRF (%)											
SiO_2	73.86	75.93	70.86	72.53	69.73	71.25	70.99	60.36	62.46	71.13	76.57
TiO_2	0.24	0.20	0.39	0.37	0.44	0.41	0.37	0.81	0.89	0.49	0.09
Al_2O_3	13.40	12.71	14.62	14.44	15.20	14.65	14.54	15.42	16.36	14.44	11.93
Cr_2O_3	b.d.l.	b.d.l.	b.d.l.	b.d.l.	0.01	b.d.l.	b.d.l.	0.01	b.d.l.	b.d.l.	b.d.l.
FeOt	1.10	0.78	1.57	1.67	2.03	1.57	1.75	5.70	4.97	2.52	1.16
MnO	0.07	0.06	0.07	0.09	0.09	0.09	0.08	0.11	0.09	0.06	0.03
MgO	0.11	0.16	0.29	0.30	0.36	0.24	0.30	3.24	1.68	0.51	0.01
CaO	0.50	0.34	0.88	0.65	0.88	0.56	0.68	4.59	3.03	1.57	0.14
Na_2O	3.78	3.46	4.70	4.38	4.49	4.54	4.97	2.79	3.11	4.27	4.39
K_2O	5.41	5.11	5.11	5.56	5.64	5.57	4.87	4.67	5.86	2.32	3.95
P_2O_5	0.02	0.01	0.06	0.06	0.07	0.05	0.06	0.35	0.39	0.06	b.d.l.
LOI	1.15	0.88	1.28	0.85	1.00	0.81	1.07	1.37	0.64	1.38	0.58
Tot	99.64	99.64	99.83	100.90	99.94	99.74	99.68	99.43	99.48	98.75	98.85
Mg#	0.15	0.27	0.25	0.24	0.24	0.21	0.23	0.50	0.38	0.27	0.02
ppm											
V	b.d.l.	b.d.l.	14	b.d.l.	17	b.d.l.	10	112	59	11	b.d.l.
Co	36	34	32	40	28	37	38	27	24	2.60	63
Ni	0.50	0.50	0.80	2.30	3.4	1.50	0.60	19	0.50	0.60	1.10
Zn	20	32	45	51	46	52	60	55	73	55	33
Rb	156	158	136	153	136	133	127	116	169	105	196
Sr	54	46	179	120	115	78	103	614	620	321	33
Y	27	20	23	27	22	23	20	16	23	21	37
Zr	223	162	397	370	423	402	360	174	257	279	181
Nb	13	13	13	14	11	12	12	7.3	11	12	23
Cs	3.2	3.9	2.10	3.10	2.60	1.80	0.70	4.2	6.2	1.70	1.60
Ba	477	310	2021	998	880	746	2243	1362	2063	1363	75
La	45	36	75	76	91	80	64	35	53	59	72
Ce	92	70	140	138	174	151	122	70	106	108	133
Pr	11	8.3	15	15	20	18	14	8.5	13	11	14
Nd	39	29	57	52	69	64	52	31	48	38	45
Sm	6.7	4.7	8.9	8.1	10	9.4	7.9	5.2	7.6	6.5	8.1
Eu	0.72	0.49	1.98	1.36	1.63	1.51	1.84	1.35	1.71	1.27	0.09
Gd	5.3	3.7	6.9	6.9	6.6	6.6	5.7	4.3	5.5	4.9	7.0
Tb	0.81	0.59	0.76	0.87	0.92	0.91	0.78	0.57	0.81	0.70	1.14
Dy	4.7	3.7	4.5	4.3	4.4	4.6	4.0	3.0	4.3	3.7	6.8
Ho	0.90	0.72	0.86	0.91	0.80	0.83	0.82	0.56	0.82	0.69	1.31
Er	2.63	2.25	2.73	2.57	2.23	2.31	2.51	1.52	2.32	1.99	3.9
Tm	0.41	0.35	0.39	0.36	0.36	0.37	0.36	0.23	0.32	0.31	0.62
Yb	2.61	2.21	2.44	2.71	2.25	2.43	2.32	1.43	2.08	1.95	4.1
Lu	0.39	0.33	0.42	0.43	0.36	0.40	0.37	0.24	0.33	0.30	0.60
Hf	6.6	5.2	8.7	8.5	9.6	9.3	8.4	4.3	6.2	7.1	7.4
Ta	1.80	1.70	1.10	1.80	1.40	1.60	1.60	0.60	1.00	0.90	7.1
Pb	16	29	137	10	17	11	28	4.0	6.9	46	36
Th	17	18	17	16	16	17	17	6.1	11	13	30
U	3.4	4.4	3.5	3.9	3.5	3.7	4.0	1.30	2.10	3.4	9.1

Table 2: continued

Region	Tapajos										
Sample	Np405	Np406	NP - 039B	NP - 073	NP - 114	NP - 121	NP – 173*	NP - 175B	NP - 182C		
Class	R	R	R	R	R	R	R	R	R		
Type	A	A	A	A	A	A	I	I	I		
XRF (%)											
SiO_2	73.67	69.79	65.32	72.82	63.80	75.09	75.58	75.03	74.44		
TiO_2	0.33	0.45	0.86	0.31	0.74	0.27	0.20	0.22	0.22		
Al_2O_3	13.09	14.72	16.61	13.84	17.99	13.16	12.96	13.46	13.50		
Cr_2O_3	b.d.l.	b.d.l.	b.d.l.	b.d.l.	b.d.l.	b.d.l.	b.d.l.	b.d.l.	b.d.l.		
FeOt	1.33	1.78	3.27	1.29	3.30	1.01	0.99	0.96	1.23		
MnO	0.05	0.05	0.09	0.04	0.05	0.03	0.07	0.09	0.02		
MgO	0.26	0.30	0.51	0.28	0.70	0.10	0.19	0.19	0.14		
CaO	0.53	0.76	2.07	0.89	1.54	0.15	0.72	0.42	0.04		
Na_2O	2.25	3.87	4.99	3.61	5.02	3.78	3.21	3.69	3.56		
K_2O	7.13	5.57	3.88	5.71	5.51	5.19	5.18	5.39	4.92		
P_2O_5	0.03	0.07	0.22	0.04	0.22	0.03	0.02	0.02	0.02		
LOI	0.55	1.26	1.50	0.75	1.45	0.95	1.49	0.83	2.09		
Tot	99.22	98.62	99.32	99.58	100.32	99.76	100.61	100.30	100.18		
Mg#	0.26	0.23	0.22	0.28	0.27	0.15	0.25	0.26	0.17		
ppm											
V	8	<8	55	14	83	18	<8	<8	<8		
Co	1.00	36	19	19	14	52	25	45	100		
Ni	0.40	2.40	2.20	3.60	1.90	0.60	0.70	0.70	1.30		
Zn	30	38	49	21	48	18	16	28	8		
Rb	232	194	96	200	153	190	156	158	133		
Sr	204	229	552	193	377	91	79	63	32		
Y	23	22	20	18	26	34	64	24	18		
Zr	272	336	228	246	265	245	173	191	189		
Nb	14	15	9.2	14	12	17	13	14	13		
Cs	2.20	2.50	2.10	2.30	1.30	3.1	4.1	3.5	1.10		
Ba	1634	1965	1615	534	1918	583	485	413	569		
La	63	62	50	57	58	62	48	41	41		
Ce	120	117	96	101	107	112	76	80	80		
Pr	12	12	11	11	13	13	10	10	10		
Nd	43	42	38	38	49	45	34	32	32		
Sm	6.6	6.9	6.4	5.6	7.5	8.4	5.4	5.8	5.4		
Eu	0.93	1.27	1.68	0.68	1.70	0.87	0.69	0.53	0.66		
Gd	5.2	5.3	5.1	4.5	5.8	7.0	5.0	4.6	3.8		
Tb	0.73	0.74	0.69	0.55	0.80	1.02	0.80	0.76	0.58		
Dy	3.9	4.0	3.8	3.0	4.4	6.1	5.2	4.2	3.6		
Ho	0.82	0.79	0.79	0.58	0.94	1.25	1.17	0.80	0.66		
Er	2.21	2.31	2.31	1.76	2.64	3.4	3.8	2.42	2.02		
Tm	0.35	0.34	0.34	0.27	0.39	0.52	0.56	0.36	0.31		
Yb	2.47	2.28	2.01	1.83	2.43	3.3	3.1	2.43	2.03		
Lu	0.39	0.37	0.30	0.26	0.35	0.53	0.54	0.36	0.33		
Hf	8	9.3	5.9	7.3	6.3	7.6	5.5	6.0	5.3		
Ta	1.00	4.5	1.00	1.50	0.80	2.30	1.60	2.20	1.50		
Pb	10	11	10	19	8.6	16	13	9.2	2.70		
Th	20	17	12	24	14	23	19	17	17		
U	4.5	3.9	2.90	5.4	3.2	6.9	5.0	4.2	2.70		